

Ninevah University

College of Electronics Engineering



Analysis and Design of a unit Cell for Reflectarrays with Improved Performance

Rosl Amer Abdaljabar

M.Sc. Dissertation

in

Communication Engineering

Supervised by

Prof. Dr. Khalil Hassan Sayidmarie

2024 A.C

1445.A.H

Ninevah University

College of Electronics Engineering



Analysis and Design of a unit Cell for Reflectarrays with Improved Performance

A Dissertation Submitted

By

Rosl Amer Abdaljabar

To

The Council of College of Electronic Engineering
University of Mosul In Partial Fulfillment of the
Requirements For the Degree of Master of Sciences

In

Communication Engineering

Supervised by

Prof. Dr. Khalil Hassan Sayidmarie

2024 A. C

1445.A.H

Supervisor's Certification

I certify that the dissertation entitled (Analysis and Design of a unit Cell for Reflectarrays with Improved Performance) was prepared by Rosl Amer Abdaljabar under my supervision at the Department of Communication Engineering, Ninevah University, as a partial requirement for the Master of Science Degree in Communication Engineering.

Signature:

Name: Prof. Dr. Khalil H. Sayidmarie

Department of Communication Engineering

Date: / /2023

Report of Linguistic Reviewer

I certify that the linguistic reviewer of this dissertation was carried out by me and it is accepted linguistically and in expression.

Signature:

Name: Prof.Dr.Wafaa A.Abdulaali

Date: / /2024

Report of the Head of Postgraduate Studies Committee

According to the recommendations presented by the supervisor of this dissertation and the linguistic reviewer, nominate this dissertation to be forwarded to discussion.

Signature:

Name: **Prof. Dr. Khalil H. Sayidmarie**

Date: / /2024

Report of the Head of Postgraduate Studies Committee

I certify that this dissertation was carried out in the Department of Communication Engineering. I nominate it to be forwarded to discussion.

Signature:

Name: **Dr: Mahmud A. Mahmud**

Date: / /2024

List of Publication

Some of the important results obtained in this work have appeared in the following publications:

Conference Paper:

1. R. A. Abdul Jabbar, and K. H. Sayidmarie," A Unit Cell Element for Reflectarrays Based on the Bowtie Shape", Accepted in the 9th International Congress on Information and Communication Technology, (ICICT 2024) 19 - 22 February 2024, London, United Kingdom.



9th International Congress on
Information and Communication Technology in concurrent with
ICT Excellence Awards (ICICT 2024)
19 - 22 February 2024, London, United Kingdom.

Dear Khalil Sayidmarie and Rosl Abdul Jabbar

Paper ID : 685

Title : A Unit Cell Element for Reflectarrays Based on the Bowtie Shape

Greetings .. !!

Congratulations! On behalf of the Program Committee of ICICT 2024 - LONDON, I am happy to inform you that your above-mentioned paper has been ACCEPTED for oral presentation in ICICT 2024 and publication in Springer LNNS series subject to fulfillment of Guidelines by Springer.

An accepted paper will be published in the Springer proceedings (LNNS) only if the final version is accompanied by the payment information (i.e. transaction reference number) subject to quality check as per Springer Guidelines.

Abstract

Highly directive antennas have a vast range of applications at microwave frequencies. The favorable features of reflector antennas and microstrip arrays were combined in a single design called “reflectarray”. These antennas have a planar reflecting surface, consisting of an array of reflecting cells that are called unit-cells, which work as receive/reflect/transmit array elements. Each of these reflecting elements is designed to have certain amplitudes and phase parameters (S11) to fulfill the design requirements.

As the bowtie antenna is known for its wide band property, this shape is proposed here as a unit cell for reflectarray antennas. Various designs for the unit cell have been investigated to achieve the desired performance of linear phase variation across a range not less than 360° , while maintaining a low slope as a function of the element size and frequency. The bowtie was developed into other derived shapes to attain a phase response of a lower slope. One design (Elliptical bowtie) gave favorable features due to the smoother edges compared to the conventional shape comprising two triangles. This shape was utilized as a single ring and then in a double ring configuration to attain the required phase slope and a range exceeding 360° . It is shown that the multiple rings can offer phase ranges of no less than 360° . By choosing suitable dimensions and scaling factors for these elements, the phase characteristics can be made approximately a linear function of their size. The CST Microwave Studio was used to model and analyze the performance of the proposed unit cells that were simulated using waveguide port excitation. The results obtained from the investigated various shapes were compared together, as well as with other published works.

TABLE OF CONTENTS

Subject		page
Abstract		I
Table of Contents		II
List of Tables		V
List of Figures		VI
List of Abbreviations		XIII
List of Symbols		XIV
CHAPTER ONE-INTRODUCTION AND RELATED WORKS		1
1.1	Introduction	1
1.2	Development History of Reflectarrays	2
1.3	Literature Review	4
1.4	Statement of the Research Problem	9
1.5	Dissertation Objectives	9
1.6	Dissertation layout	10
CHAPTER TWO-ANALYSIS OF THE REFLECTARRAY		11
2.1	Introduction	11
2.2	Definition of Reflectarray Antennas	11
2.3	Principle of Operation	13
2.4	Analysis of Reflectarray Elements	15
2.5	The Phase Tuning Approach	16
2.5.1	Elements Connected to Time Delay Lines	17
2.5.2	Elements of Variable Sizes	17
2.5.3	Rotation of The Elements	18
2.6	Specifications of The Reflectarray	18
2.6.1	Bandwidth	19
2.6.2	Efficiency of The Reflectarray Antenna	21
2.6.3	Phase Range and Slope	22
2.7	Considerations in the Selecting the Elements	23
2.7.1	Reflection Phase of the Element	23
2.7.2	Beamwidth of the Element	24
2.7.3	Spacing of the Elements	26

2.8	Various Types of Reflectarray Elements	26
2.8.1	Single Layer Elements	27
2.8.2	Multilayer Elements	30
2.8.3	Single Layer Ring and Double Ring Elements	33
CHAPTER THREE		
INVESTIGATION INTO PROPOSED UNIT CELLS FOR REFLECTARRAYS		37
3.1	Introduction	37
3.2	Simulation Framework	37
3.2.1	Overview of the Waveguide Simulator (WGS)	37
3.2.2	The Infinite-array approach	39
3.3	Considerations for the Design of Element Shapes	40
3.4	Bowtie Element as a Unit Cell	41
3.4.1	First Group	43
3.4.2	Second Group	52
3.5	Bowtie with Rounded Sides (Tapered bowtie)	54
3.5.1	The Tapered bowtie (horizontal electric field)	54
3.5.2	The Tapered Bowtie (vertical electric field)	57
3.6	The Crossed Bowtie (Third Group)	59
3.7	The Square element	61
3.8	Square Bowtie Antenna	64
3.9	The Disconnected Bowtie (Fourth group)	67
3.9.1	Disconnected triangles (tip-to-tip)	68
3.9.2	Back-to-back triangles	70
3.10	The Fractal (Dual) Bowtie Element	72
3.10.1	The Fractal Bowtie Element (horizontal electric field)	72
3.10.2	The Dual Tapered Bowtie Element (horizontal electric field)	74
3.11	Elliptical Bowtie	76
3.12	Effective dielectric constant (ϵ_{reff})	79
3.13	Resonance frequency (f_r)	80

CHAPTER FOUR		
INVESTIGATION INTO PROPOSED DOUBLE RING UNIT CELLS FOR REFLECTARRAYS		88
4.1	Introduction	88
4.2	Single-Ring Bowtie Element	89
4.3	Double Ring Bowtie Element	96
4.3.1	First Case	97
4.3.2	Second Case	103
4.3.3	Third case	104
4.3.4	Fourth case	105
CHAPTER FIVE		
CONCLUSION AND FUTUER WORK		111
5.1	Conclusions	111
5.2	Future Work	112
References		114
References		114

LIST OF TABLES

Table	Title of Table	Page
3.1	Phase response and characteristics of the bowtie unit cell for the first group.	49
3.2	Phase response characteristics of the conventional and tapered bowtie unit cell elements, at the frequency of 6.5 GHz.	57
3.3	Phase response characteristics of cross bowtie and square element cell reflectarray antenna.	64
3.4	Phase response characteristics of square bowtie and square element cell reflectarray antenna.	67
3.5	Phase response characteristics of bowtie and elliptical bowtie element cell reflectarray antenna.	78
3.6	Calculated features of bowtie element at fixed $a=4$ and various values of b .	82
3.7	K_1 and K_2 calculations	82
3.8	Calculated features of bowtie element at $W=b$.	84
3.9	Calculated features of bowtie element at fixed $b=4$ and various values of a .	85
3.10	K_1 and K_2 calculations.	86
3.11	Calculated features of bowtie element at fixed $b=4$ and various values of a .	87
4.1	Phase response and characteristics of the bowtie and bowtie ring unit cells.	93
4.2	Phase response and characteristics of the bowtie and bowtie ring unit cell.	96
4.3	Phase response and characteristics of the bowtie, ring bowtie, and double-ring bowtie unit cells.	100
4.4	Phase response and characteristics of the bowtie, bowtie ring and bowtie double ring unit cell.	102
4.5	Phase response and characteristics of the Second case.	104
4.6	Phase response and characteristics of the third case.	105
4.7	Phase response and characteristics of the elliptical bowtie elliptical bowtie ring and elliptical bowtie double ring unit cell.	110

LIST OF FIGURES

Figure	Title	Page
1.1	2D planar array (top left), Reflector antenna (down left), and a typical reflectarray (right).	2
1.2	Reflectarrays; (a) The oldest reflectarray, (b) configuration of the reflectarray, (c) Various reflectarray elements.	4
2.1	Geometry of a planar reflectarray antenna.	12
2.2	The working principle of a Reflectarray antenna with a planar metasurface.	13
2.3	Classic Microstrip antenna; (a) Microstrip antenna top view (b) side view. (c) Electric field line.	16
2.4	Multiform of reflectarray elements; (a) phase time delay lines, (b) Different types of variable size square elements, (c) variable size dipoles or loops, (d) A CP reflectarray patch with different types , (left) shows the patch with 0° phase shift and (right) the ψ rotated patch with 2ψ phase shift.	18
2.5	The variation in spatial phase delay of the reflectarray elements.	20
2.6	S-shaped graph depicting element phase changes according to variations in the element.	24
2.7	Reflectarray element pattern effect.	25
2.8	The phase variations of square and circular patches on two different kinds of substrates .	27
2.9	Element of reflectarray (left) shapes of the analyzed first group of derived element shapes, (right) Fluctuation of the reflection phase with side length L.	28
2.10	Element of reflectarray ;(a) Shapes of the analyzed second group of elements shapes, (b) Fluctuation of the reflection phase with side length L.	29
2.11	Element of reflectarray; (a)Shape of the third group of elements,(b) Fluctuation of the reflection phase with length L.	30

2.12	Double layer reflectarray;(a) Unit cell, (b) multiple layers .	31
2.13	Two layer reflectarray; (left) unit cell, (right) Reflection phase of the unit cell.	32
2.14	Ring element reflectarray; (left) Double cross loop element different arms, (right) Reflection phase response of the unit cell.	34
2.15	Ring element reflectarray.	35
2.16	Double ring element reflectarray.	35
2.17	Phase responses (left) Phase responses of double rings for square,(right) Phase responses of double rings for circular.	36
2.18	Configuration of the double ring reflectarray element .	36
3.1	Waveguide Simulator (WGS); (a) Unit cell, (b) Boundary conditions, (c) H-wall waveguide simulator.	39
3.2	Orientation of the electric field of the incident wave with respect to the array element; (a) the E-field is parallel to the width, (b) the E-field is normal to the width.	41
3.3	The bowtie unit cell of the reflectarray; (a) top view (b) side view .	42
3.4.	Geometry of the investigated bowtie dipole element at $2a=8$ mm, and E-field is along the width	44
3.5	The variation of the reflection coefficient magnitude with the frequency for various values of b, when $2a=8$ mm.	45
3.6	The variation of the reflection coefficient phase with the frequency for various values of b, when $2a=8$ mm.	45
3.7	Geometry of the investigated bowtie dipole element at $b=4$ mm.	46
3.8	The variation of the reflection coefficient magnitude with the frequency for various values of a, when $b=4$ mm.	47
3.9	The variation of the reflection coefficient phase with the frequency for various values of a, when $b=4$ mm	47
3.10	Comparison of the phase responses at the frequency of 6 GHz for the two schemes; (blue) fixed width ($a=4$) and variable height b,(brown) fixed height ($b=4$) and variable	48

	width.	
3.11	The variation of the reflection coefficient magnitude with the frequency for various values of b at $2a=8\text{mm}$.	50
3.12	The variation of the reflection coefficient phase with the frequency for various values of b at $2a=8\text{mm}$.	50
3.13	The variation of the reflection coefficient magnitude with the frequency for various values of width (2a), at $b=4\text{mm}$.	51
3.14	The variation of the reflection coefficient phase with the frequency for various values of width (2a), at $b=4\text{mm}$.	52
3.15	Geometry of the investigated bowtie unit cell when a and b were changed at the same time.	53
3.16	The variation of the reflection coefficient magnitude with the frequency for various values of width 2a and height b.	53
3.17	The variation of the reflection coefficient phase with the frequency for various values width 2a and height b.	54
3.18	Geometry of the proposed tapered bowtie unit cell with half circles on each side.	55
3.19	The variation of the reflection coefficient magnitude with the frequency for tapered bowtie for various values of a and b.	55
3.20	The variation of the reflection coefficient phase with the frequency for tapered bowtie for various values of a and b.	56
3.21	Comparison of the phase responses of the conventional and tapered bowtie unit cell elements, at the frequency of 6.5 GHz.	56
3.22	The variation of the reflection coefficient magnitude with the frequency for various values of a and b.	58
3.23	The variation of the reflection coefficient phase with the frequency for various values of a and b.	58
3.24	Geometry of the crossed bowtie unit cell.	59
3.25	The variation of the reflection coefficient magnitude with the frequency for various bowtie sizes ($a = b$).	60
3.26	The variation of the reflection coefficient phase with the	60

	frequency for various bowtie sizes ($a = b$).	
3.27	Geometry of the square unit cell, $a=b$.	61
3.28	The variation of the reflection coefficient magnitude with the frequency for the square unit cell.	62
3.29	The variation of the reflection coefficient phase with the frequency for the square unit cell.	62
3.30	Phase variation with the parameter of elements at center frequency 7GHz.	63
3.31	Geometry of the square bowtie antenna, where outer dimensions are equal to those of the square element.	64
3.32	The variation of the reflection coefficient magnitude with the frequency for the square bowtie unit cell.	65
3.33	The variation of the reflection coefficient phase with the frequency for the square bowtie unit cell.	65
3.34	The variation of the reflection coefficient magnitude with the frequency for the square unit cell.	66
3.35	The variation of the reflection coefficient phase with the frequency for the square unit cell.	66
3.36	Phase variation with the parameter a at center frequency 6.5GHz.	67
3.37	Different geometries for disconnected bowtie unit cell.	69
3.38	The variation of the reflection coefficient magnitude with the frequency for the disconnected bowtie at gap; (a) 0mm,(b) 1mm, (c) 2mm.	69
3.39	The variation of the reflection coefficient phase with the frequency for the disconnected bowtie at gap;(a) 0mm,(b) 1mm,(c) 2mm.	70
3.40	Back to back configuration of the bowtie unit cell with various gaps.	71
3.41	The variation of the reflection coefficient magnitude with the frequency for the back-back bowtie at gap; (a) 0mm, (b) 1mm, (c) 2mm.	71
3.42	The variation of the reflection coefficient phase with the frequency for the back-back bowtie at gap; (a) 0mm, (b)	72

	1mm, (c) 2mm.	
3.43	Geometries of the investigated of the fractal bowtie element.	73
3.44	The variation of the reflection coefficient magnitude with the frequency for for ratio of a2 to a1;(a)0.5,(b)0.7,(c)0.8.	73
3.45	The variation of the reflection coefficient phase with the frequency for for ratio of a2 to a1:(a) 0.5,(b) 0.7,(c) 0.8 mm.	74
3.46	Geometries of the investigated dual tapered bowtie element.	75
3.47	The variation of the reflection coefficient magnitude with the frequency for for ratio of a2 to a1;(a)0.5,(b)0.7,(c)0.8 mm.	75
3.48	The variation of the reflection coefficient phase with the frequency for for ratio of a2 to a1:(a)0.5,(b)0.7,(c)0.8 mm.	75
3.49	Geometry of the investigated elliptical bowtie element at a=b mm.	76
3.50	The variation of the reflection coefficient magnitude with the frequency for various values of element size (a).	76
3.51	The variation of the reflection coefficient phase with the frequency for various values of element size (a).	77
3.52	The variation of the reflection phase with the element width (2a) of the triangular and elliptical bowtie elements at the center frequency of 8 GHz.	78
3.53	Microstrip line, (b) effective dielectric constant.	79
3.54	Detailed design geometry of the entire structure including the solid bowtie .	81
4.1	Geometries of the bowtie shape; (a) bowtie patch with $2a=b$,(b) bowtie ring with $2a=b$ and ring width $W1= a (1-S1)/2$, (c) side view showing the substrates.	90
4.2	The variation of the reflection coefficient magnitude with the frequency for various bowtie sizes ($2a = b$) .	91
4.3	The variation of the reflection coefficient phase with the frequency for various bowtie sizes ($2a = b$).	91

4.4	The variation of the reflection coefficient phase with the width of the bowtie ring at center frequency of 8 GHz.	92
4.5	Geometries of the bowtie shape; (a) bowtie patch with $2a=b$, (b) bowtie ring with $2a=b$ and ring width $W1= a (1 - S1) /2$.	94
4.6	The variation of the reflection coefficient magnitude with the frequency for various bowtie sizes ($2a = b$) .	94
4.7	The variation of the reflection coefficient magnitude with the frequency for various bowtie sizes ($2a = b$) .	95
4.8	The variation of the reflection coefficient phase with width of bowtie at center frequency of 8 GHz	95
4.9	Geometry of the investigated of unit cell; (a)bowtie , (b)bowtie ring, (c) double ring bowtie element at $b1=2a1$.	97
4.10	The variation of the reflection coefficient magnitude with the frequency for various double ring bowtie sizes ($2a1=b1$).	98
4.11	The variation of the reflection coefficient phase with the frequency for various double ring bowtie sizes ($b1=2a1$).	99
4.12	The variation of the reflection coefficient phase with the width of the bowtie at a center frequency of 8 GHz.	99
4.13	Geometry of the investigated unit cell; (a) bowtie, (b) bowtie ring, (c) double ring bowtie element at $b1=2a1$.	100
4.14	The variation of the reflection coefficient magnitude with the frequency for various double ring bowtie sizes ($2a1 = b1$).	101
4.15	The variation of the reflection coefficient phase with the frequency for various double ring bowtie sizes ($2a1 = b1$).	101
4.16	The variation of the reflection coefficient phase with width of bowtie at center frequency 8GHz.	102
4.17	Geometry of the investigated of unit cell.	103
4.18	The variation of the reflection coefficient phase with the width of bowtie at center frequency 8GHz.	103
4.19	Geometry of the investigated unit cell.	104
4.20	The variation of the reflection coefficient phase with the	105

	width of bowtie at center frequency 8GHz.	
4.21	Geometry of the investigated unit cell;(a) elliptical bowtie (b) elliptical bowtie ring (c) elliptical bowtie double ring at $a=b$.	106
4.22	The variation of the reflection coefficient magnitude with the frequency for various elliptical bowtie sizes ($b=a$).	106
4.23	The variation of the reflection coefficient phase with the frequency for various elliptical bowtie sizes ($b=a$).	107
4.24	The variation of the reflection coefficient magnitude with the frequency for various elliptical bowtie ring sizes ($b=a$).	107
4.25	The variation of the reflection coefficient phase with the frequency for various elliptical bowtie ring sizes ($b=a$).	108
4.26	The variation of the reflection coefficient magnitude with the frequency for various elliptical bowtie double ring sizes ($b=a$).	108
4.27	The variation of the reflection coefficient phase with the frequency for various elliptical bowtie double ring sizes ($b=a$).	109
4.28	The variation of the reflection coefficient phase with width of elliptical bowtie at center frequency 8GHz.	109

LIST OF ABBREVIATIONS

Abbreviation	Name
APS	Propagation International Symposium
CP	Circularly Polarized
CST MWS	Microwave Studio
FR4	Glass-Reinforced Epoxy
IEEE	Institute of Electrical and Electronics Engineers
TEM	Transverse Electromagnetic Wave
WGS	Waveguide Simulator

TABLE OF SYMBOLS

Symbol	Name
%	Percentage
\vec{R}_{mn}	Location Vector
\vec{d}_{mn}	Location Vector
\hat{r}_0	Unit Vector
A_{mn}	Complex Excitation
ϵ_r	Relative Dielectric Constant of the Substrate
ϵ_{reff}	Effective Permittivity
λ_0	Wavelength in Free Space
d'	Spacing of Element
ϕ	Azimuth Angle
$2a$	Width
A	Complex excitation
AF	Array Factor
b	Height
BW	Bandwidth
c	Speed of Light in Vacuum
D	Diameter
d	Fraction of Free-Space
dB	Decibel unit
d_i	Distance
Et	Electric Field
F	Focal Distance
f	Frequency
fr	Resonance Frequency
GHz	Giga Hertz
h	Thickness of substrate
Ht	Magnetic Field
k_0	Wavenumber
k_o	Proportionality Factor
L	Length

mm	Millimeter (1 meter *10 ⁻³)
N	Integer
S	scale factor
S ₁₁	Reflection Coefficient
W	Width of patch
β	Progressive phase shift
δ	Delta Function
θ	Elevation Angle
λ	Wavelength
λ_{eff}	Effective Wavelength
ψ	Angle /phase shift

CHAPTER ONE

INTRODUCTION AND RELATED WORKS

1.1 Introduction

The need to communicate has been inherent in the human race since its inception. While short-range communication is relatively easy, long-range communication presents challenges, where high-gain antennas are required for the majority of systems [1]. With the recent advancements in wireless communication technology, there is a growing demand for high-gain antennas that offer wide beam scanning capabilities and can be produced at a low cost. These antennas are used in different applications like direct communication, radio cosmology, and earth remote sensing. Traditionally, the parabolic dish reflector antenna has been used for these purposes. However, the curved structure of the reflector poses challenges in manufacturing, particularly at millimeter wave frequencies. Additionally, their bulky size and weight make them less desirable compared to planar antennas. Moreover, parabolic reflectors have limitations in achieving wide-angle electronic beam scanning due to their restricted scan angle. To overcome these limitations, high-gain phased array antennas have been employed as an alternative to parabolic antennas. These arrays consist of multiple fixed elements that can achieve wide-angle beam scanning electronically by incorporating controllable phase shifters. However, the integration of amplifier modules with phased arrays becomes necessary to address the efficiency issue. To mitigate these problems, another approach was developed by introducing a flat reflector called the reflectarray. Microstrip reflectarrays have emerged as a potential solution for high-gain antennas, offering increased efficiency at lower costs by combining the advantages of planar phased arrays and reflectors [2]-[4]. So the Reflectarray antennas are the

most commonly used and most promising technology for point-to-point and 5G transmission networks because they produce highly directional pencil beams[5]. However, when it comes to applications that require higher frequencies, broadband antennas are more desirable [6]. This amalgamation of 2D planar arrays and reflector antennas is depicted in Fig.1.1, which illustrates the evolution of reflectarray antennas.

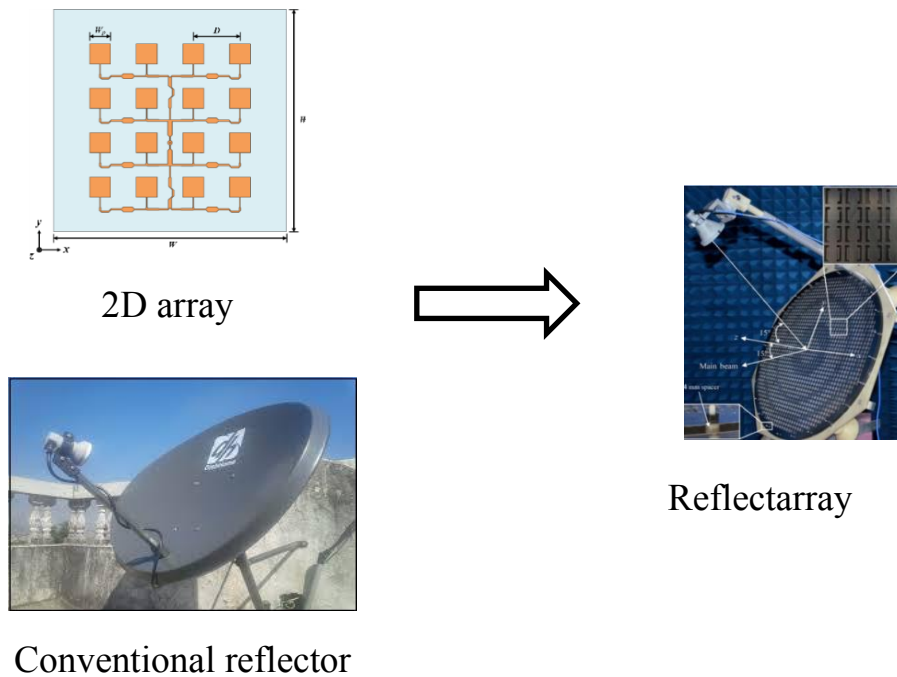


Figure 1.1. 2D planar array (top left) [7], Reflector antenna (down left), and a typical reflectarray (right) [8].

1.2 Development History of Reflectarrays

After the Second World War antenna array engineering developed quickly, especially during the 1960s and the advancement of printed circuit boards had a large effect on this development. The antenna community has been more interested in a new generation of microstrip antennas due to their low profile, low mass, and frequently affordable characteristics [5]:

The reflectarray antenna as a hybrid antenna combines numerous advantageous qualities of both reflectors and printed arrays[2]. Berry, Malech, and Kennedy proposed the idea for a reflectarray antenna in the early 1960s [4][9][10]. The ability to achieve reradiated far-field beams was demonstrated using short-ended waveguide components with variable lengths as shown in Fig.1.2a. Since the majority of wireless activities at that time were conducted at low microwave frequencies, this antenna design was seen as bulky.

The technologies of combining the reflectarray and microstrip radiators were investigated by Malagisi, who made the first reference to employing microstrip components for reflectarray in 1978. In the same year, the first attempt to investigate the microstrip reflective element was made, and Montgomery used the infinite array approach to carry out his studies [1]. To minimize antenna size, a variety of printed reflectarray antennas were proposed in the late 1980s and early 1990s, where a variety of shapes were used as seen in Fig.1.2c [1].

Starting from 2006, the IEEE Antennas and Propagation International Symposium (APS) has organized numerous sessions dedicated to reflectarray, where several hundred papers were published [5].

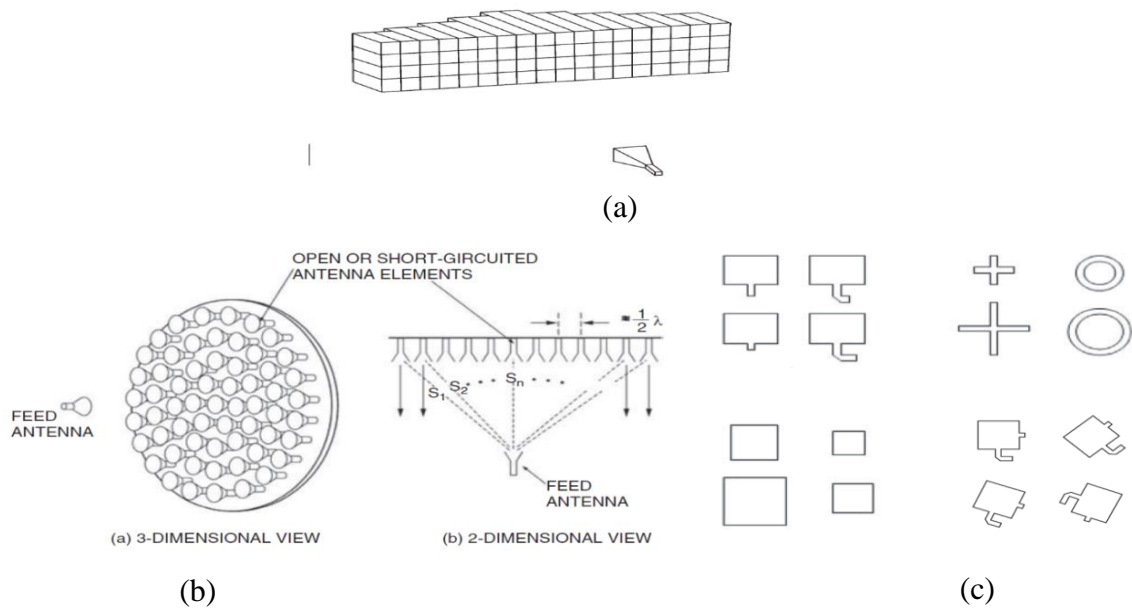


Figure 1.2. Reflectarrays; (a) The oldest reflectarray, (b) configuration of the reflectarray, (c) Various reflectarray elements[1].

1.3 Literature Review

This section focuses on presenting previous studies to gain insights into the potential developments, challenges, and applications of reflectarrays.

In [2003], M. Bozzi et al. conducted a systematic performance analysis comparing reflectarray elements of three commonly used shapes in reflectarray design. The researchers proposed the utilization of a ridge-shaped element that achieved a satisfactory trade-off among the parameters under consideration[11].

In [2008], K. H. Sayidmarie and M. E. Bialkowski presented results on polycyclic geometries of unit cells that provided an increased phase range for a single-layer printed element. It turned out that a unit cell consisting of 2 resonant elements can double the range of phases, while using three elements increases the phase range by about 3 folds with the phase response slope remaining almost unchanged. They also revealed that adjusting the relative sizes of the elements inside the cell can scale the phase responses[12]. The same

authors then reported that double square and circular ring elements produced a double response that led to enhancement in the bandwidth of the reflectarray. They concluded that properly designed multi-elements could increase the bandwidth [13]. Payam Nayeri et al. focused on examining the reflection performance of obliquely incident waves on single-layer double-ring unit cells used in reflectarray antennas. The results showed that normal incidence can provide satisfactory approximate results for the phasing response up to 30° degrees. Additionally, the investigated single-layer double-ring elements revealed an increased phasing range exceeding 600° and a notably gradual phase slope [14].

In [2010], a new element for broadband reflectarray antennas was introduced by D. Du et al. The proposed element consisted of two bent dipoles. The results showed that by using a composite substrate, a smaller slope and more linear phase performance can be obtained. Furthermore, a modified structure was designed to achieve a wider bandwidth of 6 to 10 GHz. The computed results demonstrated the desired main beam steering and a 1-dB gain bandwidth near 50%, which is significantly larger than those of conventional single-layer reflectarrays [15]. In the same year, Yuezhou Li et al. presented a comprehensive design of an X-band single-layer reflectarray consisting of 81 elements placed on two concentric circular rings. The simulation results showed that this design of multiple resonance elements has a favorable radiation pattern and an increased gain bandwidth [16].

In [2011], P. Nayeri et al. explored a method for enhancing the bandwidth of reflectarray antennas by utilizing closely spaced elements, (unit-cell sizes $< \lambda/2$) [17]. The full-wave electromagnetic simulations showed that closely spaced elements exhibit reduced phase error over a wider frequency range. The

two designed and fabricated reflectarrays were evaluated across 30 to 34 GHz frequency range. Significant improvement in gain bandwidth performance for the reflectarray designed with closely separated elements was obtained[17]. K.H. Sayidmarie et al. in the same year, investigated the phase properties of a unit cell in a single-layer reflectarray using fractal geometry. They proposed multi-resonance fractal elements and showed that patches of circular and square shape, and multiple rings that are printed on a thick substrate, can offer smaller phase slopes while providing phase ranges in excess of 360° [18].

In [2014], M. M. Fakharian et al. designed a novel reflectarray utilizing a folded stepped impedance resonator (SIR) patch-slot arrangement and using the variable size method of phase variation. The proposed structure exhibited nearly linear performance in terms of parametrics, while it offered a phase range exceeding 400° [19].

In [2017], a single-layer circularly polarized reflectarray was presented by Long Zhang et al. The antenna achieved a large axial ratio bandwidth, better gain, and higher aperture efficiency. The design utilized a proposed wideband S-shaped element that was rotated to achieve phase variations. Measurement results showed a 68.5% 3 dB axial ratio bandwidth and a 47.8% 3 dB gain bandwidth [20].

In [2020], T. Velly et al. presented a reflectarray comprising a rectangular ring and a cross patch unit cell. The reflectarray consisted of 13×13 elements and was equipped with a feed horn yielding a gain of 22.8 dB[21]. In the same year, Y. N. Phua et al. designed a new element consisting of a circular patch that is loaded with two unequal slots, so as to create a large-scale reflectarray. The design achieved 23.4 dB gain and a 42% aperture efficiency at the central frequency of 9.3 GHz. The proposed reflective element showed a

simple structure and a smooth phase curve, a minimum cross-polarized radiation field [10]. A compound unit element was proposed for the design of a reflectarray antenna operating at 28 GHz by Tahir Bashir and others. The element used a single-layer topology and integrated a variable-size phase-shifting method. The results showed that the compound element exhibited excellent characteristics in terms of a wide phase range. The proposed geometry has the potential to serve as an effective reflector for both single-beam and multi-beam reflectarray antennas in 5G applications [22]. In the same year, M. I. Abbasi et al. discussed the analysis and design of active reflectarray antennas operating in the X-band frequency range. The focus was on two types of active reflectarray designs: one utilizing PIN diodes for digital frequency switching, and the other employing liquid crystal-based substrates for analog frequency tuning. The PIN diode-based active reflectarray unit cell demonstrated a frequency tunability of 0.36 GHz and a phase range of 226° . Conversely, the liquid crystal-based design exhibited a slightly smaller frequency tunability of 0.2 GHz and a phase range of 124° . Additionally, the liquid crystal-based designs were found to have higher reflection loss and slower frequency tuning compared to the PIN diode-based active reflectarray designs [23].

In [2022], a metal-only reflectarray was introduced by Carlos Molero et al. The proposed unit cell exhibited a nearly linear phase response with a phase variation of $\pm 1^\circ$ for the orthogonal polarization. The study also investigated the reflectarray's performance under non-normal incidence and explored the frequency limitations of the unit cell. The reflectarray was capable of converting linear polarization to circular polarization [24]. The reflectarray demonstrated a simulated directivity exceeding 27 dBi [24]. In the same year, Usman Sarwar et al. presented a wide, circularly polarized reflectarray array

using a single-turn helical antenna in which the reflective element. The designed element achieved a 360° phase range [25].

Shimaa A. M. Soliman et al. in 2022 presented a reflectarray design employing elements of the shape of the pentagon. This shape was selected to convert the linearly polarized incident fields to a circular polarization. The feeder was a dipole to supply the linearly polarized wave incident on the reflectarray elements. The simulation results at 12 GHz showed an axial ratio of 2.1 dB, and a peak gain is 18 dBi [26]. In the same year, Weixiong Luo et al presented reconfigurable reflectarray, whose elements can be height-adjustable mechanically. The simulated results showed that the phase performance of the unit cell has a good linearity and exhibits broadband characteristics. The maximum phase range was found to be about 200° at a center frequency of 16 GHz. With the mechanical changes in the elevation of the elements, phase distribution among the elements of the array can be implemented and beam scanning $\pm 50^\circ$ was achieved [27].

L. Veluchamy et al. in 2023 presented simulated and experimental results of two broadband reflectarrays. The used elements were concentric square and circular rings using the basis of the Fibonacci series. The reflectarray gain bandwidth was 46.2% [28]. In the same year, E. Hedian, et al. introduced a planar reflector antenna, which consisted of metamaterial cells, different flower-like unit cells. The simulation and measurement results demonstrated that this antenna achieved a broadband and high radiation efficiency within the frequency range of 12-14 GHz [29]. In the same year, Huaiqing Zhang et al. proposed a single-layer circularly polarized reflectarray antenna with linear polarization feed [30]. The unit cell consisted of a rectangular patch and four E-shaped structures placed on the four sides. The antenna offered linear range in excess of 500° , and showed extremely low level of cross-polarization.

Experimental results achieved 3 dB bandwidth of about 38%, gain of 25.8 dB at 5.8 GHz [30]. A. Palomares-Caballero et al. in 2023 presented unit cells based on a module cell with a 3-D geometry, which allowed independent phase tuning over a wide frequency range. Phase modulation was achieved in each unit cell by adjusting the lengths of specific metal blocks within the wave propagation path. The simulation results showed a relatively linear phase response, that was maintained at oblique angles up to about 30° [31]. Ali Ali et al. focused on achieving low-divergence 3D-steered beam. The studied and simulated scenarios were normal, 2D and 3D steered beams at a frequency of 30 GHz[32].

1.4 Statement of the Research Problem

The dissertation problem statement revolves around the investigating phase characteristics of unit cell elements in a single-layer microstrip reflectarray antenna. The main goal is to achieve a phase range larger than 360° while minimizing the slope of the reflected wave phase relative to the element size. Although these two requirements seem to be in contradiction, there are some element shapes that can offer a good compromise.

1.5 Dissertation Objectives

This dissertation focuses on investigating the phase characteristics of the unit cell elements that achieve a phase range larger than 360° while minimizing the slope of the reflected wave phase with respect to the size of the elements. These characteristics are essential for achieving a wide operational bandwidth and reducing the impact of manufacturing errors. The dissertation will concentrate on the following key aspects to accomplish its objectives:

1. Examining of the operational principles of reflectarrays and analyzing the factors that impact their bandwidth.
2. Studying the characterization of the phase and amplitude responses of conventional element shapes commonly used in reflectarrays.
3. Evaluation of some proposed elements that offer favorable characteristics for reflectarray design.
4. The research methodology involves a combination of theoretical analysis and computer simulations using CST(Computer Simulation Technology) Microwave Studio (CST MWS).

1.6 Dissertation layout

This dissertation is a compilation of the studies conducted in the context of the aforementioned goals. Beyond this introductory chapter, Chapter Two examines the reflectarray antenna and the variables influencing its operation. In Chapter three, several classical and suggested elements shapes were derived through simulation using the CST microwave studio are thoroughly examined. The Fourth Chapter is an extension of the third chapter with the greatest development in the proposed forms of the unit cells that are formed of two rings. Chapter Five presents the conclusions and the future work.

CHAPTER TWO

ANALYSIS OF THE REFLECTARRAY

2.1 Introduction

Reflectarray antennas have gained considerable attention in the last decade for their properties arising from the integration of the advantages of printed arrays and high-gain parabolic reflectors. This fusion of technologies holds great promise for advancing the field of antenna systems and of high-gain communication and sensing applications. Reflectarray antennas find application in a wide range of fields, including satellite communications, contoured beam antennas that cover specified regions, and many other applications. In comparison to parabolic reflectors, reflectarrays offer a low-profile design, lightweight construction, ease of fabrication and transportation, and notably, a low cost of production due to the printing process involved [17][33][34].

This chapter provides an introduction to the key concepts and designs related to reflectarray antennas.

2.2 Definition of Reflectarray Antennas

The term "reflectarray antenna" refers to various configurations of reflective surfaces that include a set of radiating elements such as dipoles, rings, or printed patches, which reflect energy received from one or more emission sources (feeds) located in free space. It can have a flat or gently curved outer shape. The design and configuration of reflective antennas can vary widely, depending on the types of elements used, their arrangement within a mesh structure, and the feeding technology used to activate the antenna. These factors contribute to the performance of reflectarray antenna for various applications and requirements [1][33][35]. Each reflectarray element is carefully designed to

re-emit the incoming field with a precise electrical phase, enabling the formation of a flat wavefront in the distant region[1] [36]. Figure.2.1 illustrates a common configuration of a reflectarray antenna.

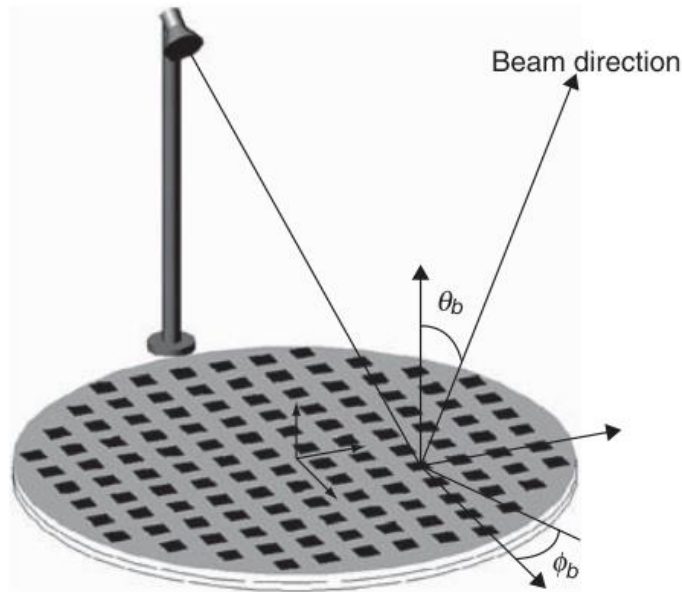


Figure 2.1 Geometry of a planar reflectarray antenna[1].

The reflectarray antenna is characterized by its flat structure, which has a simpler and more reliable folding mechanism as well as easy installation on an existing flat surface without the need to add extra volume and weight. Finally, by integrating low-loss variable phase shifters into its elements, a wide-angle electron beam scanning can be achieved. This eliminates the need for a complex, high-loss beamforming networks and/or expensive transmit/receive amplifier modules that are usually required in the typical phased arrays [1] [33] [37] [38].

2.3 Principle of Operation

Figure 2.2 demonstrates the operational principle of a reflectarray composed of a flat panel metasurface.

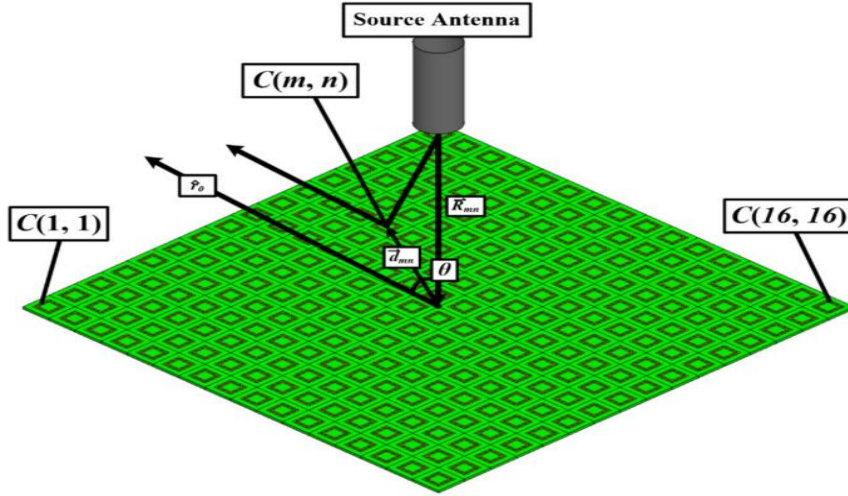


Figure 2.2. The working principle of reflectarray antenna with a planar metasurface [39].

The electromagnetic waves emitted by the source are focused towards the planar metasurface, which acts as a reflector. The metasurface consists of an array of elements, which are designed to modify the phase of the incident waves. By introducing specific phase shifts, the unit cells enable the waves to propagate in the desired direction. When the reflector is situated at the XY-plane, the array factor $AF(\theta, \phi)$ of an $M \times N$ unit-cell flat-panel metasurface reflector array can be expressed by the following equations [1]:

$$AF(\theta, \phi) = \sum_{m=0}^{M-1} \sum_{n=0}^{N-1} A_{mn} e^{jk_0(md_x u + md_y v)} \dots\dots\dots (2.1)$$

$$\begin{cases} u = \sin \theta \cos \phi + \beta_x \\ v = \sin \theta \sin \phi + \beta_y \end{cases} \dots\dots\dots (2.2)$$

In the equations, A_{mn} represents the complex excitations for elements at the (m, n) position $C(m, n)$ and k_0 denote the wavenumber in free space. β_x and β_y represent the progressive phase shifts between neighboring elements along the two directions x and y . To achieve the desired focusing of reflected waves in the direction (θ_r, ϕ_r) , the progressive phase shifts can be determined using Eq.(2.3). The parameters dx and dy represent the periodicity of element in the directions x and y , respectively[39].

$$\begin{cases} \beta_x = -\sin \theta_0 \cos \theta_0 \\ \beta_y = -\sin \theta_0 \sin \phi_0 \end{cases} \dots\dots\dots (2.3)$$

The phase shift on the unit cell $(\Delta\phi_{mn})$ at position (m, n) , denoted as $C(m, n)$, is determined based on the period of the unit cell (bx and by). By adjusting the phase of the incident waves using the element, the angle of reflection can be controlled effectively. The phase of the reflected wave at the element $C(m, n)$ can be determined by adding the phase of the incident wave to the relative phase shift imposed by the unit cell. Equation (2.4) can be used to calculate the desired phase shift distribution, $\Delta\phi$ that is necessary to achieve a specific reflection angle.

$$\Delta\phi_{mn} = 2N\pi + k_0(|\vec{R}_{mn}| - d_{mn} \cdot \hat{r}_0) \quad (N = 0, 1, 2, \dots) \dots\dots\dots (2.4)$$

In Eq.(2.4), \vec{R}_{mn} represents the location vector from the feed antenna to the element $C(m, n)$, \vec{d}_{mn} represents the location vector from the center of the surface reflector to $C(m, n)$, and \hat{r}_0 is the unit vector pointing towards the reflected wave propagation direction [39].

2.4 Analysis of Reflectarray Elements

The analysis of the reflectarray element can be conducted using similar techniques employed for classic microstrip antennas. The configuration of microstrip antennas, as shown in Fig. 2.3 comprises an extremely thin metallic patch placed a small fraction of a wavelength ($h \ll \lambda_0$, normally $0.003\lambda_0 \leq h \leq 0.05\lambda_0$, λ_0 is the wavelength in free space) top ground plane. For a rectangular elements, the length L of the element is normally $\lambda_0/3 < L < \lambda_0/2$. The radiating patch and the ground plane are separated by a substrate (dielectric layer). There is a wide range of substrate materials, with their dielectric constants in the range of $2.2 \leq \epsilon_r \leq 12$. The most desirable substrates for achieving optimal antenna performance are thick ones with a lower dielectric constant, as they offer improved efficiency and larger bandwidth [38].

Due to the finite size of the patch (along its length L and width W), the fields at the edges of the patch experience fringing. This is illustrated along the length in Fig .2.3b and Fig.2.3c. The degree of fringing is influenced by the size of the patch and thickness of the substrate. As can be seen, the lines of electric field predominantly reside within the substrate, while some portions extend into the air. Thus, fringing causes the microstrip patch to appear wider electrically than its physical dimensions. Since waves propagate through both the substrate and the air, an effective dielectric constant ϵ_{reff} as an additional term is introduced to accommodate the effects of wave propagation in the line and fringing [38]. It will be explained later in chapter three.

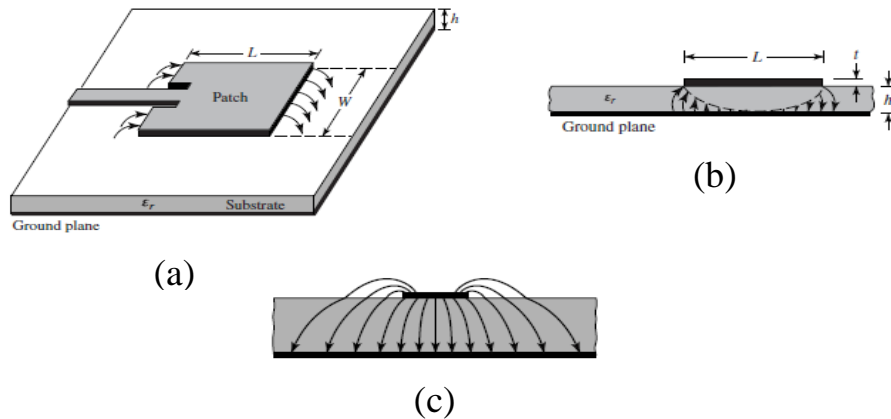


Figure 2.3. Classic Microstrip antenna; (a) Microstrip antenna top view (b) side view, (c) Electric field line[38].

2.5 The Phase Tuning Approach

Selecting an appropriate phase tuning methodology is an essential and pivotal step in the design process. This enables the reflectarray elements to attain the desired range of phase adjustment (phase tuning), which is crucial for optimizing the antenna's performance[40].

The design process of the reflectarray starts with the determination of the required phase to be supplied by each of the array elements. The second step is to choose the method for the adjustment of the compensating phases of the elements. This choice directly affects the radiation characteristics of the antenna. There are several achievable ways to modify the phase of the reflected wave from the elements, and they are usually classified into three main categories [41]:

1. Elements connected time to delay lines.
2. Elements of variable sizes.
3. Rotation of the elements.

2.5.1 Elements Connected to Time Delay Lines

In this structure, a typical reflectarray element, such as a patch, captures the electromagnetic wave emitted by the source feed. The element then transforms the captured wave into a guided wave, which travels across a transmission line. This transmission line is commonly a microstrip line and has a specific length [35][42]. To terminate the transmission line, it can either be connected to an open or a short circuit. The signal bounces off from this termination point on the transmission line and is subsequently re-emitted by the reflectarray element. Figure. 2.4a depicts a schematic representation of this kind of element, with attached phase time delay lines of two various lengths[43]. Many researches have focused on this technique in their designs [44]–[46].

2.5.2 Elements of Variable Sizes

In this method, the phase tuning of the reflectarray elements is accomplished by modifying its physical dimensions. By adjusting the length of a resonant element, it is possible to change the resonant frequency of the antenna. The variable size approach operates on the principle that resonating element of varying dimensions will yield different reflected phases. By modifying the size of the element as shown in Fig.2.4b, the desired phase shift can be achieved, allowing for precise control of the antenna's radiation characteristics. This innovative technique was initially introduced in [47]. The variable element size approach, commonly utilizing square or circular patch geometry, offers a wide range of element geometries [13]. Another approach is to employ different-sized patches, dipoles, or rings, as a result, these elements can generate various phases that compensate for the varying feed path delays as displayed in Fig.2.4c [1].

2.5.3 Rotation of The Elements

The element rotation method is an ingenious phase tuning method that is specifically applicable to circularly polarized (CP) antenna designs. It operates on the principle of turning a CP antenna element around its point of origin by an angle of ψ degrees will result in a corresponding change in the radiated phase by the same amount. The phase can be either advanced or delayed depending on the direction of rotation. This technique allows for precise control of the radiated phase and enables the fine-tuning of the antenna's performance can be seen in Fig 2.4d [36].

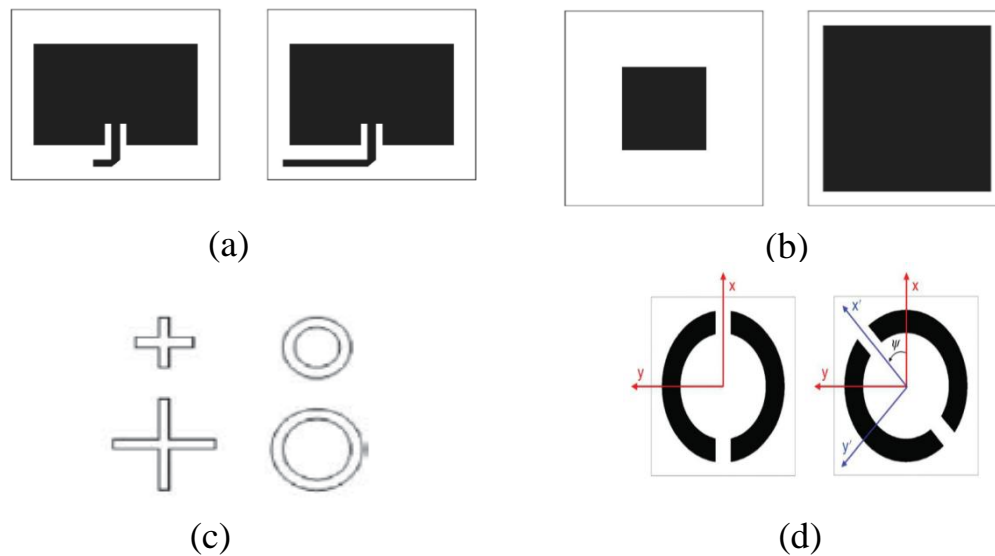


Figure 2.4. Multiformal of reflectarray elements; (a) phase time delay lines, (b) Different types of variable size square elements, (c) variable size dipoles or loops, (d) A CP reflectarray patch with different types, (left) shows the patch with 0° phase shift and (right) the ψ rotated patch with 2ψ phase shift [1][36].

2.6 Specifications of The Reflectarray

The specifications of reflectarray are determined by the description of four factors: bandwidth, efficiency, phase range, and phase slope.

2.6.1 Bandwidth

Despite its many advantages, the reflectarray antenna does have a notable drawback. Its inherent characteristic of narrow bandwidth is a limitation [4][48] [49], typically not exceeding ten percent, which depends on factors such as element design, aperture size, and the distance to the focal point. The reflectarray's bandwidth limitation can be attributed to several factors. Firstly, there is a need to compensate for the phase discrepancy between the originally curved wavefront launched by the feed and the desired planar wavefront. Secondly, typical microstrip antenna elements have limited achievable phase ranges [1]. Other factors have been discovered such as, the compensation phase is usually truncated to the 360° in each element of the array and variation phase with frequency. Recent studies have indicated that the first factor exerts the most significant impact on the gain of the reflectarray [50].

2.6.1a Bandwidth Bounded by Varied Spatial Phase Delay

A significant constraining factor in reflectarrays is the variation in spatial phase delay. The easiest way to describe the varied spatial phase delay is referring to Fig.2.5. The varied spatial phase delay, denoted as ΔS , refers to the phase discrepancy between the two paths S1 and S2 from the feed antenna to the position of the elements [51]. The path difference ΔS can have a magnitude that is several multiples of the wavelength (λ). It can be expressed as $\Delta S = (N + d) \lambda$ where d is a fraction of the free-space wavelength, and N is an integer [1].

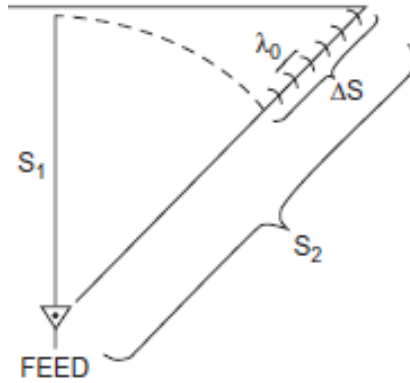


Figure 2.5 .The variation in spatial phase delay of the reflectarray elements[1].

Taking into account the coordinate system described in Fig.2.1, the progressive phase distribution on the surface of the reflectarray results in the generation of a beam directed towards (θ_b, ϕ_b) , as known from array theory, is expressed as[1].

$$\phi(x_i, y_i) = -k_0 \sin \phi_b \cos \phi_b x_i - k_0 \sin \theta_b \sin \phi_b y_i \dots\dots(2.5)$$

where k_0 is the propagation constant in vacuum, and (x_i, y_i) the coordinates of element i . The phase at each reflectarray element is determined by the sum of the phase of the incident field, resulting from propagation from the feed, and the phase shift introduced by each cell, as

$$\phi(x_i, y_i) = -k_0 d_i + \phi_R(x_i, y_i) \dots\dots\dots (2.6)$$

where $\phi_R(x_i, y_i)$ is the phase of the reflection coefficient, or phase shift, for element i , d_i is the distance from the phase center of the feed to the cell. From expressions (2.5) and (2.6), the phase shift needed at each element can be derived using the following equation:

$$\phi_R(x_i, y_i) = k_0(d_i - (x_i \cos \phi_b + y_i \sin \phi_b) \sin \theta_b) \dots\dots (2.7)$$

This phase difference has to be supplied by the element of the reflectarray for proper compensation[1]. The required phase for compensation should stay valid as the frequency of operation is changed, and eventually the violation of this leads to reduction in the gain of the reflectarray. The following formula was derived by [50] .

$$\%BW = \frac{15}{f_0 F} \left[\frac{1}{\sqrt{1+0.25(F/D)^2-1}} \right] \dots \dots \dots (2.8)$$

to estimate the bandwidth the reflectarray for certain F/D ratio where F is the focal distance and D is the diameter of the reflectarray. In this equation the units of center frequency is in GHz, and meters for D [50].

2.6.1b Bandwidth Bounded by Element

The bandwidth of a conventional microstrip patch element is typically around 3 to 5 percent. In order to achieve a wider bandwidth, various techniques have been utilized with success. These include using a thickset substrate for the patch, utilizing subarray elements in a sequential rotation and packing multiple patches. These methods have allowed for bandwidths exceeding 15 percent to be achieved [1].

2.6.2 Efficiency of The Reflectarray Antenna.

The lower gain performance of a this antenna can result in reduced efficiency. Therefore, achieving an efficiency of 50% or higher is generally considered as high efficiency for a reflectarray antenna. Improved antenna efficiency is closely linked to enhanced gain performance. One straightforward approach to increase antenna gain is by increasing the physical aperture size. However, it is important to ensure that the feed is properly positioned to avoid additional illumination or loss of extension, as this can hinder efficient operation of the reflectarray. This indicates that the maximum reflectarray

antenna efficiency can be attained by minimizing losses. Consequently, the improvement in reflecting the antenna efficiency can be evaluated by selecting an appropriate unit cell element [40].

2.6.3 Phase Range and Slope

One of the crucial considerations in the design of microstrip reflectarrays is the achieving a wide range of phase variation and a gradual change in the phase (phase slope) with respect to the variable size of the reflectarray element. A lower slope in the response of phase in relation to the element dimensions leads to greater tolerance for manufacturing errors. Consequently, a broader phase range provides the planner with increased suppleness in choosing appropriate sizes of element to achieve a desired phase value. It's important to acknowledge that the bounded phasing range of a reflectarray has two negative impacts on its operation. Firstly, some requisite phase values may need to be approximate to available ones. Secondly, truncating the required phase shift to the value of 360° range can lead to degradation in gain and bandwidth. Previous studies have explored different shapes of element, such as circular, elliptical, square, and combined shapes for reflectarray design. The main criteria for these elements are to provide a reflection phase range of at least 360° and a slow slope with frequency. These parameters significantly affect the bandwidth of the reflectarray in relation to the elements [18][52]. However, using a thicker substrate to reduce the phase slope can further limit the already inadequate phase range. To overcome this, new phasing elements in the form of variable size stacked patches have been utilized to achieve a phase range not less than 360° and a small phase slope [18].

2.7 Considerations in the Selecting of Elements

The characterization of elements plays a crucial role in the design of a reflectarray. The effectiveness of the reflectarray in scattering the signal from the feed and forming a desirable far field beam depends heavily on the optimization of element design [37]. There are three key parameters that are crucial in design and the selection of elements: Reflection Phase of element, Beamwidth of element, Spacing of element. Each of these parameters is discussed individually below.

2.7.1 Reflection Phase of the Element

The conventional design approach for a microstrip reflectarray antenna involves several key steps. Firstly, an analysis of the phase characteristics of the reflection elements is performed where the accurate calibration of phase changes with respect to element variations, such as patch size or delay line length, is crucial [53]. One commonly used technique for phase calibration is the infinite-array approach, which considers the local mutual coupling effect caused by neighboring elements. The phase-versus-element-change characteristics commonly display a nonlinear relationship, often resulting in an S-shaped curve. Figure 2.6 provides an illustration of this curve. Antenna designers aim to minimize the slope at the curve's center to avoid excessive sensitivity of the phase change to element modifications. Steep curves can pose challenges related to element changes and fabrication tolerances, particularly at higher microwave frequencies [1].

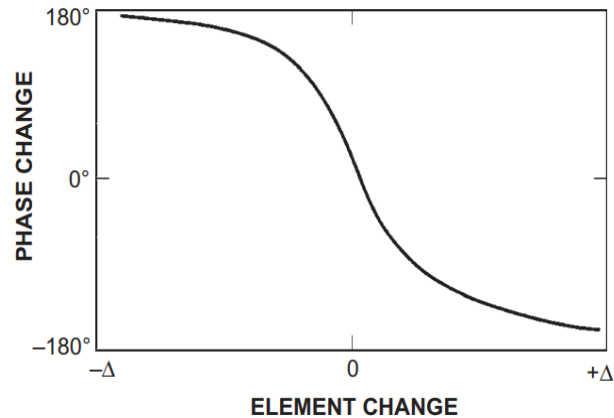


Figure 2.6. S-shaped graph depicting element phase changes according to variations in the element [1].

Ensuring an adequate range of element variation is crucial when selecting elements. It is important to guarantee that the chosen elements can produce a phase change of at least $\pm 180^\circ$. This requirement ensures that the reflectarray system can achieve the desired beamforming capabilities and fulfill its functional objectives effectively [1].

2.7.2 Beamwidth of the Element

In addition to phase, the beamwidth of the element in reflectarray is an essential design parameter. To adequately reflect incident signals, it is necessary to have a broader element beamwidth that can capture and reflect signals from the edges of the reflectarray [40]. In order to accommodate a wide range of incident angles from the feed, the element beam width needs to be suitably correlated with the reflectarray's F/D ratio. For instance, consider a reflectarray element with a narrow beamwidth achieved by using Vivaldi radiators, horns, or patches with thicker substrates, along with a small F/D ratio as shown in Fig 2.7. In this case, the elements positioned close to the edge of the reflectarray it will not effectively capture energy from the feed. Conversely, if an element in the reflectarray has an excessively wide beam and lower gain, it

can potentially impact the overall performance of the reflectarray, leading to a slightly diminished antenna gain. The gain of the array is mainly determined by the aperture size, the gain of individual elements.

Ideally, it would be beneficial to have elements positioned near the center of the reflectarray with a higher gain and narrow beamwidth, while the array elements near the edge have a broader beamwidth. This arrangement would optimize the performance of the reflectarray, maximizing the antenna gain. However, implementing such a design could introduce complexities and increased manufacturing costs for the antenna. Striking the right balance between beamwidth and gain distribution is important to optimize the reflectarray's performance while considering practical constraints[1].

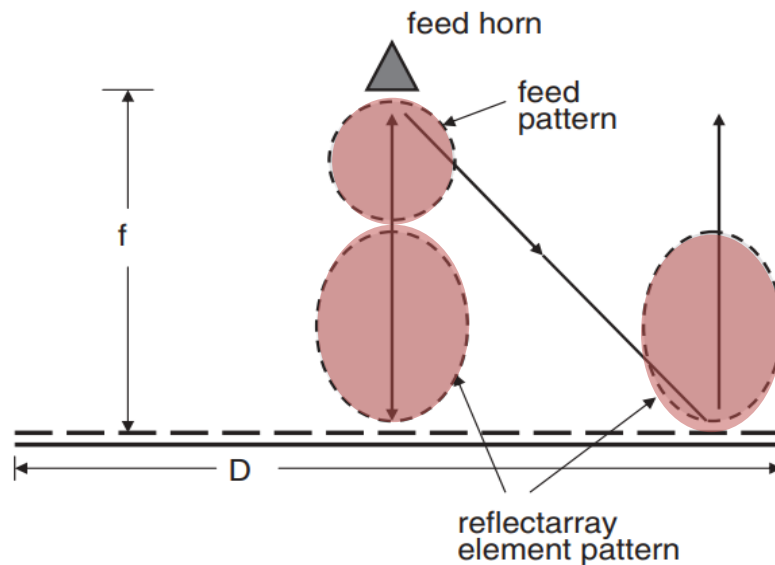


Figure 2.7. Reflectarray element pattern effect [1].

2.7.3 Spacing of the Elements

To prevent the occurrence of grating lobes in the radiation pattern, it is crucial to maintain appropriate spacing between adjacent elements in a reflectarray. When dealing with waves incident and radiated in the broadside direction, the spacing of element can be comparatively large [38], typically exceeding 0.9 times the wavelength (represented by λ). However, as we move towards the edge region of the reflectarray, the angles of incidence of the waves from the feed horn can become larger. In such cases, the spacing of element requirement becomes more stringent and should be determined by the conventional array equation:

$$d'/\lambda \leq 1/(1 + \sin \theta) \dots \dots \dots (2.9)$$

Here, d' represents the spacing of element, where λ is the wavelength of the frequency, and θ represents the maximum desired angle of wave incidence. This equation helps ensure that the spacing between elements is sufficient to avoid grating lobes [1].

2.8 Various Types of Reflectarray Elements

A reflectarray utilizes a Semi-periodic arrangement of elements to achieve the desired phase transformation within an array environment. These elements can be in the form of printed elements or volumetric structures like patches or dielectric resonators [37][54], respectively. Printed elements offer simplicity in terms of fabrication, but there exists a diverse range of reflectarray cell elements that have been developed to meet various requirements, including mechanical robustness, fabrication accuracy, bandwidth, polarization, and more. In this context, different kinds of resonant cell elements will be discussed to address these specific needs and considerations [33].

2.8.1 Single Layer Elements

The concept of manipulating the resonant sizes of microstrip patch antennas to control the phase of the reflected wave was initially documented for crossed dipoles in [55], and for rectangular elements in [47]. Developments continued using other forms such as single layer square or circular element. These forms are widely used as a form of element reflectarray. Figure 2.8 shows a comparison of performance between the square and circular element shapes [13]. Two different substrates are considered, (the first has a dielectric constant $\epsilon_r = 3.2$ and thickness $h = 1.57$ while the second one has $\epsilon_r = 2.2$ and $h = 3.175$). [13].

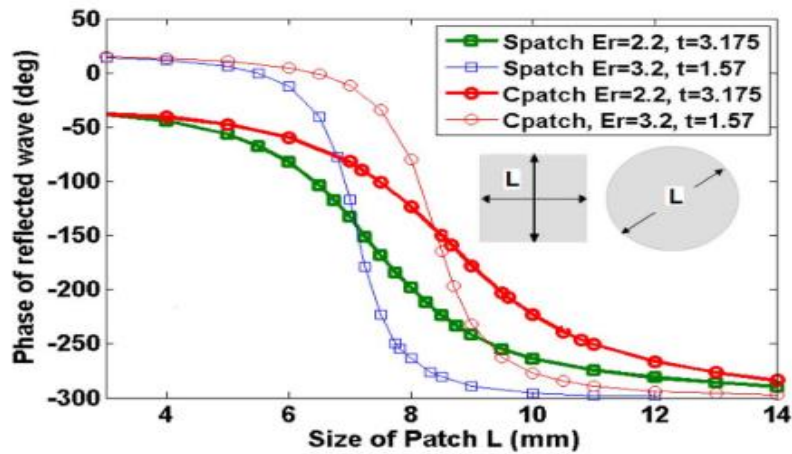


Figure 2.8. The phase variations of square and circular patches on two different kinds of substrates [13].

When comparing the results depicted in Fig. 2.7 for square and circular patches, it is evident that both shapes provide a similar phase range for the two dielectric substrates. However, the circular patch consistently exhibits a smaller phase gradient (slope). Additionally, the figure also reveals that increasing the substrate thickness and decreasing the dielectric constant lead to a less slope for two patch types. However, achieving lower slopes comes at the cost of a

smaller phase range. Specifically, the phase range for the slimmer substrate is approximately 305° , whereas for the thicker substrate, it is around 250° [13]. Another use of the square element is in [52], where sections of triangular, square, and semicircular shapes were incorporated into the four sides of a square patch. The element compositions in the initial group were created by appending isosceles triangles with a vertex angle θ to the four sides of a square patch as shown in Fig.2.9.

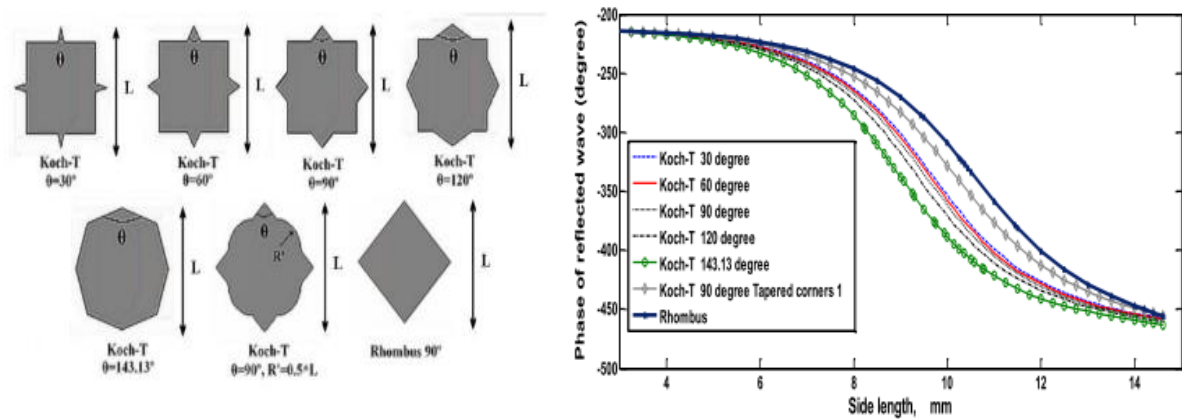
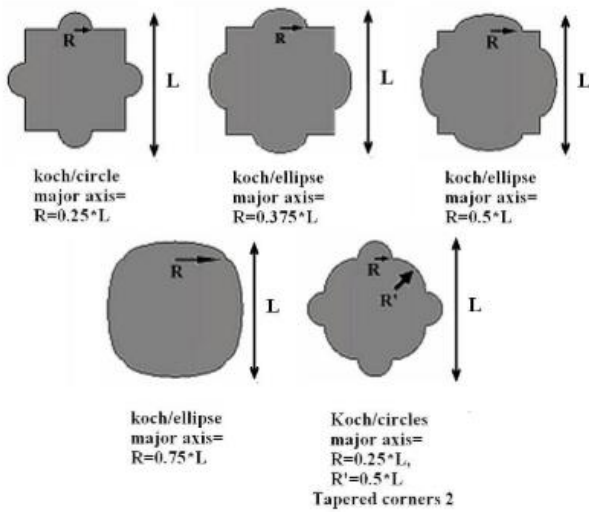
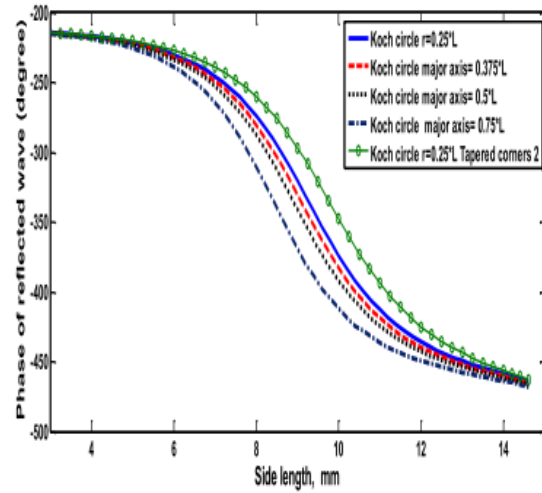


Figure 2.9 .Element of reflectarray; (left) shapes of the analyzed first group of derived element shapes ,(right) Fluctuation of the reflection phase with side length L [52].

As the angle θ of the added triangle increases, the phase slope shows a slight increase, while the phase changes with frequency slightly decreases. Additionally, the form featuring tapered corners shows the least steep changes in relation to both frequency and size. The rhombus shape demonstrates a competitive response and distinctive characteristics. The second group has shapes, illustrated in Fig.2.10, feature circular or elliptical sectors of varying radius as the added portions [52].



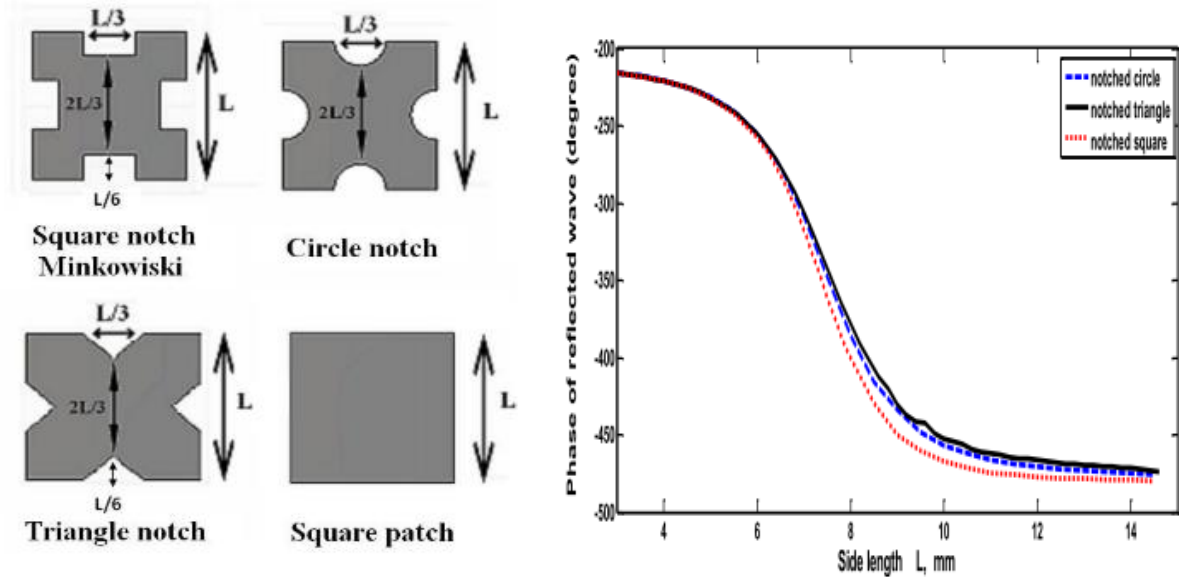
(a)



(b)

Figure 2.10. Element of reflectarray ;(a) Shapes of the analyzed second group of elements shapes, (b) Fluctuation of the reflection phase with side length L [52].

From the observation of Fig. 2.10b, it is apparent that an increase in the radius of the added portion leads to a slight increase in the phase slope, while phase change with frequency to a small extent decreases. The shape of tapered corners exhibits relatively small values for two slopes in relation to frequency and size. It is worth noting that all the shapes examined in that study have phase ranges that are less than 300. The elements in the third group are characterized by notched patches, where sections are removed from the borders of the square patch, as depicted in the illustration Fig.2.11[52].



(a) (b)
 Figure 2.11 .Element of reflectarray ;(a)Shape of the third group of elements,(b) Fluctuation of the reflection phase with length L [52].

The results obtained from the third group of shapes are larger than those from the first two groups. Furthermore, in contrast to the first two groups, these shapes exhibit larger phase ranges, although they are still less than 300° [52]. Many developments have considered the shape of the square and circle patches as [56] , where the element was composed of a square slot positioned at the center of the unit cell, accompanied by four L -slots. Also [57][58].

2.8.2 Multilayer Elements

One approach to achieve a smoother phase behavior with respect to length involves increasing thickness of the substrate. However, this leads to a significant reduction in the total phase range. It is crucial to consider that for the create of a reflectarray, it is necessary to have phase shift values covering a range of 360° , which cannot be achieved with a thickness substrate alone. To address this, one potential solution is to stack two or more array layers, as

illustrated in Fig.2.12. Each layer operates as a resonant circuit., with the phase of the reflected field varying in a similar manner to that of a single layer. However, through the utilization of multiple layers, the phase shift can attain values several magnitudes larger than 360° . Thus, by increasing the isolation between the layers and the isolation between the last layer and the metallic plane, a smoother and more linear phase behavior with respect to patch size can be achieved, while still maintaining a phase shift range greater than 360° . Figure 2.12 shows sample of the multilayer structure utilizing rectangular patches [1] [38].

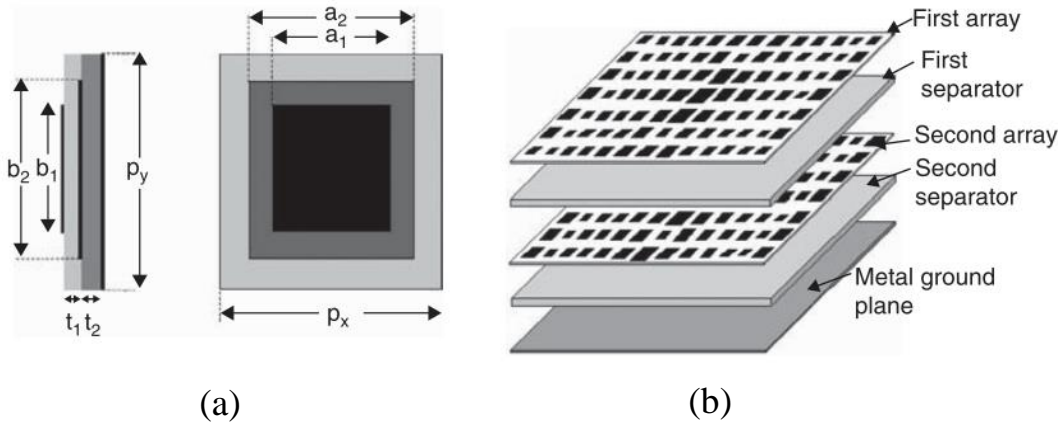


Figure 2.12 .Double layer reflectarray; (a) Unite cell, (b) multiple layers [1]

In[59], a multi-layered structure with circular spots was investigated. The structural unit comprised of two circular conductive elements positioned in two FR4 dielectric slabs stacked on top of each other, with a dielectric constant ($\epsilon_r = 4.4$). The upper substrate had a height (h_T) of 3 mm, whereas the lower substrate had a height (h_B) of 1.5 mm. The stacked patches were supported by a ground plane. The diameter of the lower circular patch was indicated as d_B , while the diameter of the top patch was 0.75 times d_B ($d_T = 0.75 d_B$). The unit cell had dimensions $dx = dy = 17.65$ mm. The phase of the reflection coefficient for the unit cell was plotted in Fig.2.13 against the size of the lower circular

patch. The results demonstrated that by varying the size of the lower patch between 5 and 14 mm, varied the phase of the reflected field within a range of 0° to -500° . The use of a stacked structure was necessary to achieve such a wide phase range, as a single-layer structure would not suffice. This extensive phase control range proved beneficial for achieving the desired phase distribution in various scenarios for the proposed reflectarray antennas

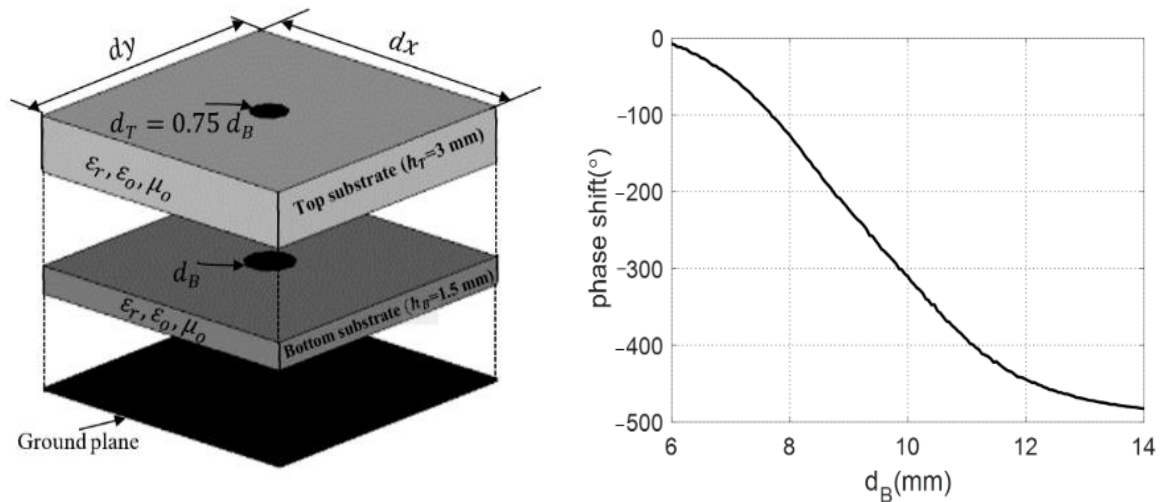


Figure 2.13. Two layer reflectarray; (left) unite cell, (right) Reflection phase of the unit cell [1].

The multi-layer variable dimensions patch reflectarray poses a challenge in terms of manufacturing, as each layer needs to be produced individually and carefully aligned and bonded to prevent any air gaps. This requirement results in higher manufacturing costs. To overcome this, there has been a growing interest in exploring new arrangements of single layer for reflectarrays that can give an expanded phase range and increased bandwidth, researchers in [12] [55] [60][61] suggested employing "loop" elements to enhance the phase range and bandwidth of a single layer reflectarray. Their research showcased notable improvements, such as a phasing range extension of more than 600° and an expanded bandwidth of 9% (1-dB gain reduction). These findings highlight the

potential of employed loop cell elements to enhance the performance of single-layer printed reflectarrays.

2.8.3 Single Layer Ring and Double Ring Elements

Reflectarray antennas typically have a limited bandwidth, usually around 4%, which is lower compared to conventional reflector technology. One method to enhance the bandwidth is to use a thicker substrate for printing the reflectarray element, the slope of the phase response is effectively reduced. However, this approach results in a smaller achievable phase range, which negatively affects the gain and overall radiation efficiency. To overcome the bandwidth limitations of single layer reflectarrays, multi-layer structures have been proposed. However, these structures bring their own drawbacks, including increased weight, loss and complexity of manufacturing [55]. A simple architecture addresses these challenges as shown in Fig.2.14. The suggested architecture manages the reflection phase by modifying the length of a double crossed loop unit cell. This control enhances the bandwidth of the reflectarrays while preserving the ease of manufacturing associated with a single layer antenna [55].

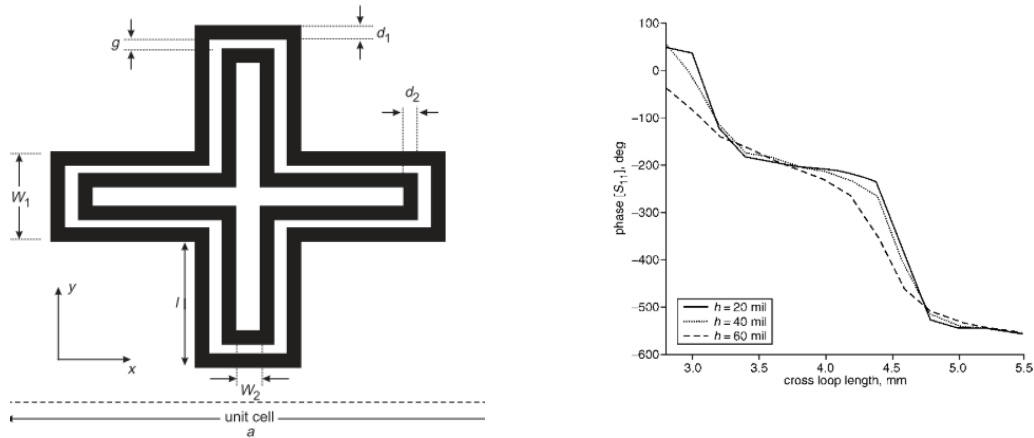


Figure 2.14; Ring element reflectarray,(left) Double cross loop element different arms, (right) Reflection phase response of the unit cell [55].

Other work dealt with ring [62] and also in [13] comparison was made between square and circular rings with different substrate as shown in Fig.2.15. It can be observed that the phase range is nearly 360° for the substrate $\epsilon_r=3.2$ with a thickness $h=1.57$ mm. The circular ring displays a gentler slope in comparison to the square ring. Alterations such as increasing the substrate thickness and decreasing the dielectric constant led to reduced slopes for two ring shapes. Nevertheless, this reduction in slopes also corresponds to a decrease in the phase range. As illustrated in Fig. 2.15, the phase range is reduced from approximately 350° to 300° . The phase results obtained for a unit cell, which consists of either a single patch or a square/circular ring on a substrate for single layer, demonstrate the challenge of achieving both a small phase slope and a phase range of 360° . To address this issue, uniplanar phasing elements in the shape of double rings are proposed as shown in Fig.2.16.

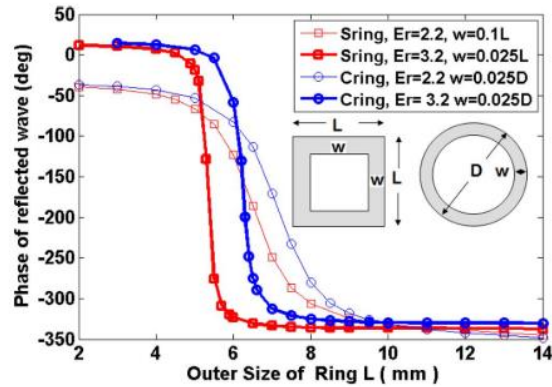


Figure 2.15; Ring element reflectarray[13].

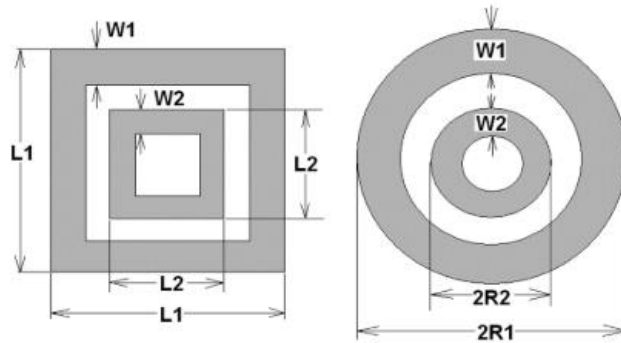


Figure 2.16. Double ring element reflectarray [13].

The results in Fig.2.17 indicate that the phase range achieved with the double square ring is imminent 700° . By utilizing a thicker substrate with a reduced dielectric constant, the slope of the phase response is decreased, resulting in a more linear behavior. However, this comes at the expense of a slightly reduced phase range, which is imminent 650° . The circular rings have slopes which are less steep compared to their square counterparts for both types of substrates. The same comparison was in [62].

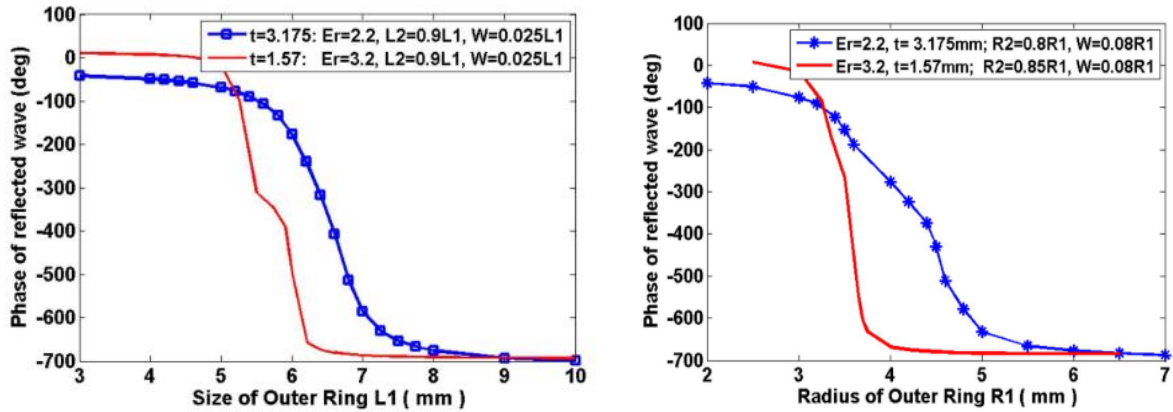


Figure 2.17. Phase responses (left) Phase responses of double rings for square, (right) Phase responses of double rings for circular [13].

In [63], the design entailed a reflectarray single layer employing double elliptical ring. It is specifically designed to operate at a frequency of 11.5 GHz. The phasing of elements are positioned in a square lattice with a periodicity of 15mm, which corresponds to approximately 0.6 wavelengths (λ) at 11.5 GHz. The reflectarray arrangement is depicted in Fig.2.18. The elliptical rings are on a thin dielectric substrate with a relative permittivity (ϵ_r) of 1.96 and with thick of 0.254 mm. This substrate is bolstered by a thick foam with an ϵ_r of 1.06 and a thickness of 6 mm. A ground plane is also included in the design. The phasing elements incorporated in this design provide a phase variation range that surpasses the necessary 360° . Additionally, they exhibit a slower slope compared to conventional elements [63].

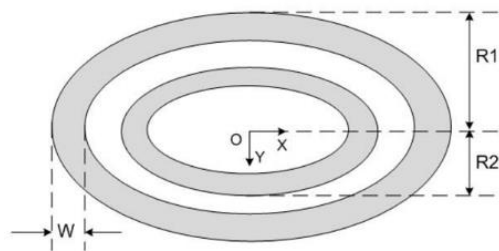


Figure 2.18. Configuration of the double ring reflectarray element [63].

CHAPTER THREE

INVESTIGATION INTO PROPOSED UNIT CELLS FOR REFLECTARRAYS

3.1 Introduction

Various element shapes were suggested to use as unit cells for the reflectarrays. The element should provide the desired phase range of not less than 360° , as well as having a linear phase variation with either frequency and the size of the element. In this chapter, a few shapes are suggested for the unit cell elements aiming to search for better performance. Therefore, the following sections present the results of the investigation of the proposed elements.

3.2 Simulation Framework

To assess the performance of the proposed elements, computer simulations were conducted using CST Microwave Studio 2016 (CST MWS). This is a leading software suite in the field of electromagnetic simulation and analysis. It provides engineers and researchers with advanced tools for modeling, simulating, and optimizing various electromagnetic phenomena. It allows to use the virtual prototyping, optimizing device performance, reducing the number of physical prototypes required, and mitigating risks related to test failures.

3.2.1 Overview of the Waveguide Simulator (WGS)

In this approach of analyzing the reflectarray, the array is assumed to consist of a very large number of similar elements, or approximately an infinite array. Then the analysis is applied to one of the similar elements using the Waveguide Simulator (WGS) of the CST software. This is an effective method

for simulating the performance of antenna elements within an array configuration. It is especially useful for analyzing periodic structures like array antennas. By modeling the array elements as a unit cell within a periodic structure, this technique takes advantage of the periodicity of the array, streamlining the simulation process. Rather than simulating the entire array, only a single unit cell is simulated, representing a small portion that exhibits similar characteristics when repeated periodically. Implementing the WGS approach significantly reduces computational resources and simulation time compared to simulating the entire array. This is particularly beneficial for large antenna arrays, where simulating the complete structure would be impractical due to size and computational constraints. The WGS technique has found widespread application in the design and analysis of various array antennas, including planar microstrip arrays, reflectarray antennas, and phased array antennas.

Figure 3.1 depicts a commonly used method known as the H-wall waveguide simulator, also referred to as a parallel-plate waveguide simulator. In this setup, the waveguide's top and bottom surfaces function as electric conducting walls, while the right and left walls act as magnetic field walls. When vertically polarized waves enter the waveguide, they encounter the element positioned at the end of the waveguide in the broadside direction. These waves are then scattered back in the same broadside direction, carrying amplitude and phase information. In order to obtain comprehensive data, it is necessary to capture a second set of amplitude and phase information. This involves introducing a 90° phase shift to the incoming wave. This procedure should be repeated for various element changes until a complete 360° rotation is achieved [1][38].

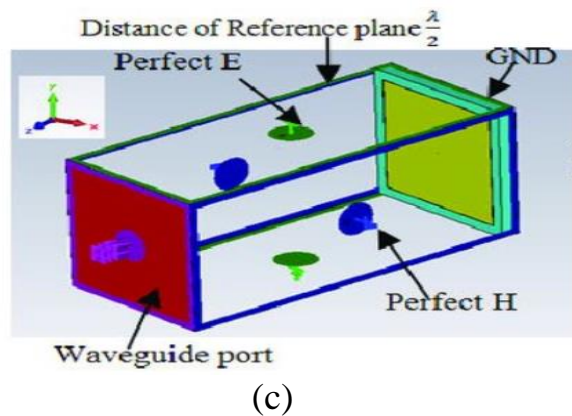
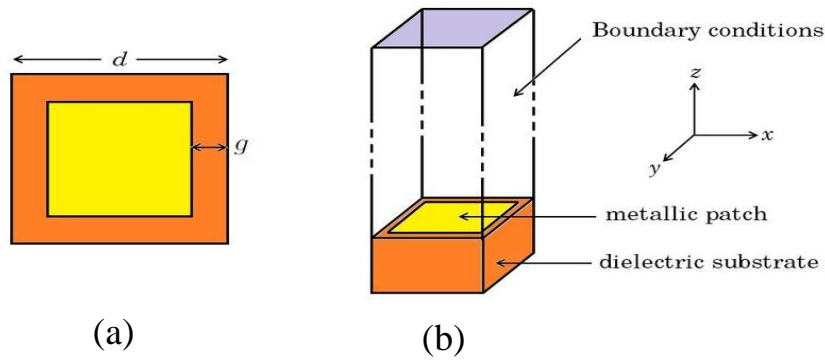


Figure 3.1. Waveguide Simulator (WGS); (a) Unit cell, (b) Boundary conditions [64], (c) H-wall waveguide simulator [65].

3.2. 2 The Infinite-array approach

Using the WGS the parameters (magnitude and phase) of the reflected wave can be determined. Thus for any element size, the reflection coefficient can be characterized by these two values (magnitude and phase). Then a table that relates these two values to the size of the investigated element can be formulated.

Similarly, the magnitude and phase of the reflected wave can be determined for each frequency of operation leading to another table. This process was termed as a calibration process. The calibration process for the phase change and element change (such as patch size and delay line length)

should be done accurately, so that it will result in designs leading to better and more accurate performance. One popular method for phase calibration is to utilize the infinite-array approach. When dealing with reflectarrays that consist of a large number of elements, the infinite array model can be employed using Floquet's theorem. This approach allows the analysis to be simplified to just a single periodic cell. Additionally, this technique offers accurate predictions for each individual element of the array by automatically considering the mutual coupling effect. Instead, the infinite-array approach assumes that all surrounding elements are identical and employs periodic solutions using Floquet modes [1]. An infinite array approach can be simulated using a mathematical waveguide simulator [4].

3.3 Considerations for the Design of Element Shapes

In this chapter, a few shapes of elements were examined and their performances were compared to determine the shape that provides the required results (adequate phase range, low slope). To ensure a fair comparison, the following factors were taken into consideration:

- 1-All elements utilize the same substrate type and thickness.
- 2-The element shapes were simulated using different bands of frequency for the reason that the response region differs.
- 3-The direction of the electric field of the incident wave, at the input of the WGS, was set into two cases with respect to the element. In the first case, the direction of the applied electric field was parallel to the width, with the boundary conditions:
at X_{min} ; $E_t=0$, at X_{max} ; $E_t=0$, at Y_{min} ; $H_t=0$, at Y_{max} ; $H_t=0$,
as illustrated in Fig.3.2a.

In the second case, the direction of the applied electric field was normal to the width, with the boundary conditions:

(at X_{min} ; $H_t=0$, at X_{max} ; $H_t=0$, at Y_{min} ; $E_t=0$, at Y_{max} ; $E_t=0$), As illustrated in Fig. 3.2b.

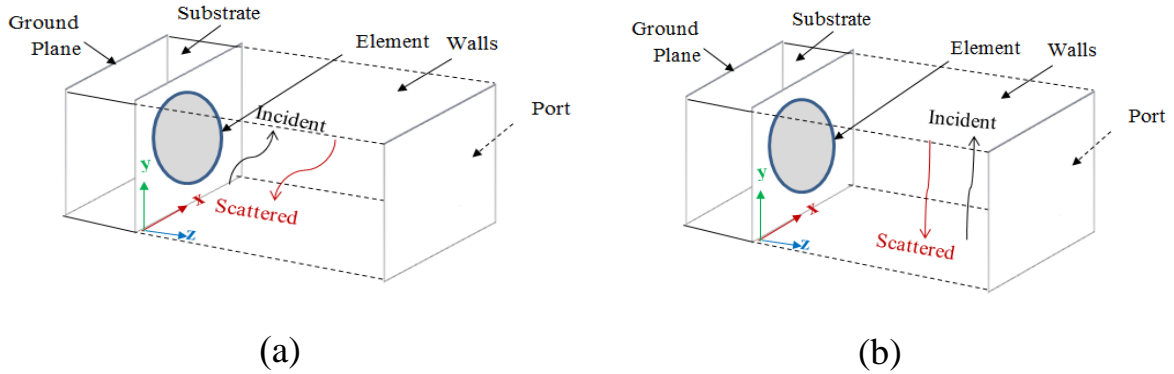


Figure 3.2. Orientation of the electric field of the incident wave with respect to the array element; (a) the E-field is parallel to the width, (b) the E-field is normal to the width.

3.4 Bowtie Element as a Unit Cell

The bowtie antenna has good performance in transmission and reception, as it offers a large bandwidth compared to other types. Many researchers conducted analyses on various bowtie shapes with the aim of using them as antennas of one element [66]-[68]. Some developed forms of a bowtie have been studied as possible elements of reflectarrays antennas, comparing them with classical ones. The study included the following groups where each group consists of the classical form first along with the developed one, comparing them in terms of phase range and slope in order to investigate and determine the optimal element. Therefore, this section proposes the use of the bowtie shape as a unit cell element for the design of reflectarrays. The bowtie shape has three main parameters namely; width ($2a$), height (b), and angle (θ) of the tip of the

two triangles, as shown in Fig.3.3. These can be considered as design parameters that can be manipulated to achieve the desired performance. The effects of these parameters are investigated in the following sections. The values of mentioned parameters will determine the angle of the tip of the two triangles. An example of the bowtie antenna as an element for the reflectarray is shown in Fig.3.3. In reflectarray design, the elements are backed by a conducting ground plane as the reflectarray has to work as a reflector. The space between the bowtie element and ground plane is filled with an FR4 substrate having a relative dielectric constant $\epsilon_r = 4.3$ loss tangent $\tan\delta = 0.025$, and height $h = 3.2\text{mm}$. This element was modeled using the CST Microwave suite with WGS, and the obtained results are discussed in the following sections. Fig. 3.3 shows the general unit cell simulation, where the element is placed in the XY-plane, and the incident electromagnetic wave is propagating along the negative Z-direction. Various modifications were performed on the basic bowtie shape, and the resulting shapes were categorized into a few groups as illustrated in the following sections.

The WGS produces results of the reflection coefficient (in magnitude and phase) of the investigated element. The phase data are more important since the design of the reflectarray relies on supplying proper phase compensation.

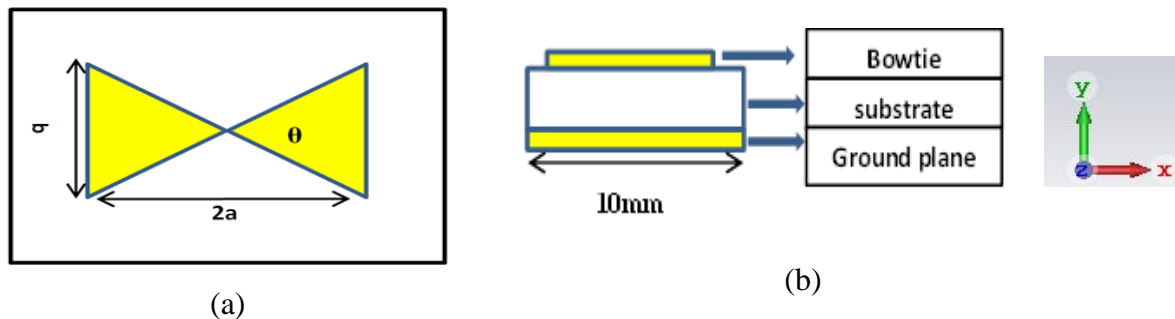


Figure 3.3. The bowtie unit cell of the reflectarray; (a) top view ,(b) side view.

To quantitatively evaluate the phase responses, the obtained data was used to calculate the following features:

1. Phase range: This is defined as the difference between the maximum and minimum phase values observed.
2. Phase center: It is determined by calculating the mean of the maximum and minimum phase values.
3. Element size for phase center: This refers to the size of an element that produces a phase equal to the mean value.
4. Rate of phase variation with size (slope): It measures the change in phase per unit length (in degrees per millimeter) for the linear region
5. Rate of phase change with frequency: This measures the change in phase per unit frequency (in degrees per gigahertz).

The investigated bowtie shapes of the proposed element were grouped according to which parameter was changed, and which one was kept constant. The groups are illustrated in the following sub-sections.

3.4.1 First Group

In this group, the performance of the unit cell was tested in two different manners. The first one is fixing the value of the patch width (2a) while changing the patch height parameter (b), whereas the second state can be described by the reverse as fixing the parameter (b) and changing the element width (2a).

3.4.1-a Fixed width (2a) and variable height (b)(horizontal electric field)

In this case, of the bowtie element, the width was kept constant, while the height was varied and the response of the element was investigated. The

simulations started with classic bowtie but with fixed width ($2a$) at $2a = 8$ mm, and changing height (b) as shown in Fig.3.4. The obtained results of the unit cell simulations are displayed in the following figures in the form of the magnitude of the reflection coefficient $|S_{11}|$ and the phase of the reflection coefficient.

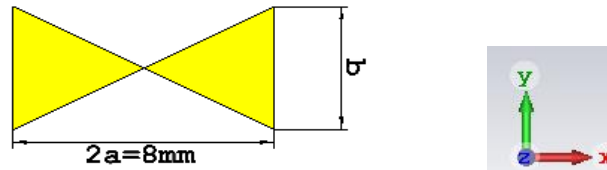


Figure 3.4. Geometry of the investigated bowtie dipole element at $2a=8$ mm, and E-field is along the width.

Figure 3.5 shows that there is a full reflection ($S_{11}=0$ dB) for a wide range of frequencies, but the reflection coefficient drops down to about -6 dB at certain frequencies. The response area starts at 6.8GHz and decreases towards a lower frequency of 5.8GHz. This resonance frequency decreases slightly as the dimension b is increased, which can be related to the fact that larger objects resonate at lower frequencies.

For the phase response, it can be seen from Fig. 3.6 that as the height b is increased, the response moves to a lower frequency, and this can be attributed to the fact that parts of larger size resonate at lower frequency. The slopes of the phase responses are almost the same for the various values of the height b .

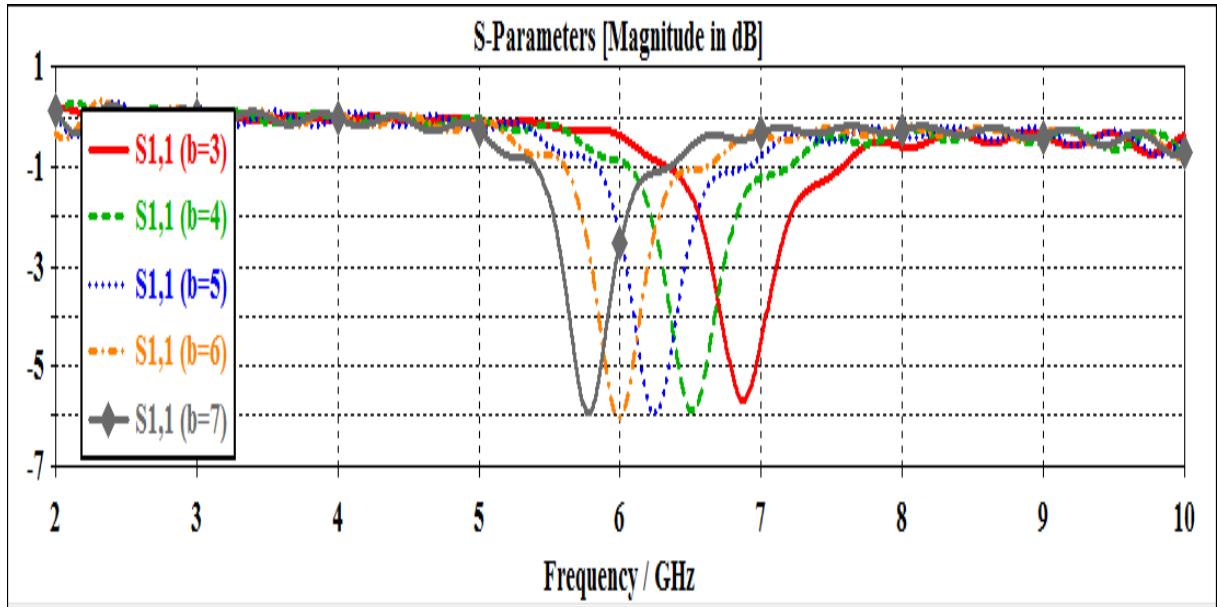


Figure 3.5. The variation of the reflection coefficient magnitude with the frequency for various values of b , when $2a=8\text{mm}$.

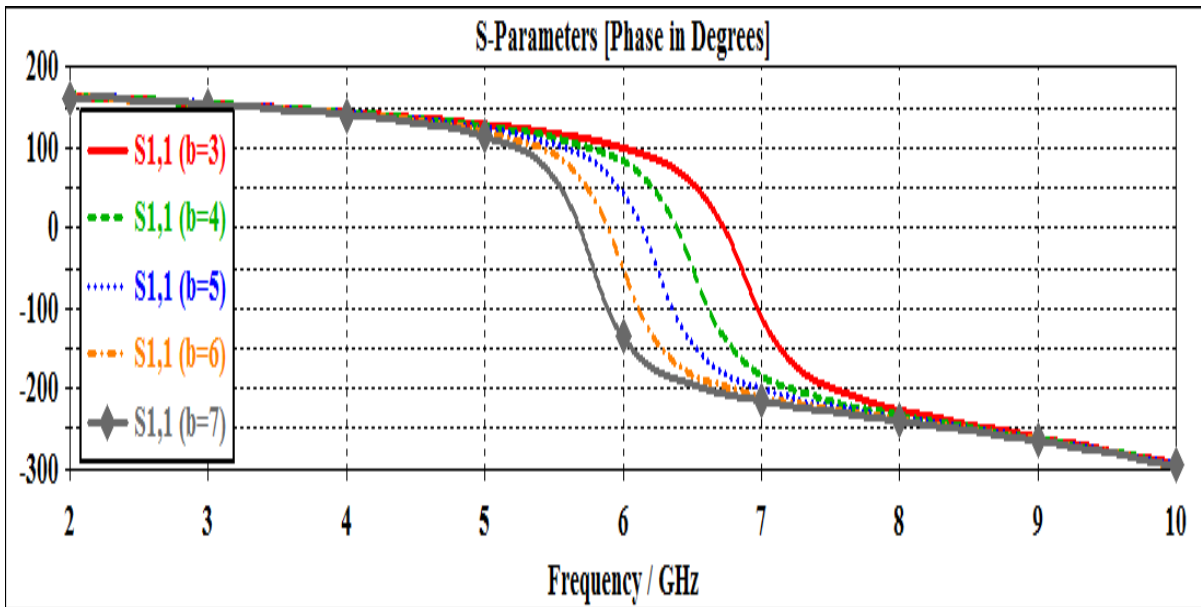


Figure 3.6. The variation of the reflection coefficient phase with the frequency for various values of b , when $2a=8\text{mm}$.

3.4.1-b Fixed height ($b=4$ mm) and variable width ($2a$) (horizontal electric field)

In this state of the bowtie element, the height (b) was kept constant, while the width ($2a$) was varied and the response of the element was investigated. The simulations started with classic bowtie but with fixed height (b) at $b = 4$ mm, and changing width ($2a$) as shown in Fig.3.7.

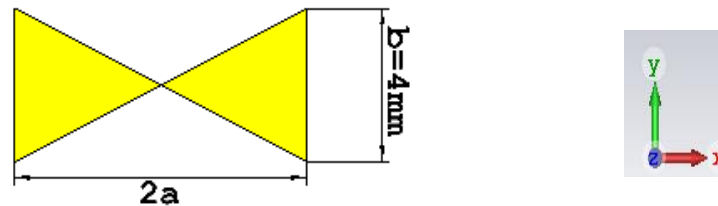


Figure 3.7. Geometry of the investigated bowtie dipole element at $b=4$ mm.

Figure 3.8 shows that there is a full reflection ($S_{11}=0$ dB) for a wide range of frequencies, but the reflection coefficient drops down to about -7.2 dB. The response area starts at 8 GHz and decreases towards lower frequency ending at 4.2GHz. This resonance frequency decreases even more than in the case of a change in (b) with an increase in the dimension a , which can be related to the fact that larger objects resonate at lower frequencies. In addition, Fig. 3.9 shows the variation of the reflection coefficient phase with the frequency for various values of a , and at fixed $b=4\text{mm}$. It can be seen that as the width ($2a$) is increased, the resonance frequency decreases.

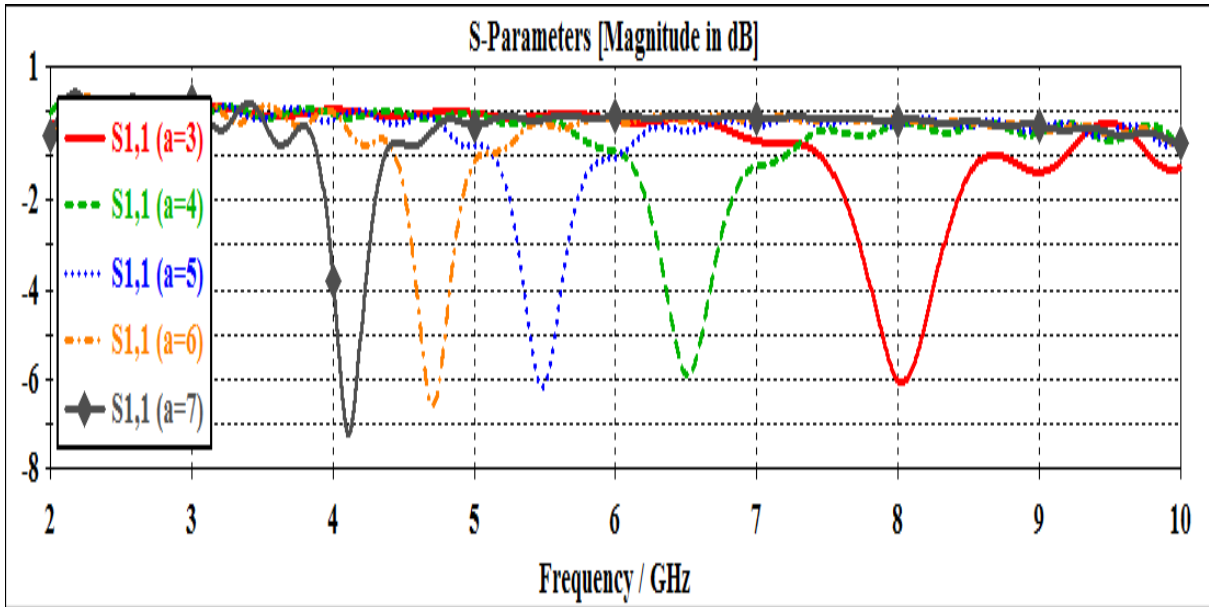


Figure 3.8. The variation of the reflection coefficient magnitude with the frequency for various values of a , when $b=4\text{mm}$.

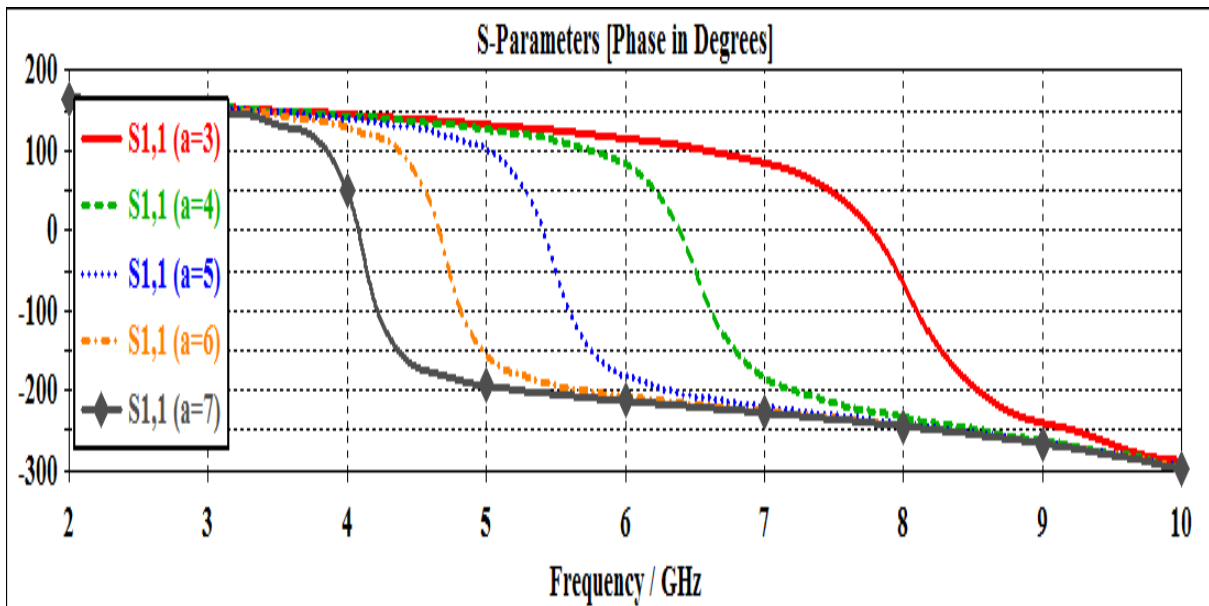


Figure 3.9. The variation of the reflection coefficient phase with the frequency for various values of a , when $b=4\text{mm}$.

Figure 3.10 shows the phase response of a bowtie unit cell at a frequency of 6 GHz, at a fixed width $2a=8\text{mm}$ compared to the phase response of a bowtie unit at a fixed width $b=4\text{mm}$ at same frequency. Upon analysis, it becomes apparent that the phase of the reflection coefficient undergoes a predictable change of less than 360 degrees when there is a modification in the height (b) of element or the width ($2a$) of the element. The variation with the height (fixed width) has lower slope as compared to the variation with the width (fixed height). The designer can use this figure, for example, to set the size of the bowtie element to achieve the required phase value of the element of the reflectarray. This is also evident from the comparison in the Table 3.1.

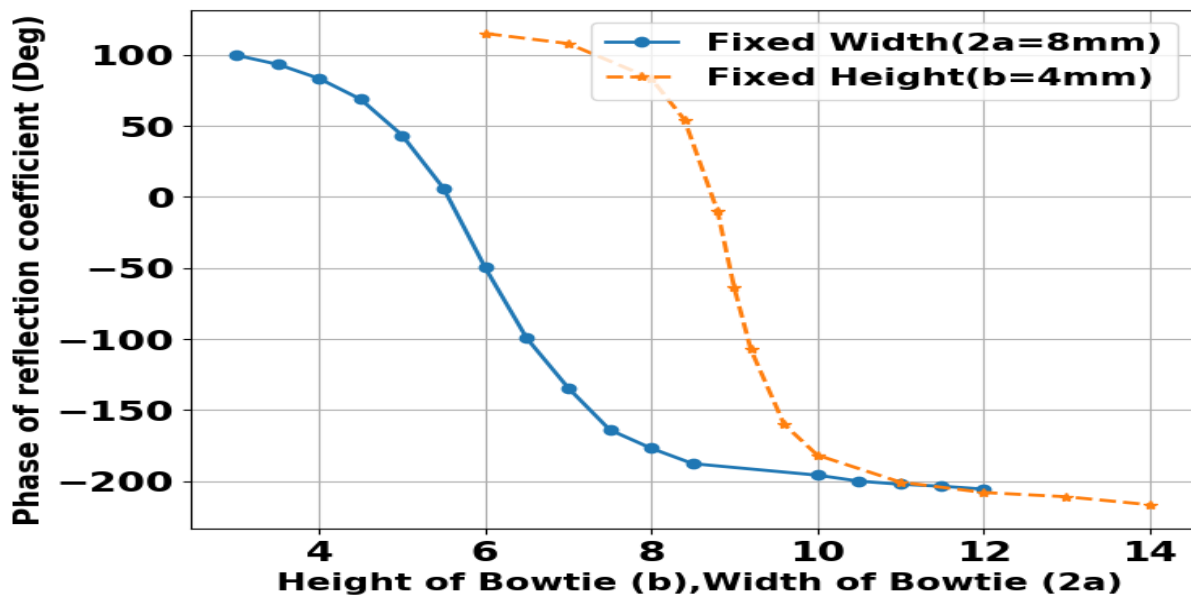


Figure 3.10. Comparison of the phase responses at the frequency of 6 GHz for the two schemes; (blue) fixed width ($2a=8$) and variable height b , (brown) fixed height ($b=4$) and variable width.

Table 3.1. Phase response and characteristics of the bowtie unit cell for the first group.

Name	Variable height, and fixed width (2a=8mm)	Variable width, and fixed height (b=4mm)
Max phase	99.7	115
Min phase	-205.6	-212.6
Center phase	-52.9	-48.8
Element size for phase center	6.2	4.5
Phase range	305.3	327.6
Slope(deg /mm)	105.3	132.5
Slope (deg /GHz)	384.6	352.2

3.4.1-c Fixed width (2a) and variable height (b) (vertical electric field)

After changing the direction of the electric field to be in the vertical direction (parallel to the height of the bowtie), the results shown in Figs.3.11 and Fig.3.12 were obtained. The results of Fig.3.11 show that as the height b is increased from 3 mm to 7 mm ,the resonance frequency decreases slightly from 10.8 GHz to 9.8 GHz. This is in line with the fact that larger objects have lower resonance frequency. The phase response shows variant changes with frequency as can be seen in Fig.3.12. When the height is at 3 mm and 4 mm, the phase changes slowly with frequency compared to the cases when the height is larger than 4 mm.

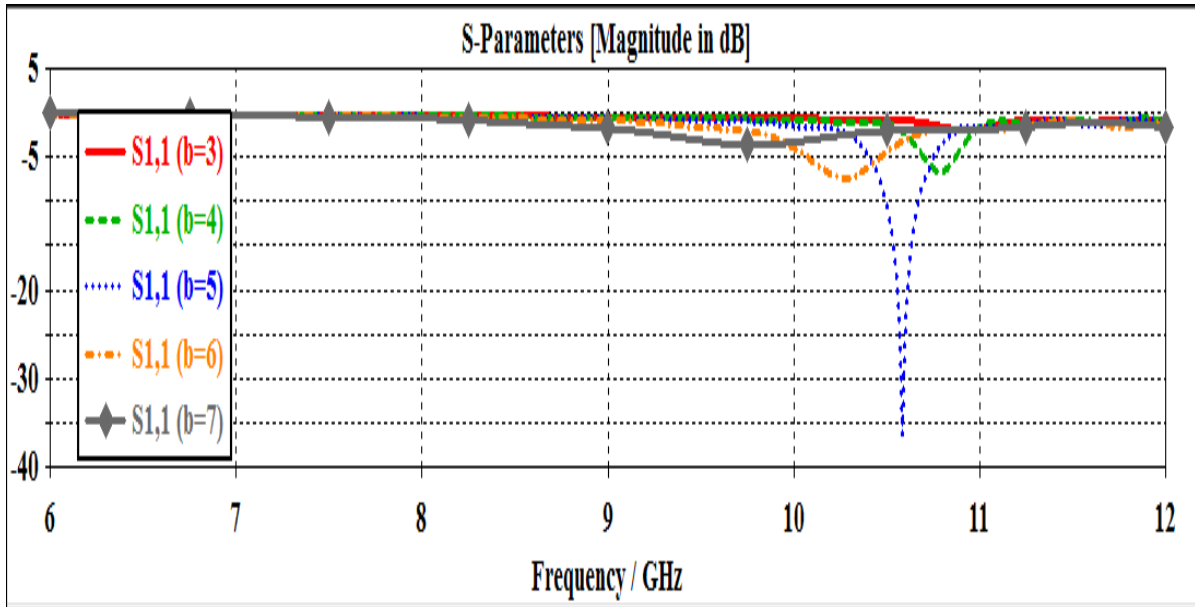


Figure 3.11. The variation of the reflection coefficient magnitude with the frequency for various values of b at $2a=8\text{mm}$.

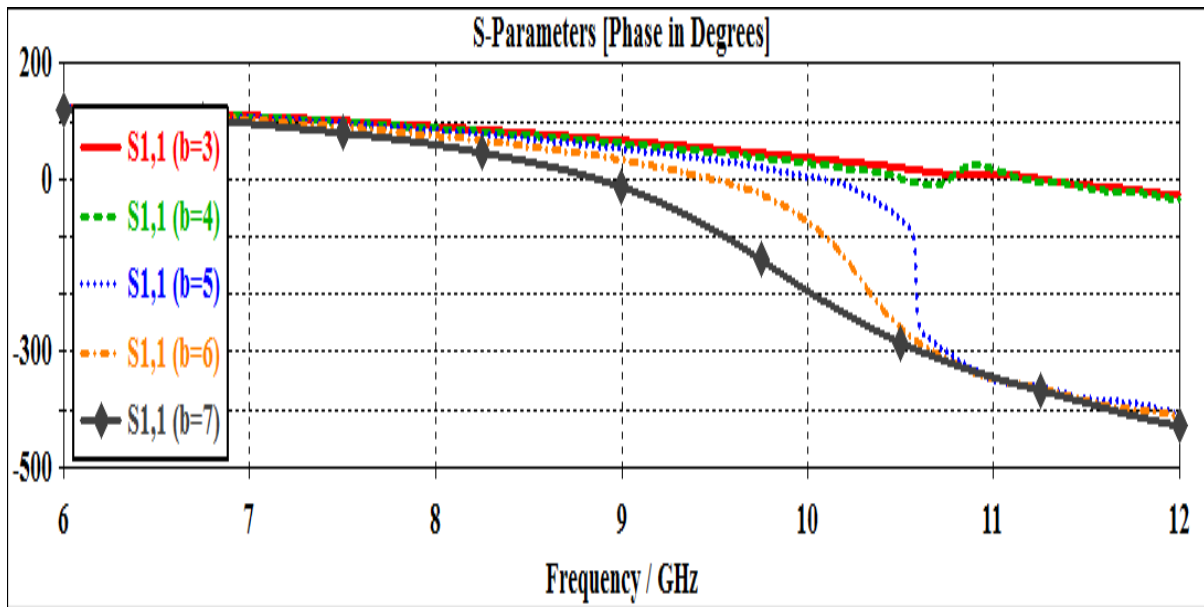


Figure 3.12. The variation of the reflection coefficient phase with the frequency for various values of b at $2a=8\text{mm}$.

3.4.1-d Fixed height (b) and variable width (2a) (vertical electric field)

The direction of the electric field was changed to be vertical, i.e. parallel to the height. The width of the element was changed while the height b was fixed at $b=4$ mm. The obtained results are shown in Figs. 3.13 and 3.14. It is observed that a slight effect occurs on the resonance frequency when changing parameter (a). The electric field is perpendicular to the direction of varying the length of the element. The phase response is shown in Fig. 3.14, where it can be seen that the phase is very slightly affected by the variation in the width ($2a$). Compared with the former cases, it can be concluded that appreciable phase changes can be obtained when the dimension parallel to the electric field is changed.

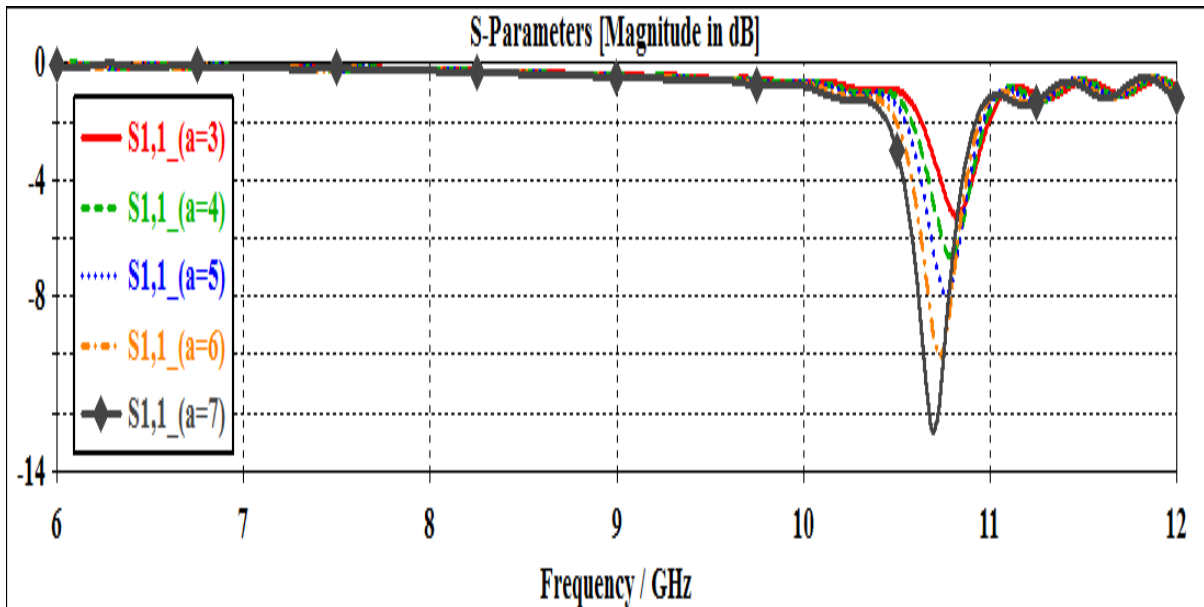


Figure 3.13. The variation of the reflection coefficient magnitude with the frequency for various values of width ($2a$), at $b=4$ mm.

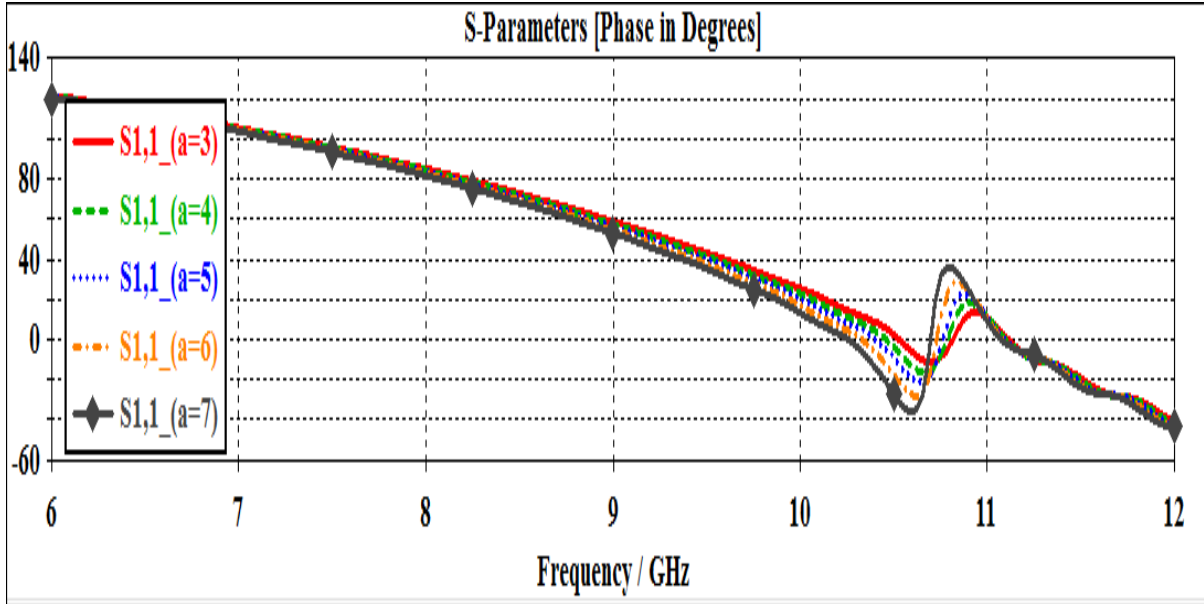


Figure 3.14. The variation of the reflection coefficient phase with the frequency for various values of width ($2a$), at $b=4\text{mm}$.

3.4.2 Second Group

In this group, the a/b ratio was kept constant when changing the size of the bowtie element. Thus, the angle (θ) was kept constant, which means the shape of the bowtie element was preserved during the changes.

3.4.2-a Changing the height b and width $2a$ (horizontal electric field)

When both the width $2a$ and height b are changed at the same time, the ratio a/b stays constant and consequently the angle of the bowtie shape stays constant.

The size of the bowtie unit cell can be modified, which may have a significant impact on its performance and characteristics. Figure. 3.15 shows the geometry of the investigated bowtie dipole element when a and b were changed at the same time such that $a=b$.

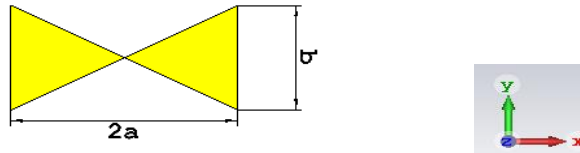


Figure 3.15. Geometry of the investigated bowtie unit cell when a and b were changed at the same time.

The effect of both variables is shown together in Fig. 3.16 for the response of the magnitude. The results indicate that the resonance frequency decreases as the size of the bowtie is increased. This is in line with the fact that the resonant frequency is inversely proportional to the size of the element.

For the phase response, it can be seen from Fig.3.17 that as the dimensions a and b are simultaneously increased, the response moves to lower frequency, which can be attributed to the fact that parts of larger size resonate at lower frequency. The slope of the phase responses is almost the same for the various combinations of a and b .

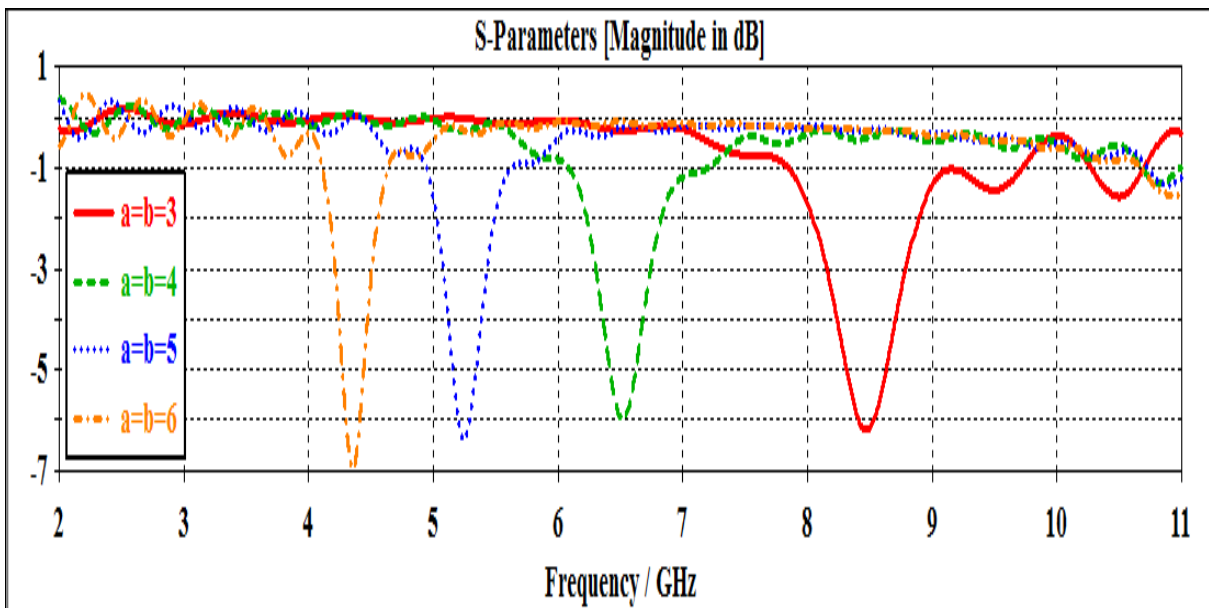


Figure 3.16. The variation of the reflection coefficient magnitude with the frequency for various values of width $2a$ and height b .

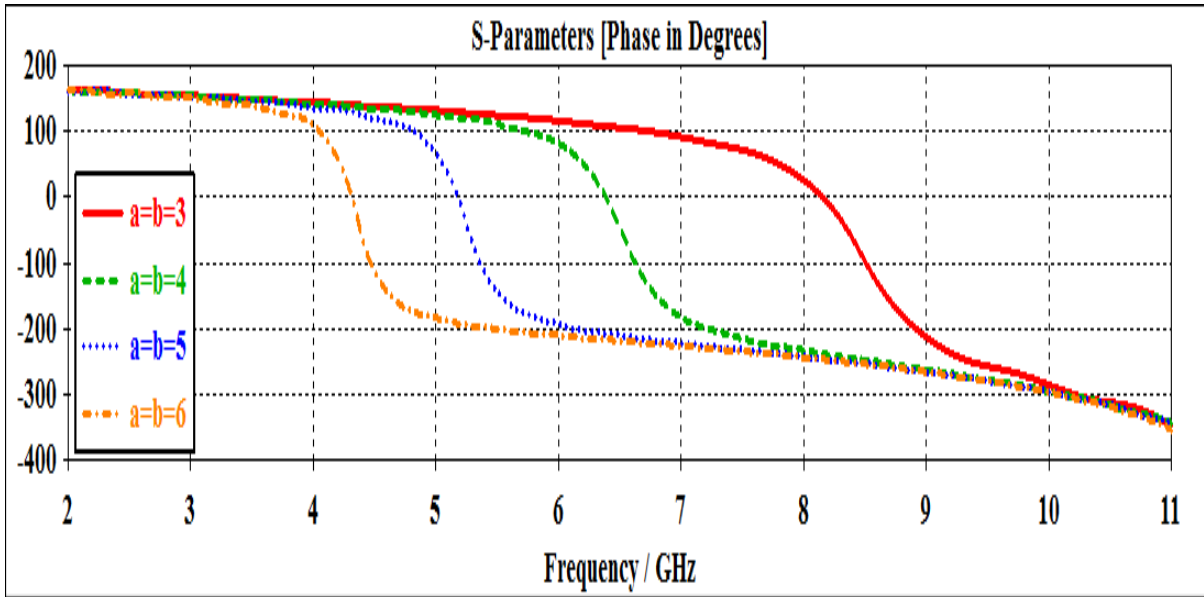


Figure 3.17. The variation of the reflection coefficient phase with the frequency for various values width $2a$ and height b .

3.5 Bowtie with Rounded Sides (Tapered bowtie)

The bowtie shape was modified by tapering its two sides, and this was performed by attaching half of a circle at both sides. The circle has a diameter equal to b as shown in Fig. 3.18. The proposed development was inspired by the former finding [52], which showed tapered sides and smooth edges help to reduce the variation of the phase response. The tapered bowtie was simulated using the WGS, where the following two cases were considered, can see also in [69].

3.5.1 The Tapered bowtie (horizontal electric field)

In this set of simulations, the incident wave has an electric field parallel to the X-axis (along the width of the bowtie). The obtained results from the various simulations are shown in Figs. 3.19 and 3.20. We notice from Fig. 3.19 that the resonance frequency decreases as either the width, height, or both increase. Thus, an increase in the size results in a decrease in the resonance

frequency. Figure.3.20 reveals the variation of phase shift with frequency as a function of the parameters for the given unit cell configuration. The phase response also shifts to lower frequency as the dimensions of the elements are increased.

Figure 3.21 shows a comparison of the phase responses with element size for the conventional and tapered bowtie elements that were obtained at the center frequency 6.5 GHz. Detailed parameters of the two responses are shown in Table 3.2. It can be seen from the phase responses and data listed in Table 3.2 that the tapered bowtie has smaller phase slopes with respect to both frequency and size. The two shapes have almost the same phase range.

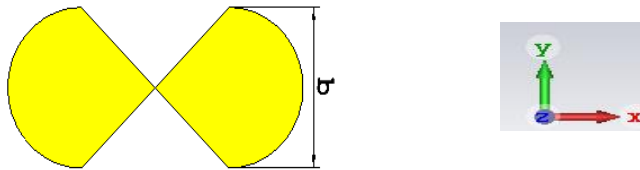


Figure 3.18. Geometry of the proposed tapered bowtie unit cell with half circles on each side.

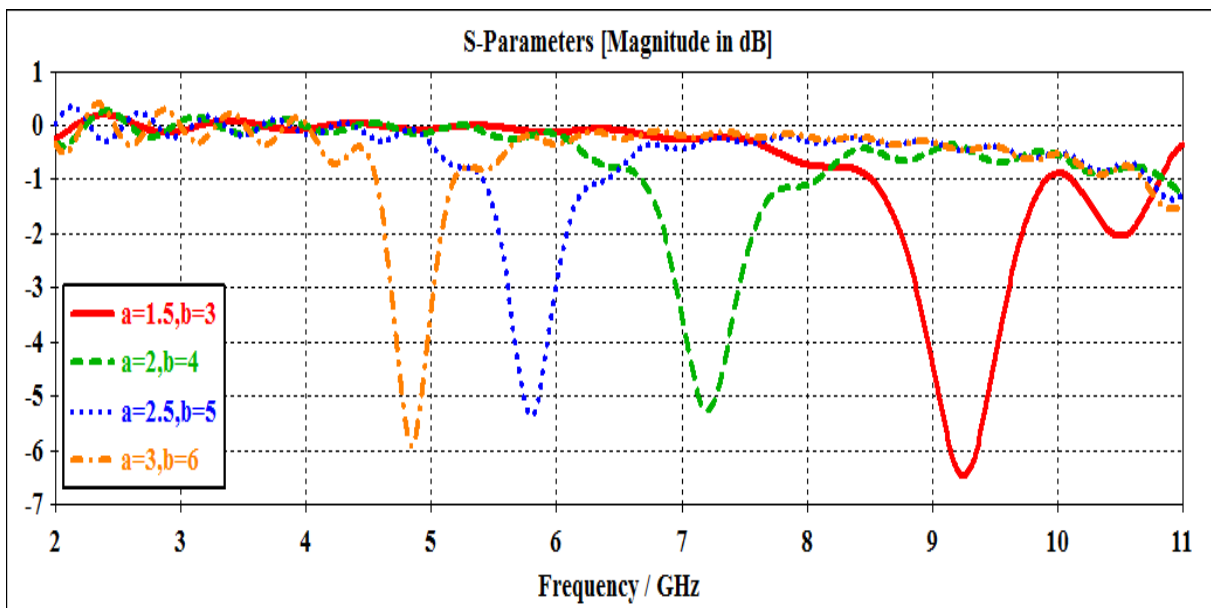


Figure3.19.The variation of the reflection coefficient magnitude with the frequency for tapered bowtie for various values of a and b.

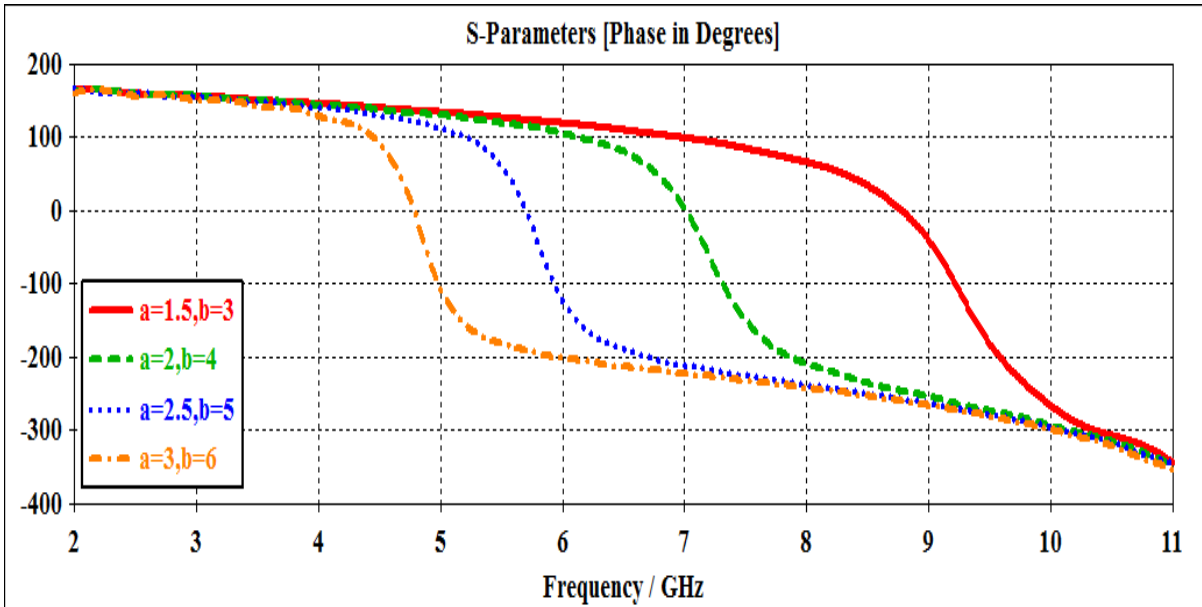


Figure 3.20. The variation of the reflection coefficient phase with the frequency for tapered bowtie for various values of a and b .

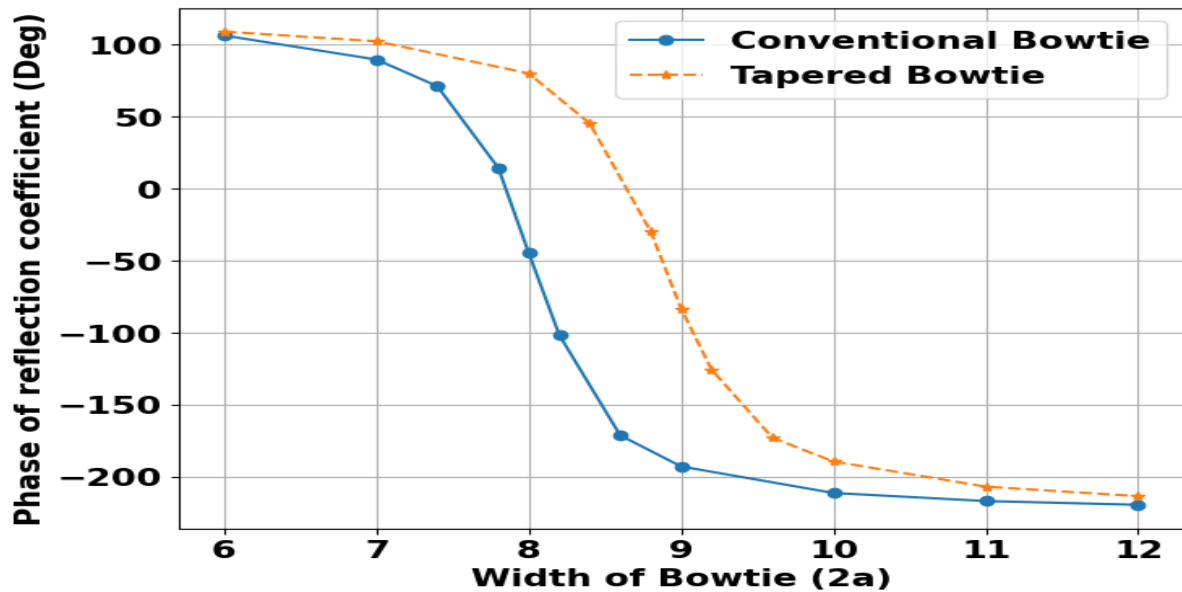


Figure 3.21. Comparison of the phase responses of the conventional and tapered bowtie unit cell elements, at the frequency of 6.5 GHz.

Table 3.2. Phase response characteristics of the conventional and tapered bowtie unit cell elements, at the frequency of 6.5 GHz.		
Parameter	Conventional bowtie	Tapered bowtie Fig. 3.18
Max	106.5	109.2
Min	-219.2	-213.2
Center phase	-56.3	-52
Element size for phase center	8.1	8.9
Phase range	325.7	322.4
Slope (deg / mm)	289.7	213.6
Slope (deg /GHz)	258	371.2

3.5.2 The Tapered Bowtie (vertical electric field)

In this set of simulations, the incident wave has an electric field normal to the width of the bowtie (along the Y-axis). The obtained results from the various simulations are shown in Figs. 3.22 and 3.23. The response of the magnitude of the reflection coefficient shown in Fig. 3.22, exhibits the same trend of decreasing resonance frequency with the increase in the size of the bowtie (increasing either width or height).

The phase response shown in Fig. 3.23 exhibits similar variation to those obtained for the conventional bowtie that were shown in Fig. 3.12. For heights of 3 mm and 4 mm, the phase changed slowly with frequency compared to the cases when the height was larger than 4 mm.

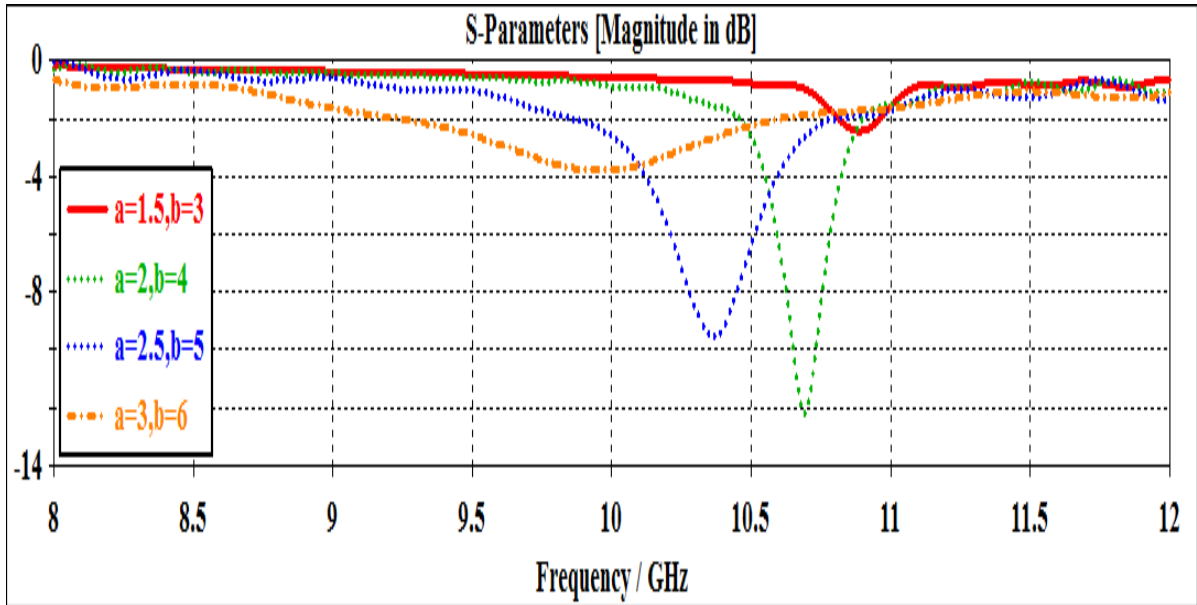


Figure 3.22. The variation of the reflection coefficient magnitude with the frequency for various values of a and b .

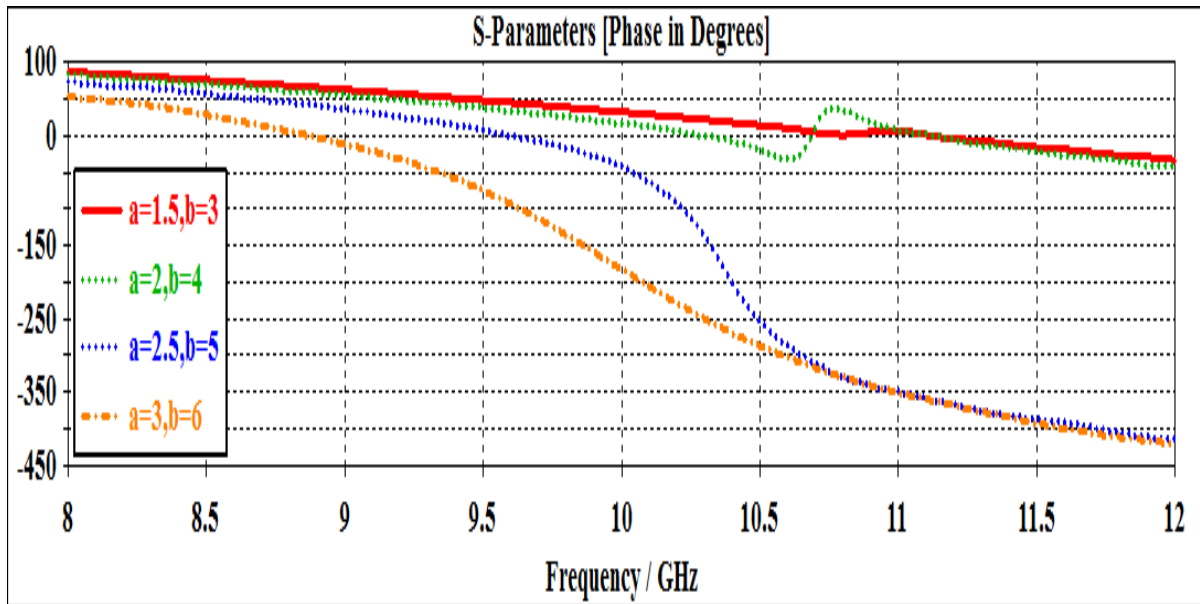


Figure 3.23. The variation of the reflection coefficient phase with the frequency for various values of a and b .

3.6 The Crossed Bowtie (Third Group)

As was noticed in the responses of previous groups, the performances of the bowtie elements were different for the two types of polarizations. This result has motivated a search for an element shape that responds equally to both polarizations. The suggestion was to combine two bowtie elements in quadrature, to form the crossed bowtie shape that is shown in Fig.3.24. The suggested element was investigated for the two types of polarizations.

Figure 3.25 shows the obtained results when the electric field of the incident wave was in the horizontal direction. The response shows that the resonance frequency decreases as the bowtie element is increased. The phase response, depicted in Fig.3.26 reveals the same trend. Notably, the slopes of the phase responses remain nearly unchanged for different values of the dimensions a and b . It was also found that when the electric field of the incident wave was rotated by 90° , the results were exactly the same, (they were not placed here for brevity). Therefore, the crossed bowtie responds to both polarizations equally, and this is a consequence of the two-dimensional symmetry of the bowtie shape. Many researchers have addressed this form of bowtie [70] [71].

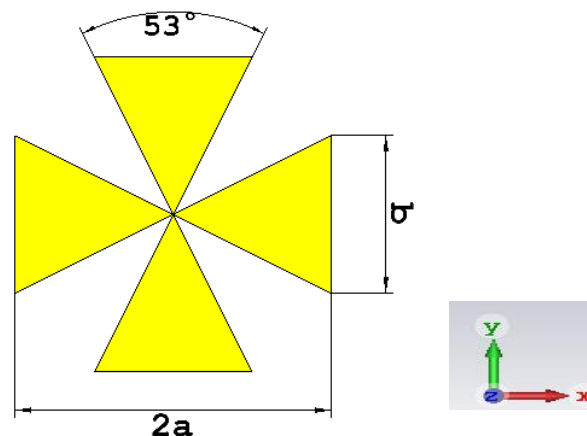


Figure 3.24. Geometry of the crossed bowtie unit cell.

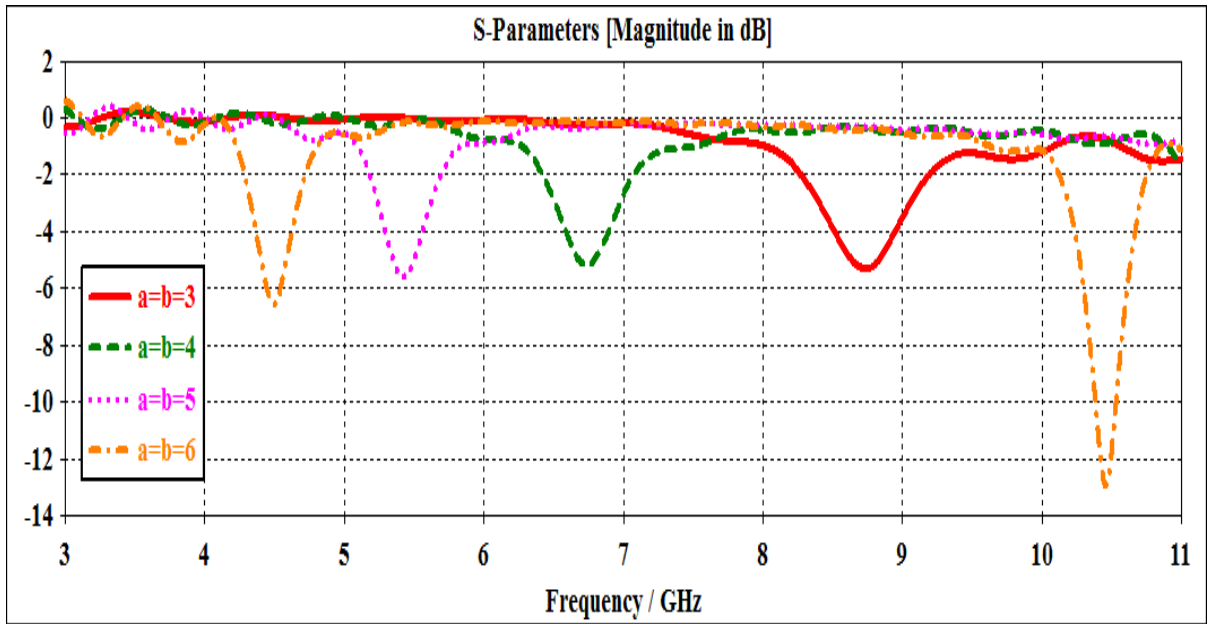


Figure 3.25. The variation of the reflection coefficient magnitude with the frequency for various bowtie sizes ($a = b$).

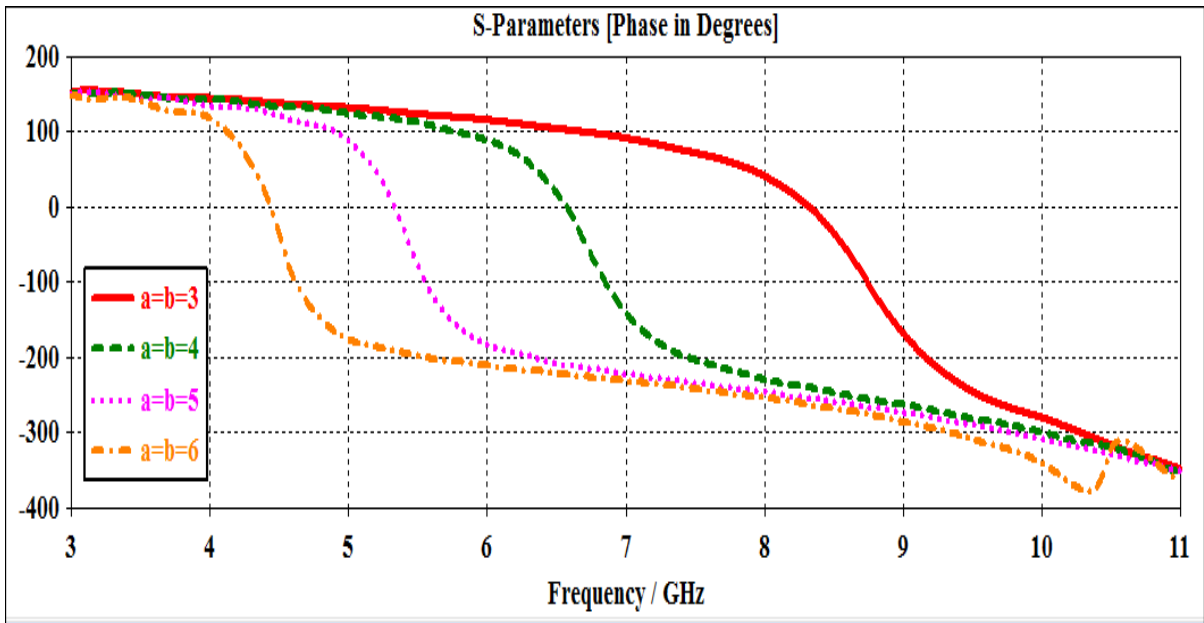


Figure 3.26. The variation of the reflection coefficient phase with the frequency for various bowtie sizes ($a = b$).

3.7 The Square element

Square element unit cell, as the name implies, have a conductive element in the shape of a square. The designed square element antenna is shown in Fig.3.27. The square element was simulated for the case when the electric field of the incident wave was along the X-axis, and the obtained results are shown in Figs. 3.28 and 3.29. The response of the magnitude of the reflection coefficient, shown in Fig.3.28, indicates the decrease of resonance frequency with the increase of the side length of the square. The phase response of the square element indicates a shift towards lower frequencies as the side length of the square is changed, as it can be seen in Fig.3.29. The performed simulations when the electric field of the incident wave was rotated to be along the Y-axis produced similar results, and the results are not presented here to avoid repetition. The finding is due to the symmetry of the element across the XY axes.

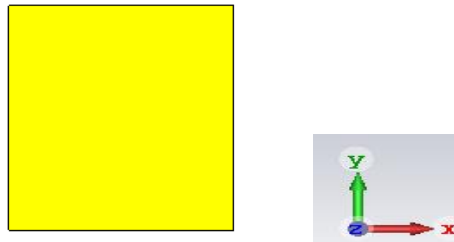


Figure 3.27. Geometry of the square unit cell, $a=b$.

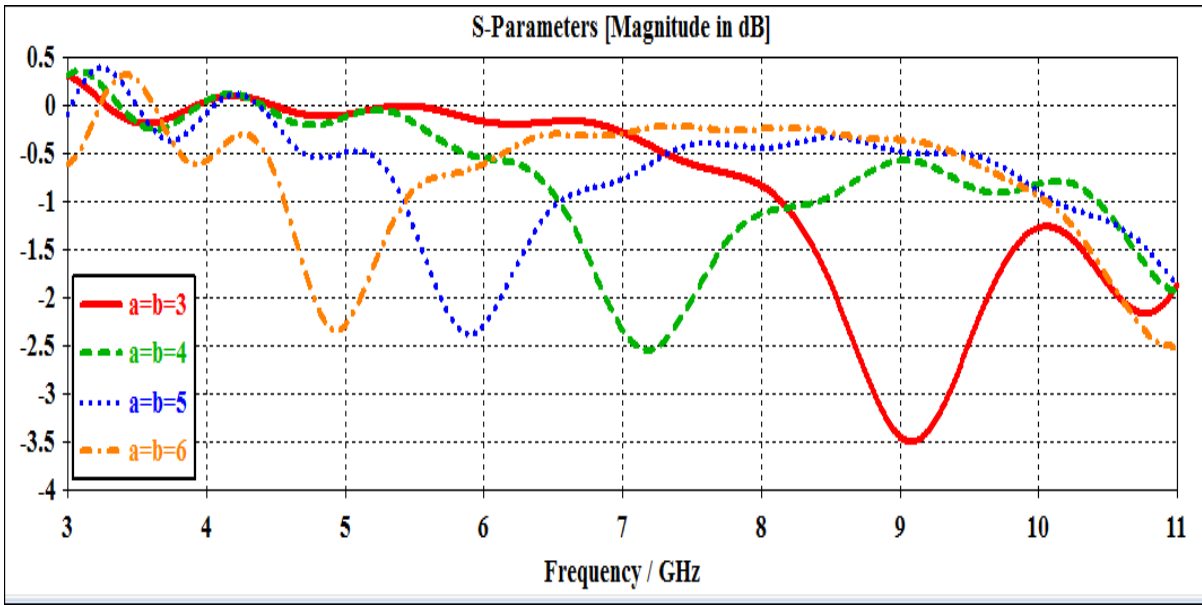


Figure 3.28. The variation of the reflection coefficient magnitude with the frequency for the square unit cell.

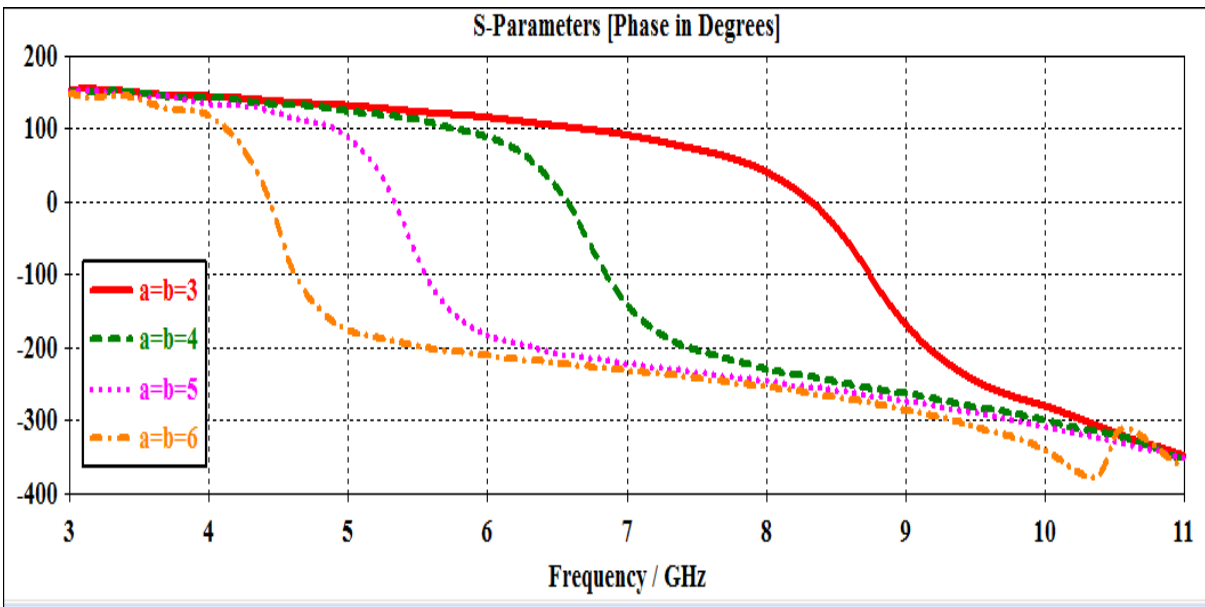


Figure 3.29. The variation of the reflection coefficient phase with the frequency for the square unit cell.

Based on the information given in Figure 3.28 and Fig.3.29, the phase relationship with the size of the element is plotted in Fig.3.30. It is compared with the phase response of the cross bowtie antenna (see Table 3.3). It can be seen from the phase responses and the table that the cross bowtie offers wider phase range but on the account of larger slope.

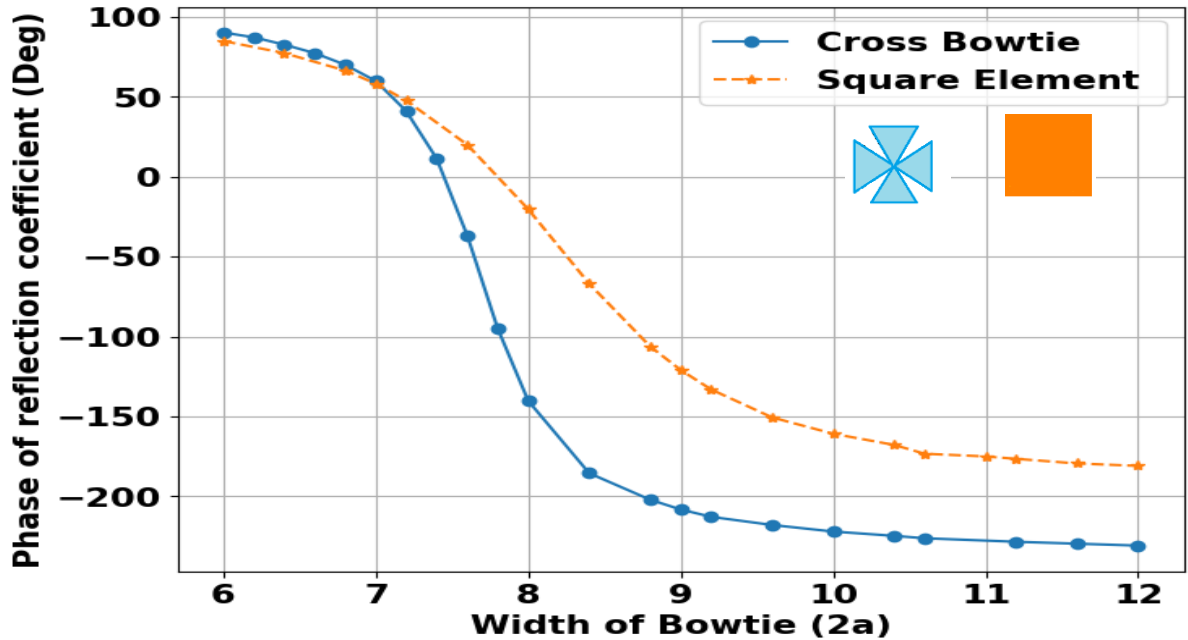


Figure 3.30. Phase variation with the parameter of elements at center frequency 7GHz.

Table 3.3. Phase response characteristics of cross bowtie and square element cell reflectarray antenna.		
The name	Cross bowtie	Square element
Max	90.5	84.9
Min	-230.9	-181
Center phase	-70.2	-48
Element Size for center phase	7.8	4.2
Phase range	321.4	265.9
Slope(deg /mm)	226.6	117.5
Slope (deg/GHz)	235.5	147.8

3.8 Square Bowtie Antenna

In this configuration, a comparison was also made here between a square element but here with a bowtie shape with the same horizontal and vertical dimensions, where horizontal dimensions for bowtie is equal $2a$ and vertical dimensions $b=2a$, for square the dimensions equal $2a$.

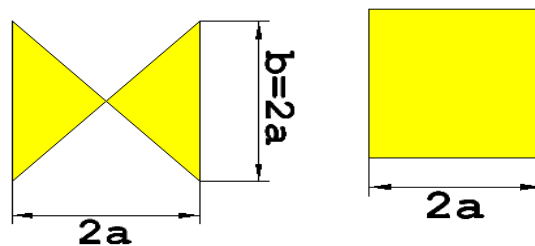


Figure 3.31. Geometry of the square bowtie antenna, where outer dimensions are equal to those of the square element.

Figure 3.32 to Fig. 35 for two elements, it turns out that we are still in line, and the resonance frequency decreases slightly with increasing dimensions,

which may be related to the fact that large objects resonate at low frequencies. Figure 3.36 and Table 3.4 show phase variation with width of bowtie at center frequency 6.5 GHz. It can be seen from the phase responses and the table that wider phase range for two elements when compared with the previous case but still bowtie offers wider phase range but on the account of larger slope.

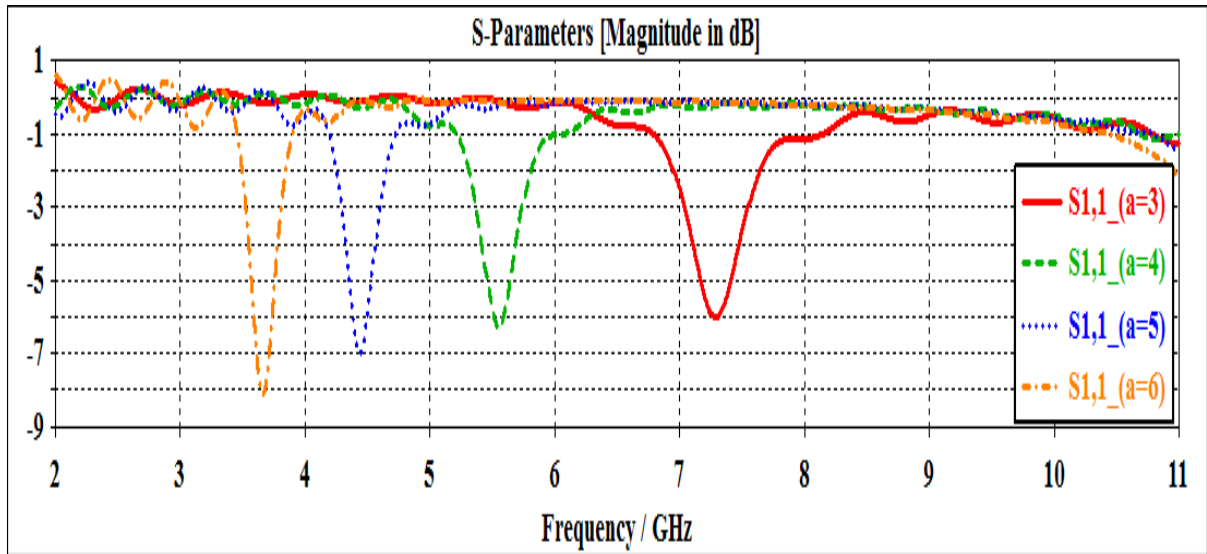


Figure 3. 32.The variation of the reflection coefficient magnitude with the frequency for the square bowtie unit cell.

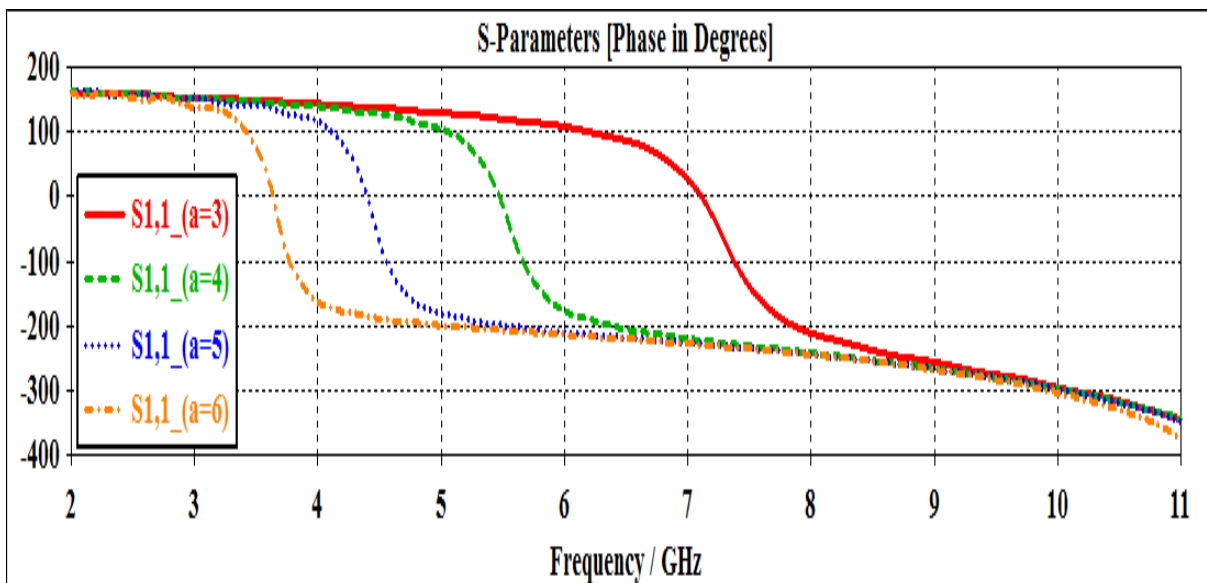


Figure 3. 33. The variation of the reflection coefficient phase with the frequency for the square bowtie unit cell.

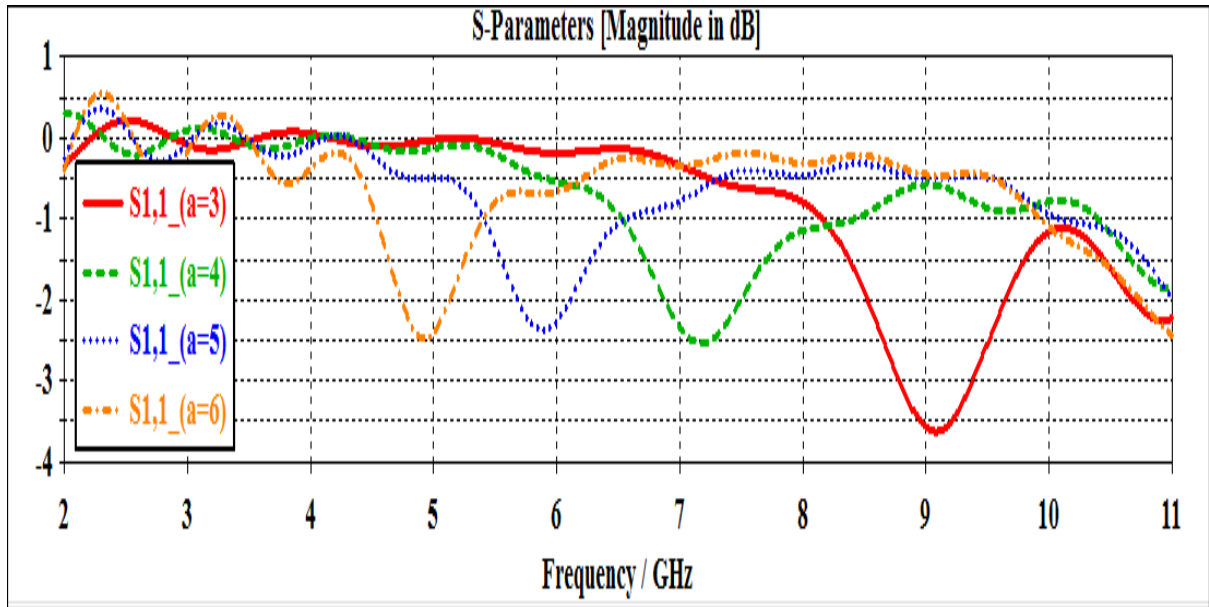


Figure 3. 34. The variation of the reflection coefficient magnitude with the frequency for the square unit cell.

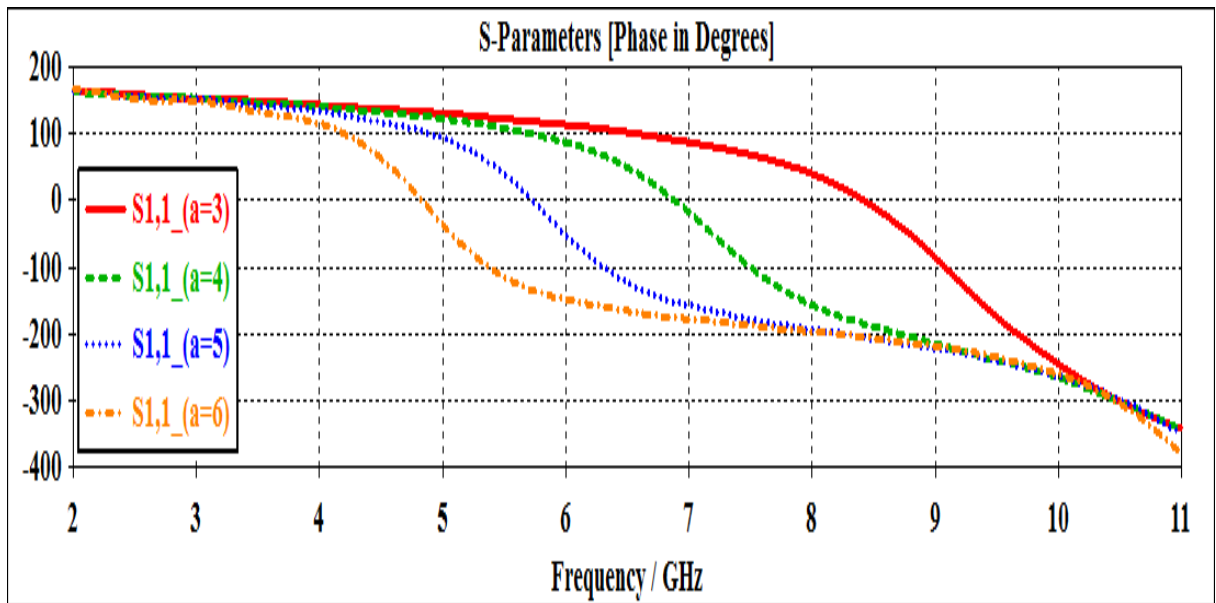


Figure 3. 35. The variation of the reflection coefficient phase with the frequency for the square unit cell.

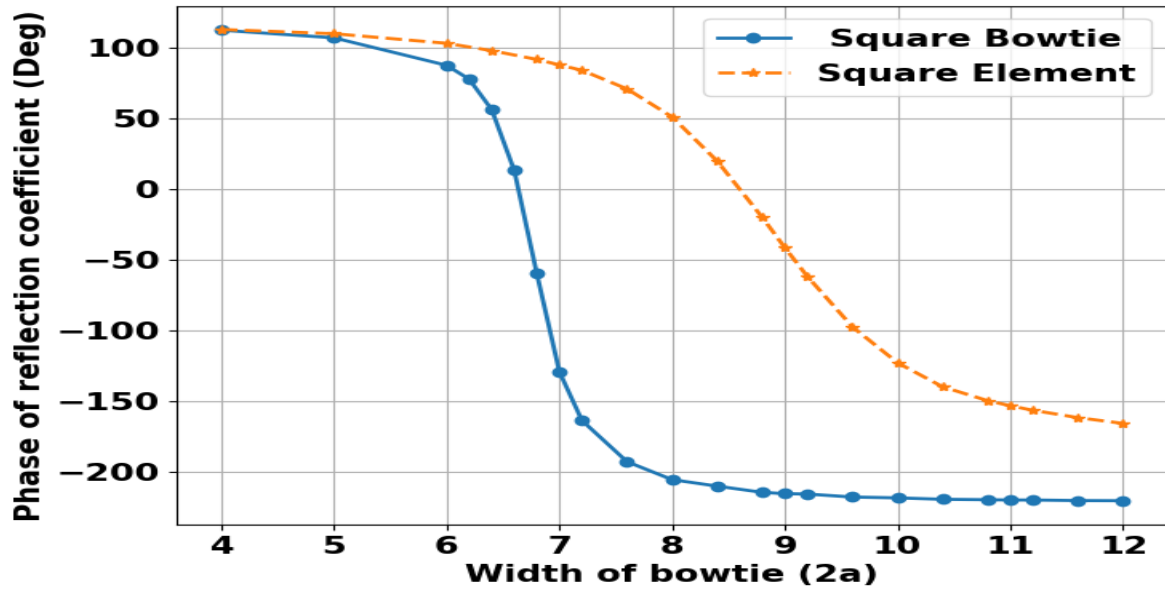


Figure 3.36. Phase variation with the width of bowtie at center frequency 6.5GHz.

Table 3.4. Phase response characteristics of square bowtie and square element cell reflectarray antenna.		
The name	Square bowtie	Square element
Max	112.3	112.8
Min	-220.3	-166.1
Center phase	-54	-26.6
Size for center phase	6.8	8.8
Phase range	332.6	278.9
Slope(deg/mm)	275	86.8
Slope (deg/GHz)	347	166.6

3.9 The Disconnected Bowtie (Fourth group)

In the search for unit cells that can offer better performance, it was suggested to investigate the case when the two parts of the bowtie are disconnected. This

design can be grouped into firstly when the two triangles are facing each other (tip-to-tip orientation), and secondly when the bases of the two triangles are parallel. Both shapes are investigated in the following sections.

3.9.1 Disconnected triangles (tip-to-tip)

The disconnected bowtie unit cell, when the tips of the two triangles are facing each other is shown in Fig.37. The dimensions are set at $2a = 10$ and $b = 5$, while the gap between the triangles was varied from zero to 2 mm. The incident wave is assumed to have an electric field parallel to the width of the bowtie.

The key variation in this design is the gap between the triangles, which can range from zero to some value. When the gap is set to zero, the two triangles are in electrical direct contact forming a single conductor. It is assumed that by varying the gap, the design allows for different configurations.

The obtained results from the simulations are shown in Fig.3.38 and Fig.3.39. When the gap was increased above zero (the two triangles were separated) the resonance frequency increased from about 5.3 GHz to the range around 11 GHz. This means that the resonance frequency is almost doubled, which can be attributed to the fact that the width (horizontal distance) of each triangle is half that of the former bowtie element (connected triangles). In other words, halving the size results in double the resonance frequency.

The other note is that changing the gap length will change the mutual coupling between the two triangles, and thus influence the resonance frequency as can be seen in Fig.3.38.

The phase variations with frequency are shown in Fig. 3.39, and reveal fast changes around the frequency of 11GHz, where there is resonance. Such

variations are larger than those obtained from the conventional bowtie unit cells. The case with the vertical electric field did not offer better results.

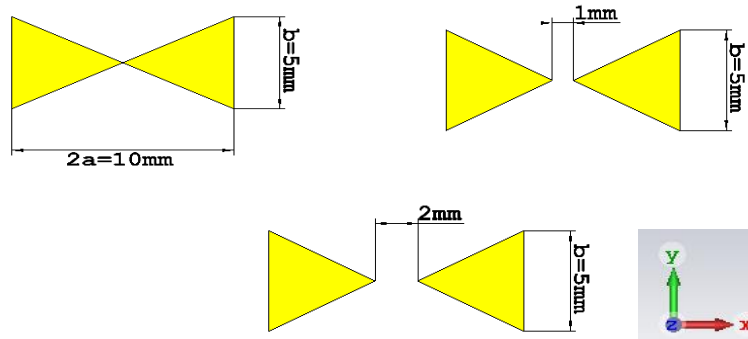


Figure 3.37. Different geometries for disconnected bowtie unit cell.

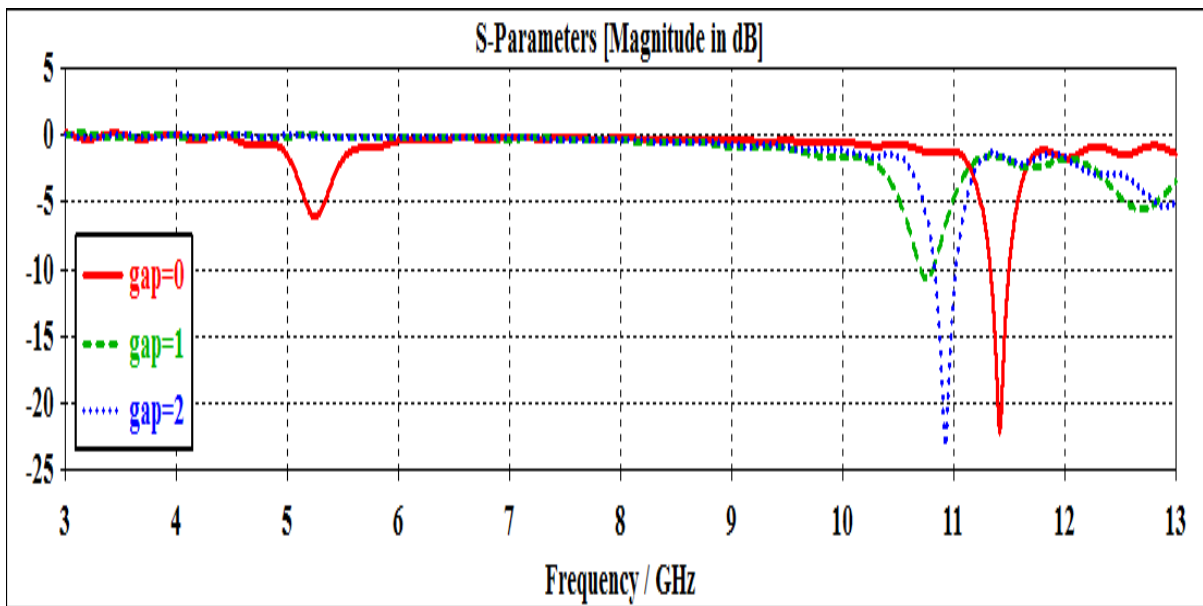


Figure 3.38. The variation of the reflection coefficient magnitude with the frequency for the disconnected bowtie at gap; (a) 0mm,(b) 1mm, (c) 2mm.

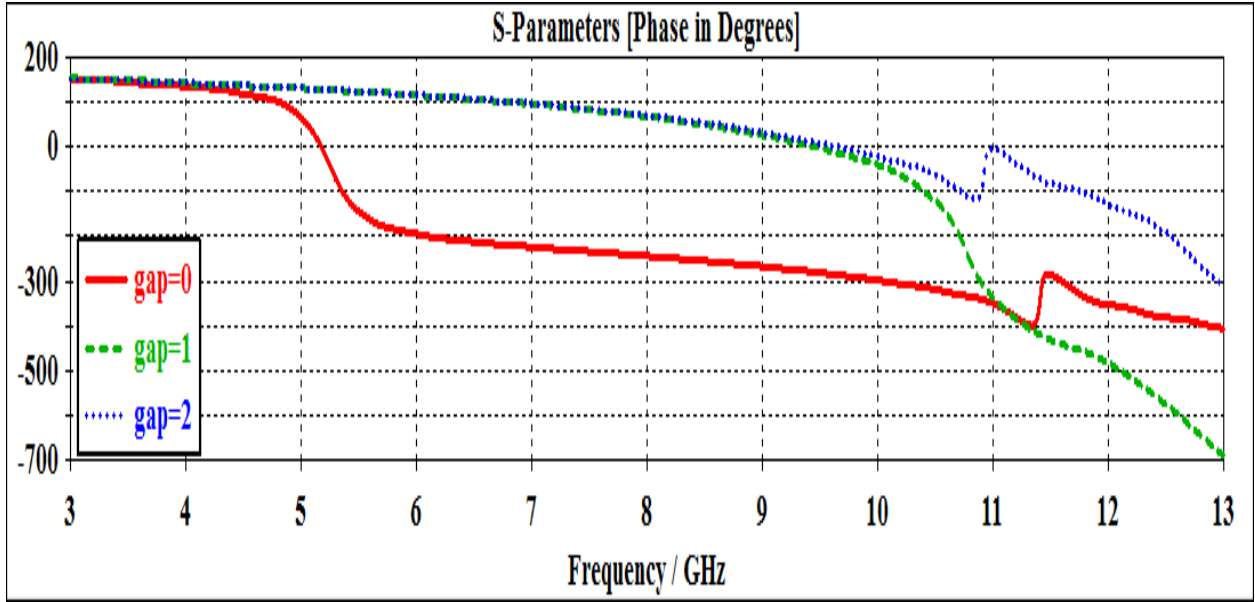


Figure 3.39: The variation of the reflection coefficient phase with the frequency for the disconnected bowtie at gap;(a) 0mm,(b) 1mm,(c) 2mm.

3.9.2 Back-to-back triangles

In this configuration, the two triangles were placed such that their bases are parallel as shown in Fig.3.40. The close proximity produces mutual coupling that results in a capacitor whose value decreases as the gap between the bases is increased. When the gap between the triangles is set to zero, the two triangles are in direct contact, creating a single conducting surface in the shape of rhombus. As the gap increases, the two triangles start to separate, resulting in an open space between them. By varying the gap the designer allows for various configurations.

The proposed unit cell was simulated assuming an incident wave with an electric field along the X-axis, and dimensions ($a= 5\text{mm}$, and $b= 5\text{mm}$). Three gap values of 0, 1 mm, and 2 mm were assumed, and the obtained results are shown in Fig.3.41 and Fig.3.42. The magnitude response shows resonance frequency in the range from 10 GHz to 12 GHz. The phase response, shown in

Fig.3.42, exhibits a slow phase variation when the gap is set to zero, while the variation tend to be faster when the gap is increased.

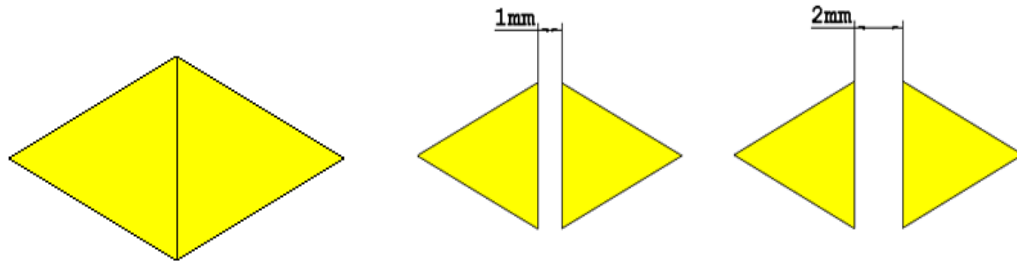


Figure 3.40. Back to back configuration of the bowtie unit cell with various gaps.

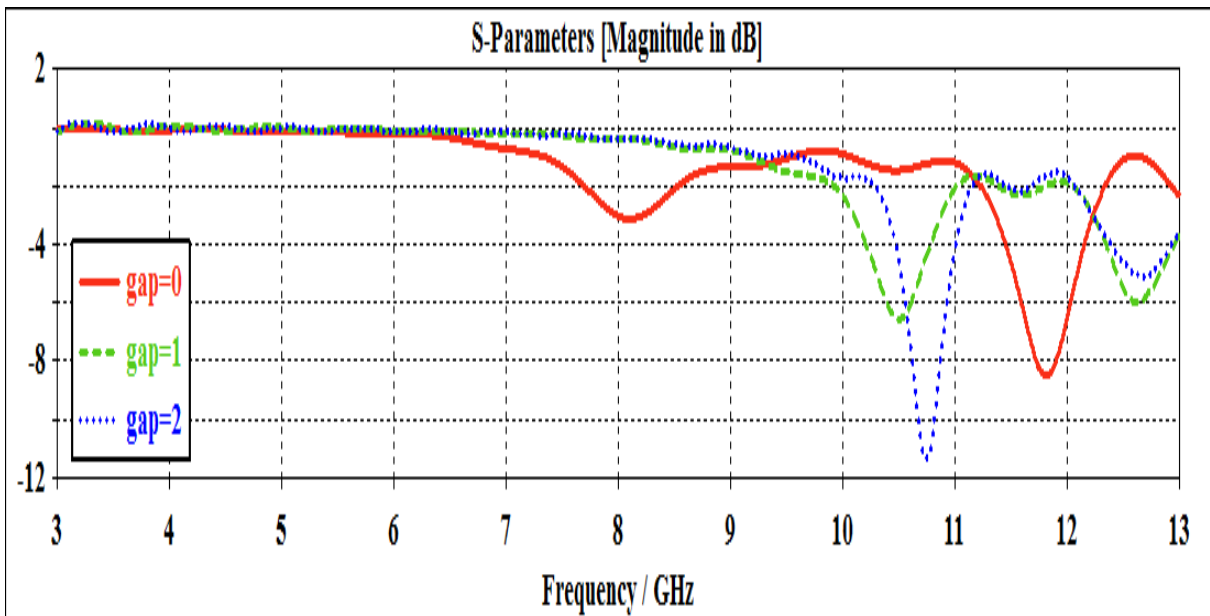


Figure 3.41. The variation of the reflection coefficient magnitude with the frequency for the back-back bowtie at gap; (a) 0mm, (b) 1mm, (c) 2mm.

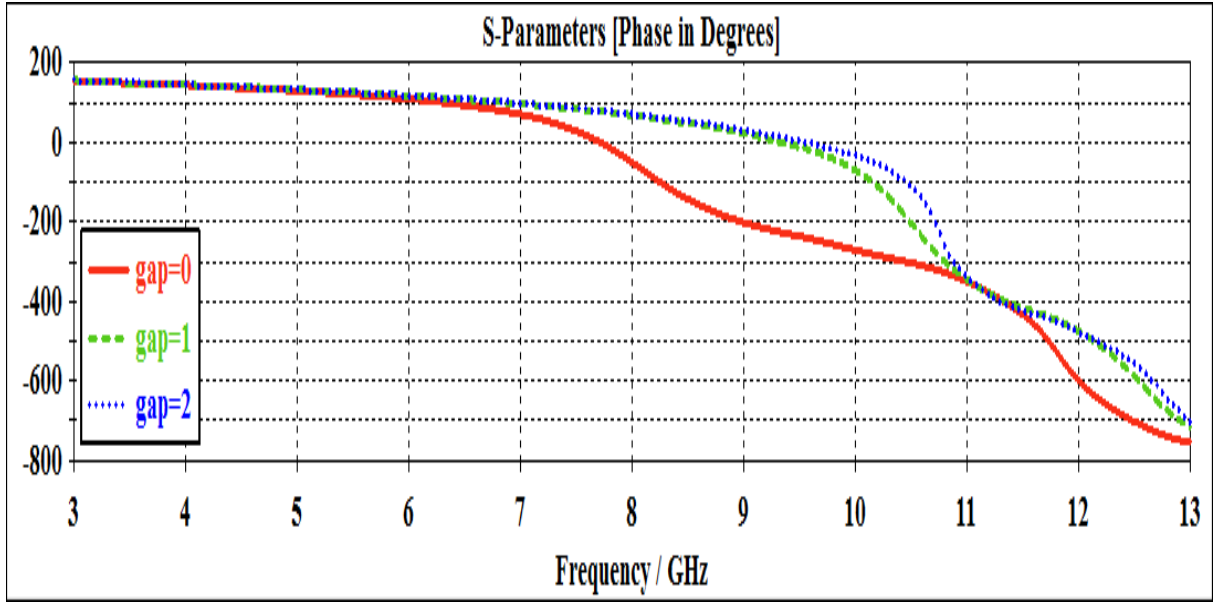


Figure 3.42. The variation of the reflection coefficient phase with the frequency for the back-back bowtie at gap; (a) 0mm, (b) 1mm, (c) 2mm.

3.10 The Fractal (Dual) Bowtie Element

In the model, two bowtie elements are combined into a single layer. The ratio between the sizes of the two shapes is (a_2/a_1) where a_2 is the width of the inner bowtie and a_1 is the width of the outer bowtie as shown in Fig.3.43. This shape was inspired by the fractal antenna proposed in [72]. Here the repetition idea of the fractal geometry is utilized. The idea behind this is to achieve larger bandwidth and hence lower phase slope.

3.10.1 The Fractal Bowtie Element (horizontal electric field)

The fractal bowtie element, that is shown in Fig.3.43, was simulated with an incident wave having a horizontal electric field. It is noticeable from Fig 3.44 and Fig.3.45 that the effect of changing the ratio on the response is very small, as the disparity between the three curves is very small the reflection point for all tested values of (a_2/a_1) takes place at a frequency approximately 5.3 GHz with a steep slope. The outer dimension of the three cases was 10 mm, and

hence the resonance frequency was around 5.3 GHz. This indicates that the inner bowtie has small effect on the resonance frequency.

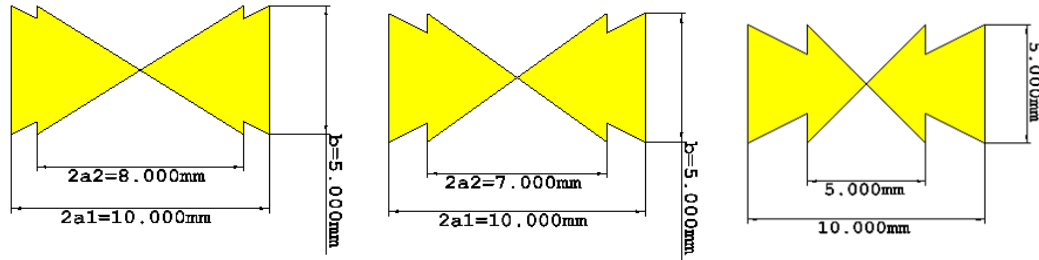


Figure 3.43. Geometries of the investigated of the fractal bowtie element.

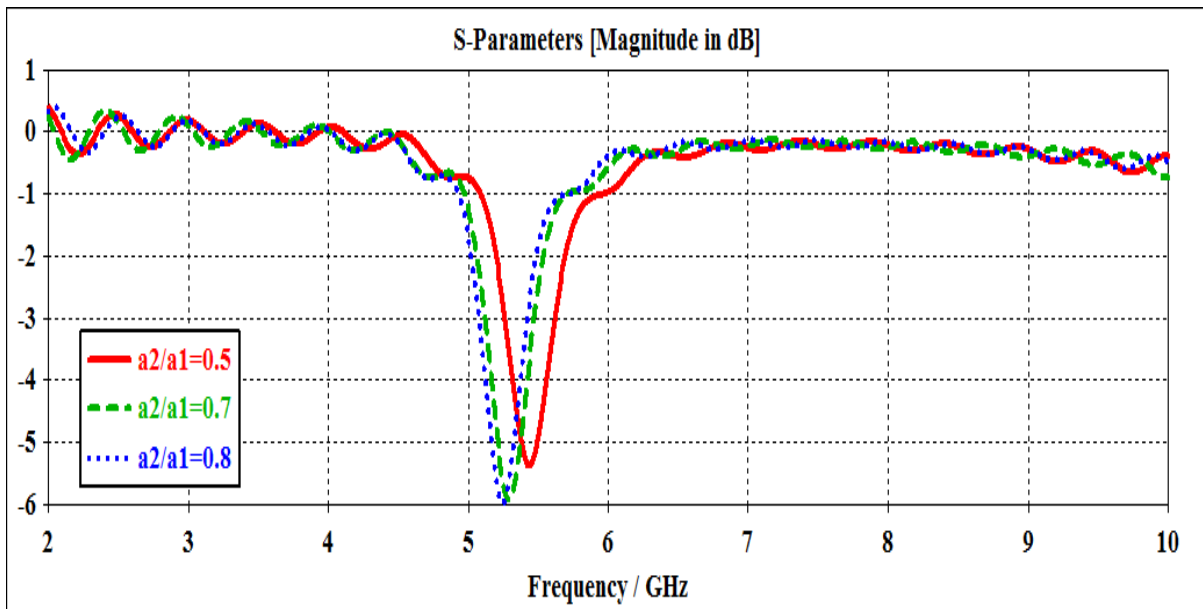


Figure3.44.The variation of the reflection coefficient magnitude with the frequency for for ratio of a_2 to a_1 ; (a)0.5, (b)0.7, (c)0.8.

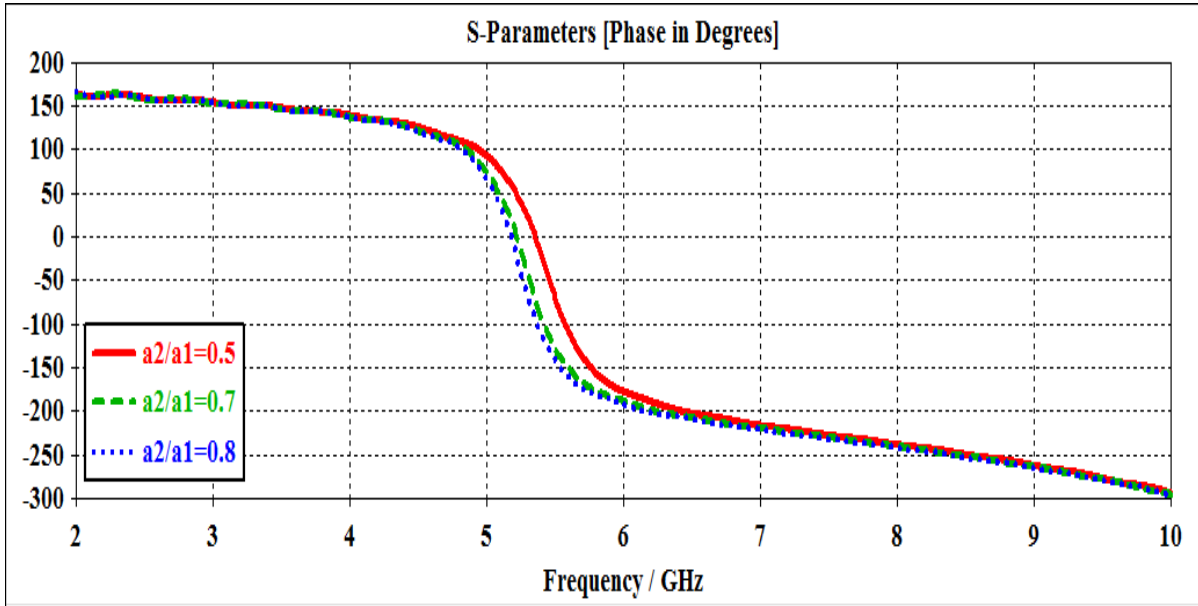


Figure 3.45. The variation of the reflection coefficient phase with the frequency for for ratio of a_2 to a_1 ; (a) 0.5, (b) 0.7, (c) 0.8.

3.10.2 The Dual Tapered Bowtie Element (horizontal electric field)

The same idea adopted in section 3.5.1 was used here, but the sides of the bowtie shape was tapered by half circles, as shown in Fig. 3.46. The ratio (a_2/a_1) where a_2 is the width of the inner bowtie and a_1 is the width of the outer bowtie is also used to describe the shape of the elements. As indicated in Fig. 3.47 and Fig. 3.48 the reflection point for each tested values of a_1 and a_2 occurs at frequency around 6 GHz with sharp linear phase region at the same frequency as the disparity between the three curves. The outer dimension (width) of the three cases was 10 mm, and hence the resonance frequency was around 6 GHz. This indicates that the inner bowtie has small effect on the resonance frequency.

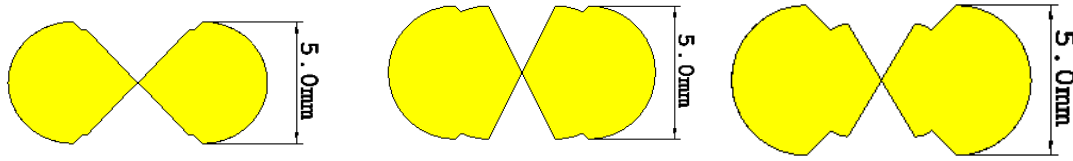


Figure 3.46: Geometries of the investigated dual tapered bowtie element.

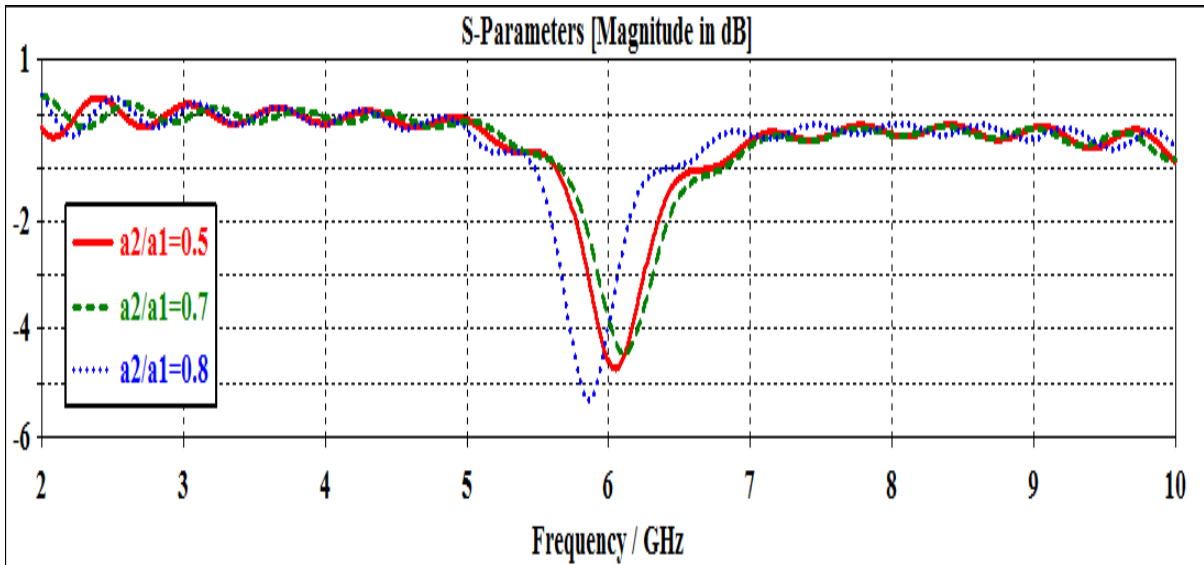


Figure3.47. The variation of the reflection coefficient magnitude with the frequency for for ratio of a2 to a1;(a)0.5,(b)0.7,(c)0.8.

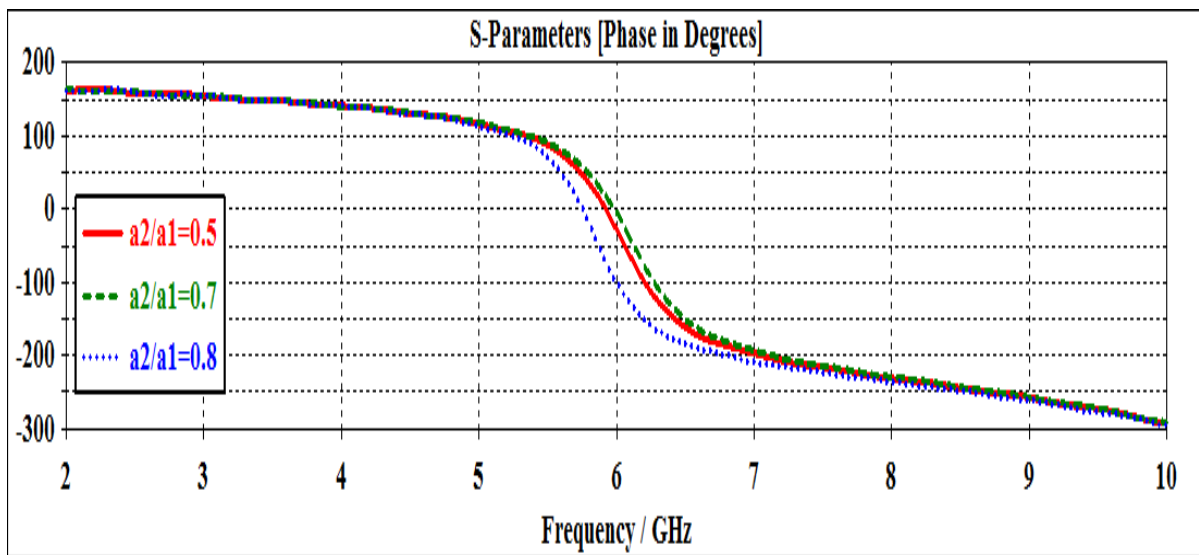


Figure3.48. The variation of the reflection coefficient phase with the frequency for for ratio of a2 to a1;(a)0.5,(b)0.7,(c)0.8.

3.11 Elliptical Bowtie

The proposed last model aims to reduce the sharp edges of the bowtie by replacing the use of a triangle with an elliptical shape, while still maintaining the conventional bowtie appearance as illustrated in the Fig.3.49. The obtained results from the various simulations are shown in Figs. 3.50 and 3.51.

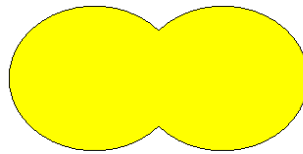


Figure 3.49 Geometry of the investigated elliptical bowtie element at $a=b$ mm.

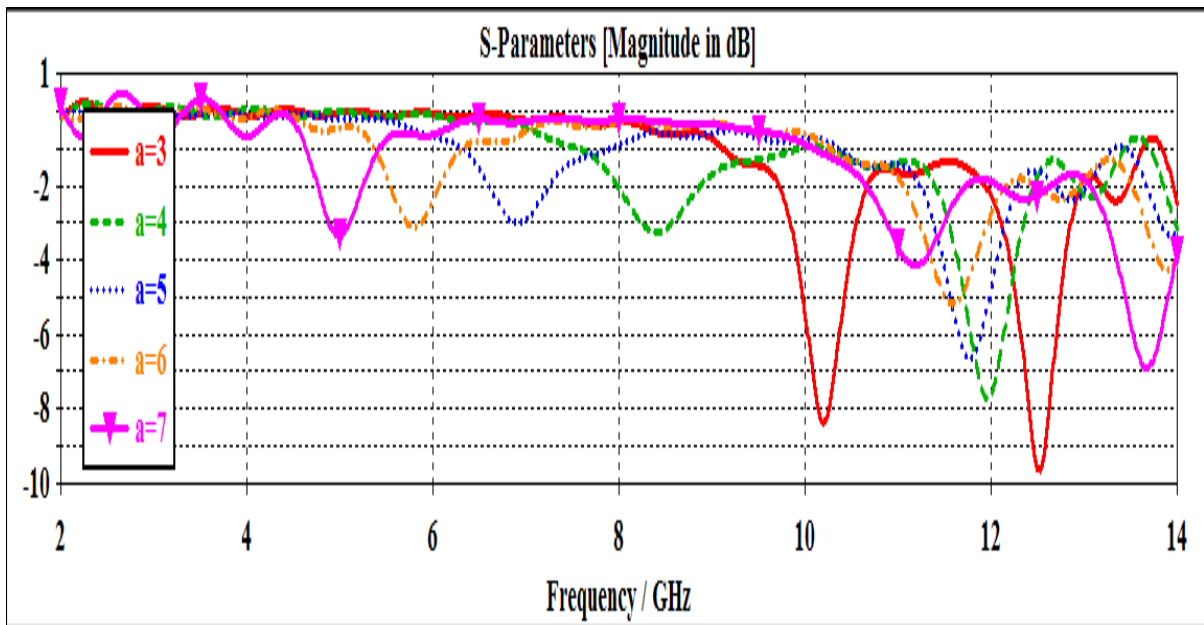


Figure 3.50. The variation of the reflection coefficient magnitude with the frequency for various values of element size.

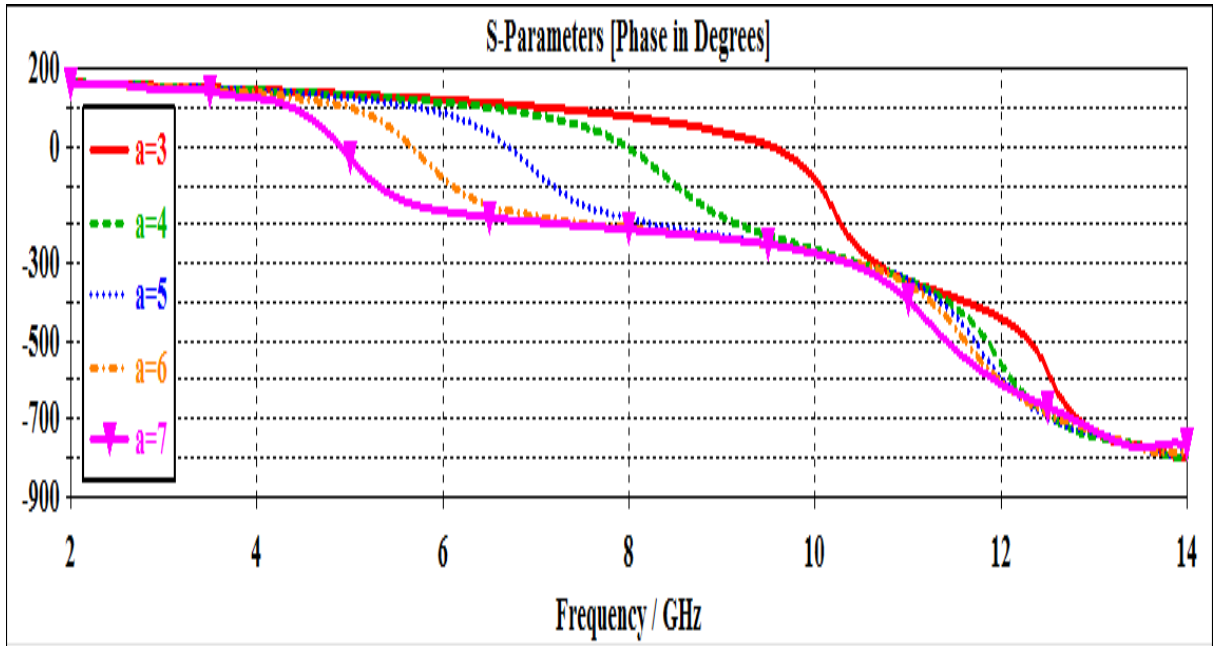


Figure 3.51. The variation of the reflection coefficient phase with the frequency for various values of element size.

Based on the information given in Fig.3.50 and Fig.3.51, the phase relationship with the width of the element is plotted in Fig.3.52. It is compared with the phase response of the classic bowtie antenna under the same conditions $a=b$, (see Table 3.5). It can be seen from the phase responses and the table that the elliptical bowtie offers smaller slope compared to the bowtie but at the expense of reduced phase range.

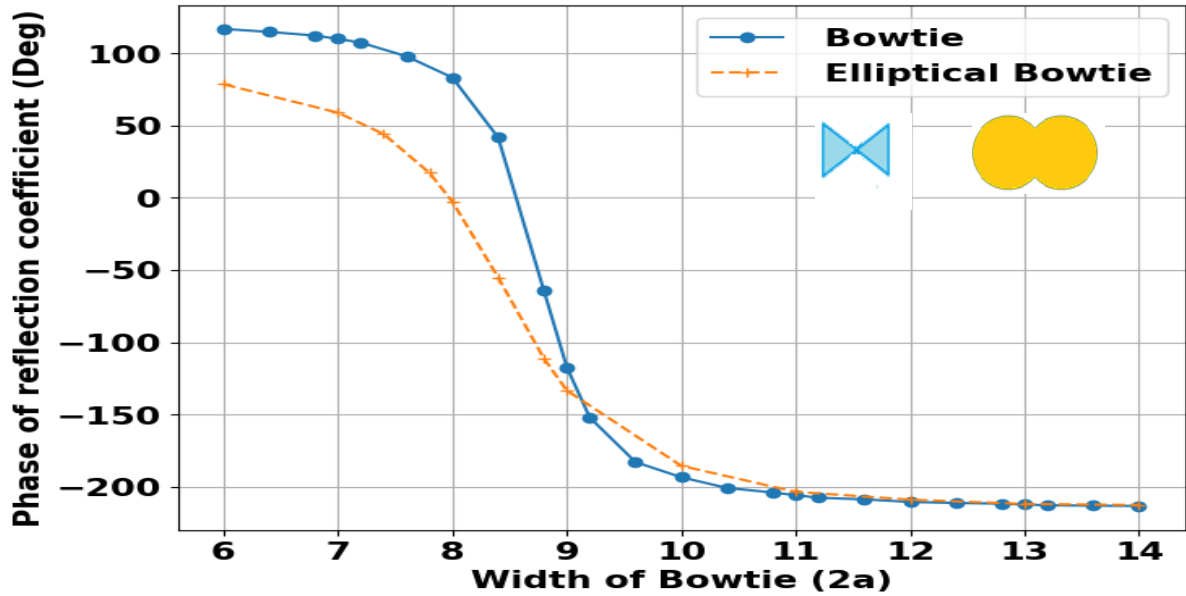


Figure 3.52. The variation of the reflection phase with the element width ($2a$) of the triangular and elliptical bowtie elements at the center frequency of 8 GHz.

Table 3.5. Phase response characteristics of bowtie and elliptical bowtie element cell reflectarray antenna..		
Name	Bowtie	Elliptical bowtie
Max phase	117	78.7
Min phase	-212.3	-212.6
Phase Center	-47.6	-66.9
Element size for phase center	8.4	8.4
Phase range	329.3	291.3
Slope ($^{\circ}/\text{mm}$)	166.3	96.1
Slope (linear region) ($^{\circ}/\text{GHz}$)	386.4	132.2

3.12 Effective dielectric constant (ϵ_{reff}):

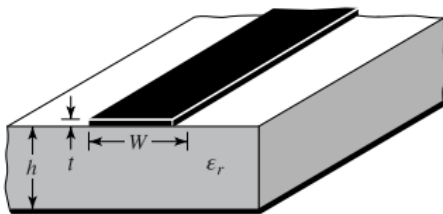
The unit cell representing the reflectarray is formed of a conducting patch on a grounded dielectric substrate. The electric field cannot be confined between the patch and the ground plane and some its fraction fringes outside. The electric field lines thus extend in the air. The effective dielectric constant is defined as value of a uniform dielectric material, which allows patch shown in Fig.3.53b to have the same electrical characteristics as the actual patch without fringing. The effective dielectric constant is given by this formula [38]:

$$\epsilon_{\text{reff}} = \frac{\epsilon_r + 1}{2} + \frac{\epsilon_r - 1}{2} \left[1 + 12 \frac{h}{w} \right]^{-1/2} \dots\dots\dots (3.1)$$

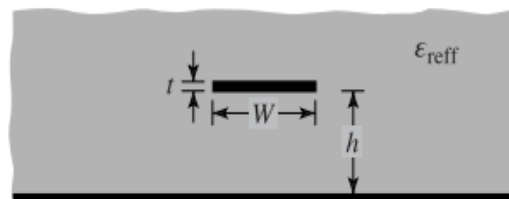
Where ϵ_r is the relative permittivity of the substrate that has a thickness of h , the patch size is W .

As the effective relative permittivity is defined by Eq.3.1, then the effective wavelength λ_{eff} corresponding to a frequency f can be given by Eq.3.2: Where c is speed of light in vacuum, λ_0 is wavelength in free space .

$$\lambda_{\text{eff}} = \frac{c}{f\sqrt{\epsilon_{\text{reff}}}} = \lambda_0 / \sqrt{\epsilon_{\text{reff}}} \dots\dots\dots (3.2)$$



(a) Microstrip line



(b) Effective dielectric constant

Figure3.53.(a) Microstrip line ,(b) Effective dielectric constant[38].

3.13 Resonance frequency (fr)

The resonance frequency of an antenna is that specific frequency at which the antenna operates most efficiently. The resonance frequency of an antenna is determined by its physical dimensions, such as length or geometry, and the electrical properties of the surrounding environment. The resonant frequency of the bow-tie patch's dominant TM_{10} mode can be determined using a modified set of design equations. These equations are derived from the semi-empirical design equations for rectangular patch, as referenced in [73]. By utilizing the modified design equations, one can accurately calculate the resonant frequency of the solid bowtie patch for its dominant mode.

$$f_r = \frac{c}{2\sqrt{\epsilon_e}L} \left(\frac{1.152}{R_t} \right) \dots\dots\dots (3.3)$$

$$R_t = \frac{L}{2} \frac{(W+2\Delta l)+(W_c+2\Delta l)}{(W+2\Delta l)(S+2\Delta l)} \dots\dots\dots (3.4)$$

$$\Delta l = h \frac{0.412(\epsilon_e+0.3)\left(\frac{W_i}{h}+0.262\right)}{(\epsilon_e-0.258)\left(\frac{W_i}{h}+0.813\right)} \dots\dots\dots (3.5)$$

$$W_i = \frac{W+W_c}{2} \dots\dots\dots (3.6)$$

since $W_c=0$, because there is no cut at the tip of the triangle, then

$$W = \frac{0+b}{2} = \frac{b}{2} \dots\dots\dots (3.7)$$

This set of design equations involves variables denoted as the thickness, relative permittivity, and effective permittivity of the substrate and effective wavelength, represented as: h , ϵ_r and ϵ_e , λ_{eff}

respectively. The geometric parameters are defined in Fig. 3.54 where W represented in our design by b and s by $2a$.

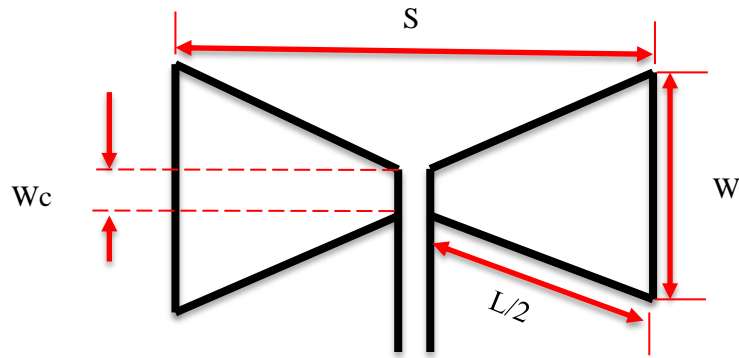


Figure 3.54. Detailed design geometry of the entire structure including the solid bowtie .

Table 3.6 is a tabular representation of various design parameters for a solid bowtie antenna with different configurations for case fixed (a) at 4mm and changing b according to [73] where $W=b/2$.The effective relative permittivity ϵ_{reff} as given by the above equations, increases as the value of b increases. The increase in ϵ_{reff} leads to a decrease in the effective wavelength according to the following relation (3.2). A dipole resonates at a certain frequency when its length is $\frac{1}{2}$ wavelength. However, in bowtie ,the height of the dipole (b) also affects the resonance frequency. Such relation describing such effect can be deduced from the data listed in Table 3.6

It can be seen from the Table that the ratio $2a/ \lambda_{\text{eff}}$ is changing between 0.312 to 0.260 for the lower resonance frequency. On the other hand, it changes from 0.523 to 0.54 for the upper resonance frequency. The changes can be attributed to the variation in height b of the bowtie shape.

The resonance frequency found from the results shown in Table 3.6, as were found from the CST simulation, can be related to the dimensions of the bowtie shape by the following formula.

$$f = K_1 \times \text{Horizontal Dimention} + K_2 \times \text{Vertical Dimension} \dots\dots\dots (3.8)$$

Here f is in GHz, dimensions are in mm, K_1 and K_2 are proportionality factors. For the shown dimensions in Fig.3.4 we have

$$f = K_1 \times 2a + K_2 \times b \dots\dots\dots (3.9)$$

The two constants K_1 and K_2 can be found from the data listed in Table 3.7. We find the K_1 and K_2 for lower band and upper band. The error rate is approximately 1.5%, and at high frequencies, it appears that it does not depend on the dimensions.

Table 3.6. Calculated features of bowtie element at fixed a=4 and various values of b.								
a	b	fr(GHz)	W	ϵ_{reff}	$\lambda_o(\text{mm})$	$\lambda_{\text{eff}}(\text{mm})$	$2a/\lambda_{\text{eff}}$	b/λ_{eff}
4	3	6.8	1.5	2.96	44.1	25.6	0.312	0.11
4	3	11.4	1.5	2.96	26.3	15.28	0.523	0.196
4	4	6.5	2	3.017	46.1	26.54	0.30	0.15
4	4	11.4	2	3.017	26.3	15.14	0.528	0.264
4	5	6.2	2.5	3.057	48.3	27.6	0.289	0.18
4	5	11.4	2.5	3.057	26.3	15.04	0.531	0.332
4	6	6.0	3	3.09	50	28.4	0.281	0.21
4	6	11.4	3	3.09	26.3	14.96	0.534	0.401
4	7	5.7	3.5	3.12	52.6	29.7	0.269	0.23
4	7	11.4	3.5	3.12	26.3	14.88	0.537	0.47
4	8	5.5	4	3.15	54.5	30.7	0.260	0.26
4	8	11.4	4	3.15	26.3	14.81	0.54	0.54

Table 3.7 K_1 and K_2 calculations.									
Lower Band					Upper Band				
a	b	fr	K_1	K_2	a	b	fr	K_1	K_2
4	3,4	6.8,6.5	0.96	-0.3	4	3,4	11.4,11.4	1.425	0
4	4,5	6.5,6.2	0.96	-0.3	4	4,5	11.4,11.4	1.425	0
4	5,6	6.2,6	0.9	-0.2	4	5,6	11.4,11.4	1.425	0
4	6,7	6,5.7	0.975	-0.3	4	6,7	11.4,11.4	1.425	0
4	7,8	5.7,5.5	0.88	-0.2	4	7,8	11.4,11.4	1.425	0
average			0.935	-0.26	average			1.425	0

According to [74] where the authors considered $W = b$, then $\lambda_{\text{eff}} = \lambda_o/\sqrt{\epsilon_{\text{reff}}}$. Table 3.8 is a continuation of the previous table representing different

design configurations of a bowtie antenna along with their corresponding parameters. In this dataset, the unit cell width "W" is equal to the unit cell height "b", and the effective wavelength " λ_{eff} " is calculated using the formula " $\lambda_0/\sqrt{\epsilon_{\text{reff}}}$ ".

Table 3.8 is a confirmation of what was deduced with the difference of the values of the b. The variations in dimensions and resonant frequencies allow for optimizing the antenna's performance for specific applications. Shows various dimensions of the bowtie antenna "a" and "b" and their corresponding resonant frequencies for different configurations. Additionally, it provides values for the effective relative permittivity ϵ_{reff} , free space wavelength λ_0 (mm), effective wavelength λ_{eff} (mm), as well as the ratios " $2a/\lambda_{\text{eff}}$ " and " b/λ_{eff} ".

The resonance frequency is typically based on its length, generally half a wavelength in this case of a bowtie configuration, the height of the dipole (b) additionally impacts the resonance frequency.

It can be seen from the table that the ratio $2a/\lambda_{\text{eff}}$ is changing between 0.318 to 0.267 for the lower resonance frequency. On the other hand, it changes from 0.534 to 0.55 for the upper resonance frequency. The changes can be attributed to the variation in height b of the bowtie shape. This type of data is often crucial in antenna design research and development, as it provides valuable insights into the antenna's characteristics and helps engineers and researchers select the most suitable configuration for their intended applications .

Table 3.8 Calculated features of bowtie element at W=b.								
a	b	fr(GHz)	W	ϵ_{reff}	$\lambda_o(\text{mm})$	$\lambda_{\text{eff}}(\text{mm})$	$2a/\lambda_{\text{eff}}$	b/λ_{eff}
4	3	6.8	3	3.09	44.11	25.09	0.318	0.119
4	3	11.4	3	3.09	26.3	14.96	0.534	0.20
4	4	6.5	4	3.15	46.15	26	0.30	0.153
4	4	11.4	4	3.15	26.3	14.81	0.540	0.27
4	5	6.2	5	3.21	48.38	27	0.296	0.185
4	5	11.4	5	3.21	26.3	14.67	0.545	0.34
4	6	6.0	6	3.25	50	27.73	0.288	0.216
4	6	11.4	6	3.25	26.3	14.58	0.548	0.411
4	7	5.7	7	3.29	52.63	29	0.275	0.241
4	7	11.4	7	3.29	26.3	14.49	0.552	0.48
4	8	5.5	8	3.33	54.54	29.88	0.267	0.267
4	8	11.4	8	3.33	26.3	14.41	0.555	0.555

Table 3.9 is a tabular representation of various design parameters for a solid bowtie antenna with different configurations but here for case fixed b at 4mm and changing a according [73] where $W=b/2$. The Table 3.9 also includes same parameters previous Tables 3.6, 3.8. The effective relative permittivity ϵ_{reff} is value is not affected by the change a because the equation depends on the value of b.

A dipole resonates at a certain frequency when its length almost 1/4 wavelength for lower band and its length almost 1/2 wavelength for upper band. However, in bowtie dipole, the width of the dipole "a" also affects the resonance frequency. Such relation describing such effect can be deduced from the data listed in Table 3.9. It can be seen from the table that the ratio $2a/\lambda_{\text{eff}}$ is changing between 0.27 to 0.3 for the lower resonance frequency. On the other hand, it changes from 0.4 to 1 for the upper resonance frequency. The changes can be attributed to the variation in width a of the bowtie shape. The resonance

frequency found from the results shown in Table 3.9, as were found from the CST simulation, can be related to the dimensions of the bowtie shape by same formula .

$$f=K1 *horizontal dimension + K2 * vertical dimension$$

Here f is in GHz, dimensions are in mm, K1 ad K2 are proportionality factors.

$$we\ have\ f= K1 *2a + K2 * b$$

The two constants K1 and K2 can be found from the data listed in Table 3.10

$f=K1 *horizontal dimension + K2 * vertical dimension$.For the data in the table 3.9, we have $f= K1 *2a + K2 * b$,We find the K1 And K2 for lower band and upper band at Table 3.10, highest error rate is approximately 13.2%.

Table 3.9. Calculated features of bowtie element at fixed b=4 and various values of a .								
a	b	fr(GHz)	W(mm)	ϵ_{reff}	$\lambda_o(mm)$	$\lambda_{eff}(mm)$	$2a/ \lambda_{eff}$	b/ λ_{eff}
3	4	8	2	3.017	37.5	21.5	0.27	0.18
3	4	11.5	2	3.017	26	14.96	0.4	0.26
4	4	6.5	2	3.017	46.15	26	0.3	0.15
4	4	11.4	2	3.017	26.3	15.14	0.52	0.26
5	4	5.5	2	3.017	54.5	31.37	0.31	0.12
5	4	11.4	2	3.017	26.3	15.14	0.79	0.26
6	4	4.7	2	3.017	63.36	36.47	0.32	0.10
6	4	11.3	2	3.017	26.5	15.25	0.78	0.26
6	4	13.8	2	3.017	22	12.66	0.94	0.31
7	4	4.1	2	3.017	73.1	42	0.33	0.09
7	4	11.2	2	3.017	26.7	15.37	0.91	0.26
7	4	13.5	2	3.017	22.2	12.7	1.1	0.314
8	4	3.6	2	3.017	83.3	47.9	0.33	0.03
8	4	10.8	2	3.017	27.7	15.9	1	0.25
8	4	13	2	3.017	23	13.2	1.2	0.30

Table 3.10. K_1 and K_2 calculations									
Lower Band					Upper Band				
a	b	fr	K1	K2	a	b	fr	K1	K2
3,4	4	8,6.5	-0.75	3.125	3,4	4	11.5,11.4	-0.05	2.96
4,5	4	6.5,5.5	-0.5	2.625	4,5	4	11.4,11.4	-0.5	2.625
5,6	4	5.5,4.7	-0.4	2.375	5,6	4	11.4,11.3	-0.05	2.975
6,7	4	4.7,4.1	-0.3	2.075	6,7	4	11.3,11.2	-0.05	2.975
7,8	4	4.1,3.6	-0.25	1.9	7,8	4	11.2,10.8	-0.2	3.625
average			-0.44	2.4	average			0.17	3

In order to confirm what has been concluded, the following Table 3.11 will be similar to the previous table, but according to [74] researcher considered that $W=b$, that The effective relative permittivity ϵ_{reff} and its value is not affected by the change a because the equation depends on the value of b but resonance frequency is affected because to change the size. But the difference here. It can be seen from the table that the ratio $2a/\lambda_{\text{eff}}$ is changing between 0.28 to 0.34 for the lower resonance frequency. On the other hand, it changes from 0.41 to 1.2 for the upper resonance frequency and this is due to the difference in resonance frequency.

Table 3.11. Calculated features of bowtie element at fixed b=4 and various values of a .								
a	b	fr(GHz)	W(mm)	ϵ_{reff}	$\lambda_o(\text{mm})$	$\lambda_{\text{eff}}(\text{mm})$	$2a/\lambda_{\text{eff}}$	b/λ_{eff}
3	4	8	4	3.15	37.5	21.12	0.28	0.18
3	4	11.5	4	3.15	26	14.6	0.41	0.27
4	4	6.5	4	3.15	46.15	26	0.30	0.15
4	4	11.4	4	3.15	26.3	14.8	0.54	0.27
5	4	5.5	4	3.15	54.5	30.7	0.32	0.13
5	4	11.4	4	3.15	26.3	14.8	0.67	0.27
6	4	4.7	4	3.15	63.36	35.6	0.33	0.112
6	4	11.3	4	3.15	26.5	14.9	0.8	0.26
6	4	13.8	4	3.15	22	12.3	0.97	0.32
7	4	4.1	4	3.15	73.1	41.1	0.34	0.09
7	4	11.2	4	3.15	26.7	15	0.93	0.26
7	4	13.5	4	3.15	22.2	12.5	1.12	0.32
8	4	3.6	4	3.15	83.3	46.9	0.34	0.08
8	4	10.8	4	3.15	27.7	15.6	1	0.25
8	4	13	4	3.15	23	12.9	1.2	0.31

CHAPTER FOUR

INVESTIGATION INTO PROPOSED DOUBLE RING

UNIT CELLS OF THE REFLECTARRAYS

4.1 Introduction

The reflectarrays consist of multiple elements that reflect the incident rays from a feed antenna located in front of the array. Each element must provide the required reflection phase, which was set in the design stage, or the reflectarray performance will be degraded because of reflection phase errors. The errors can also occur if the array element fails to provide the exact value of the required reflection phase range. To cover all possible phase values, a phase range of no less than 360° must be provided. Various approaches have been proposed in the past to provide phase range of more than 360° . Those included the use of variable-size patches for obtaining the required phase range with a small slope [75]. In the case of microstrip patch elements, achieving a phase range close to 360° comes at the cost of a steep slope in the phase as the patch size varies. Unfortunately, this sharp slope brings about a reduction in the bandwidth of the array elements and poses challenges in manufacturing. Striking a balance between these two aspects, phase range and small slope, consequently restricts the bandwidth of the reflectarray. Aiming to solve the problem of limited phase range and consequently small bandwidth in single-layer patch reflectarrays, there are two possible approaches. The first is to utilize multilayer variable-size patches [76]-[78], while the second option is to employ multiresonant broadband elements [55] [79][80]. Both these methods offer improved phasing range, lower slopes, and enhanced operational bandwidth for the reflectarray antenna as a whole. However, it is worth noting that multilayer variable size

patch reflectarrays come with their own set of challenges. Each layer needs to be manufactured individually, and the alignment and assembly of these layers must be done meticulously without any gaps. Consequently, this leads to increased manufacturing costs associated with this approach [81]. An enhanced version of a single-layer microstrip reflectarray element has been proposed, featuring a configuration of ring or double ring structures. This modification is designed to improve the performance of the reflectarray. By adjusting the size of these elements and increasing the thickness of the substrate, a significantly wider range of phase variation with a lower slope is achieved. This represents a notable improvement compared to conventional single-layer elements[7] [8][16][52]. Based on the selected shapes investigated in Chapter Three, ring and double-ring element configurations were designed and investigated in this chapter. This chapter focuses on the examination of these rings, and double-ring elements through simulation to verify their performance.

4.2 Single-Ring Bowtie Element

To enable a complete phase response range of 360° , the feasibility of using printed ring elements was explored. This approach aims to extend the operational capacity of the reflectarray by allowing the full swing of phase variation. Therefore, the designer can choose the right size of the element to supply the required phase shift of the element.

In this chapter, it is proposed to convert the bowtie shape into a ring with the same profile. The investigations start with evaluating the performance of the unit cell elements of the bowtie shape in the form of a ring and compare it with the patch shape, as shown in Fig.4.1. A microstrip reflectarray operating at center frequency of 8 GHz is considered using the unit cell approach. The reflectarray is assumed to be formed of identical elements arranged in a square

array of 20 mm periodicity. The used substrate is assumed to be comprised of two layers. The first layer used Taconic TLY-5 having relative permittivity $\epsilon_r = 2.2$, thickness $h_1=0.16$ mm, and tangent loss $\tan\delta=0.009$. The second layer is formed of foam having $\epsilon_r = 1.05$, thickness $h_2=3$ mm and zero loss. The unit cell was analyzed using the commercial electromagnetic software CST Microwave Studio. The overall shape was chosen to be a square with an outside length of 20 mm. The ring shape was generated in the CST software by scaling the initial bowtie shape with a factor S_1 , and subtracting the resulting shape from the original one. Therefore, the width of the ring $W_1= a (1- S_1)/2$, where S_1 is a scale factor less than unity.

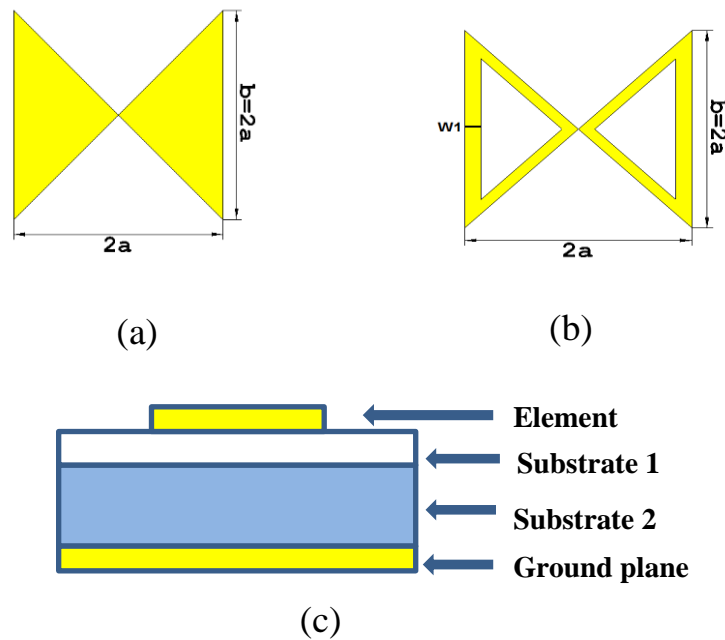


Figure 4.1. Geometries of the bowtie shape; (a) bowtie patch with $2a=b$, (b) bowtie ring with $2a=b$ and ring width $W_1= a (1- S_1)/2$, (c) side view showing the substrates.

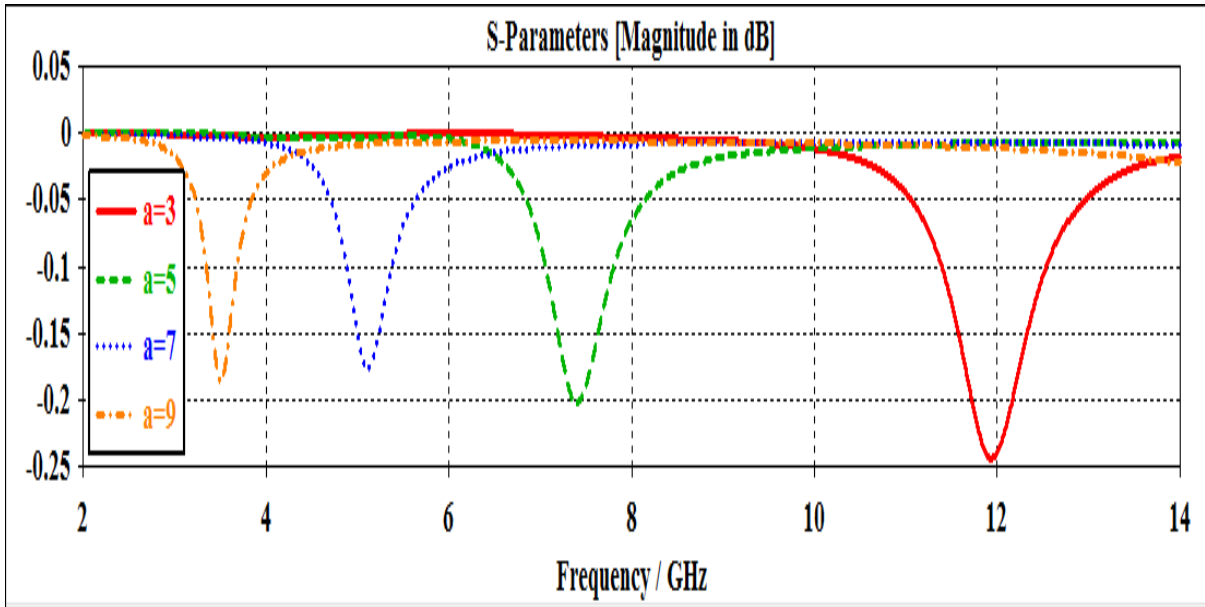


Figure 4.2. The variation of the reflection coefficient magnitude with the frequency for various bowtie sizes ($2a = b$).

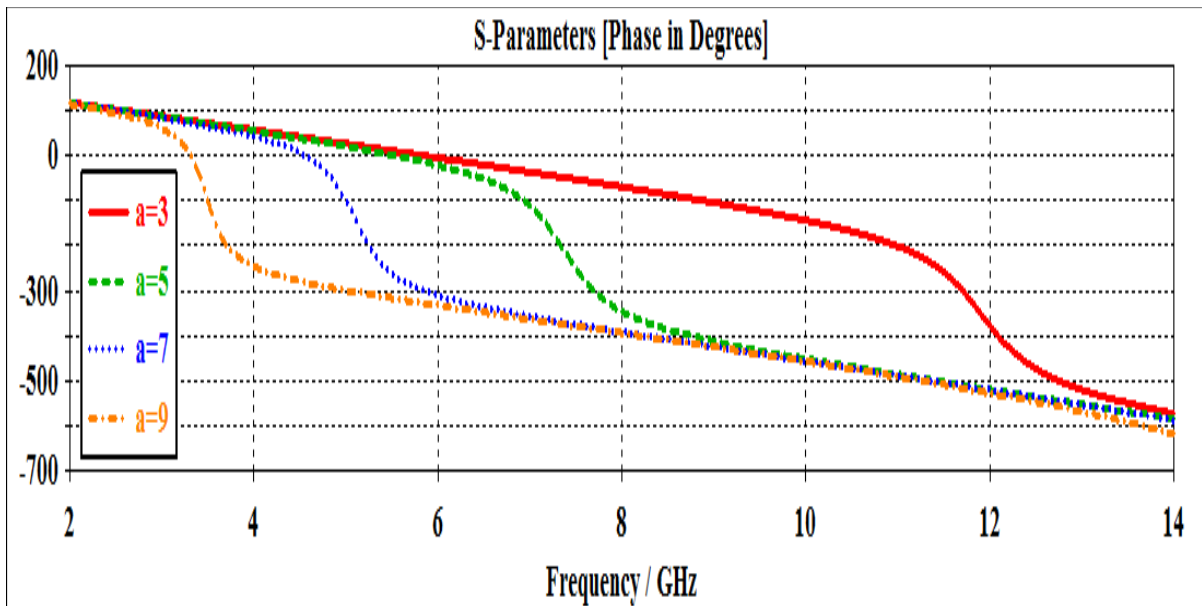


Figure 4.3. The variation of the reflection coefficient phase with the frequency for various bowtie sizes ($2a = b$).

In order to assess the effect of the width of the ring on the performance of the unit cell element, rings of various widths were simulated by varying the scale factor $S1$. The phase responses were determined from the resulting reflection coefficient, as shown in Fig.4.4, where the phase is plotted against the outer width $2a$ or the size of the bowtie ring. It can be seen from the figure that as the scale factor increases (smaller ring width), the phase slope increases. The smallest phase slope is obtained for the filled bowtie ($S1=0$). The detailed characteristics of the obtained responses are listed in Table 4.1.

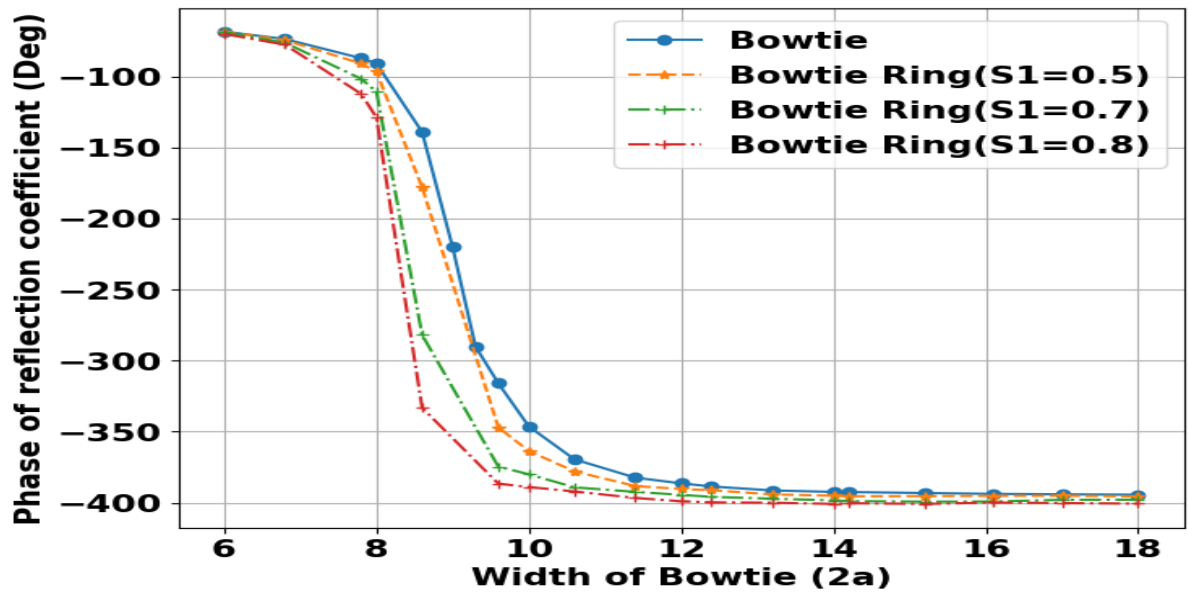


Figure 4.4. The variation of the reflection coefficient phase with the width of the bowtie ring at center frequency of 8 GHz..

Table 4.1. Phase response and characteristics of the bowtie and bowtie ring unit cells.				
Name	Bowtie	Bowtie ring S1 (0.5)	Bowtie ring S1(0.7)	Bowtie ring S1 (0.8)
Max phase	-68.2	-68.3	-68.6	-68.9
Min phase	-394.4	-395.6	-397.9	-400
Center phase	-231.3	-231.9	-233.2	-234.4
Element size for center phase	9	8.7	8.5	8.3
Phase range	326.2	327.3	329.3	331.1
Slope(deg /mm)	176.9	250.5	285.5	340.6
Slope (deg /GHz)	528.7	436.2	359.5	236

The configuration shown in Fig. 4.5 is generally similar to the previous case, but the two side rings are connected at the center of the bowtie to form a single conducting layer. The performance of this configuration is shown in Fig. 4.6 and 4.7. Fig. 4.8 shows the obtained phase response for various widths of the ring compared to that for the filled bowtie. It can be seen that as the width of the ring is reduced the phase slope increases and the phase range increases. Table 4.2 shows detailed comparison of the properties of the phase responses.

The improvement in slope is evident here as it gave a lower inclination compared to the previous case. This is due to the decrease in sharp edges in the center [82] .

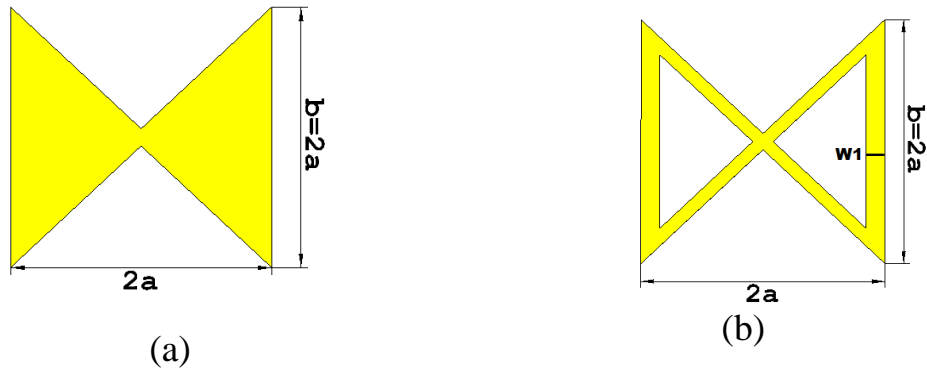


Figure 4.5. Geometries of the bowtie shape: (a) bowtie patch with $2a=b$, (b) bowtie ring with $2a=b$ and ring width $W1= a (1 - S1) / 2$.

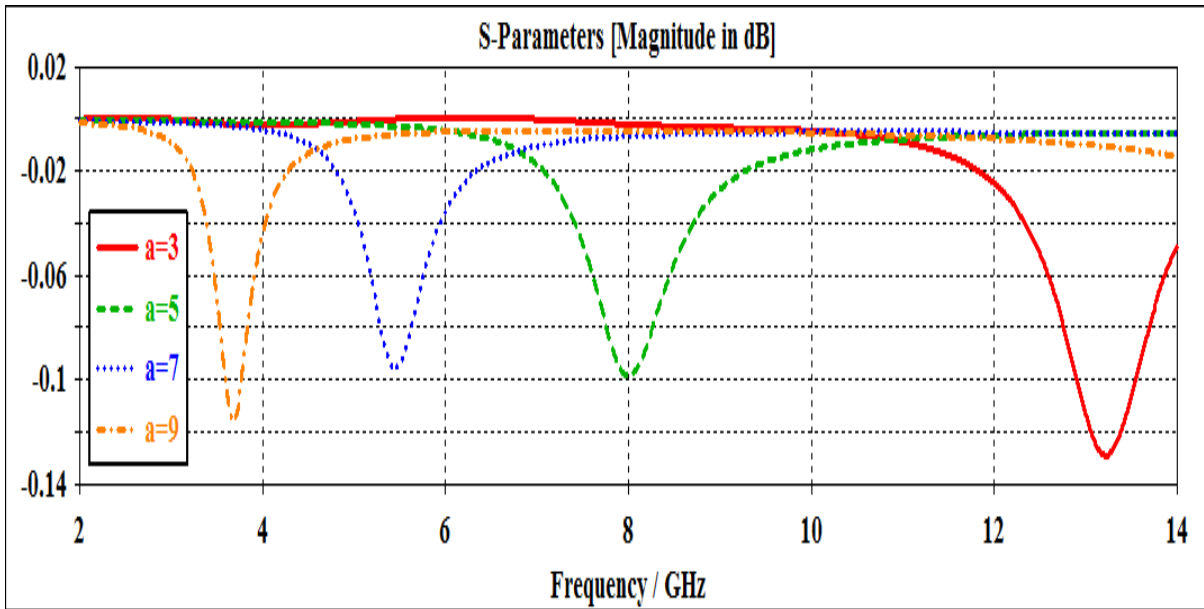


Figure 4.6. The variation of the reflection coefficient magnitude with the frequency for various bowtie sizes ($2a = b$).

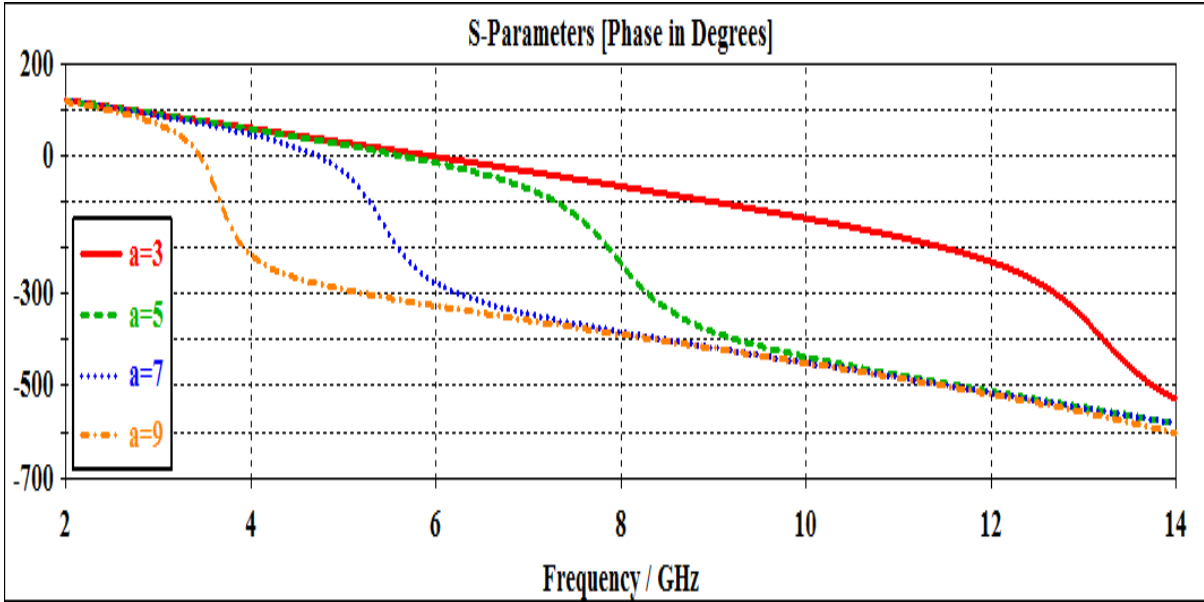


Figure 4.7. The variation of the reflection coefficient magnitude with the frequency for various bowtie sizes ($2a = b$).

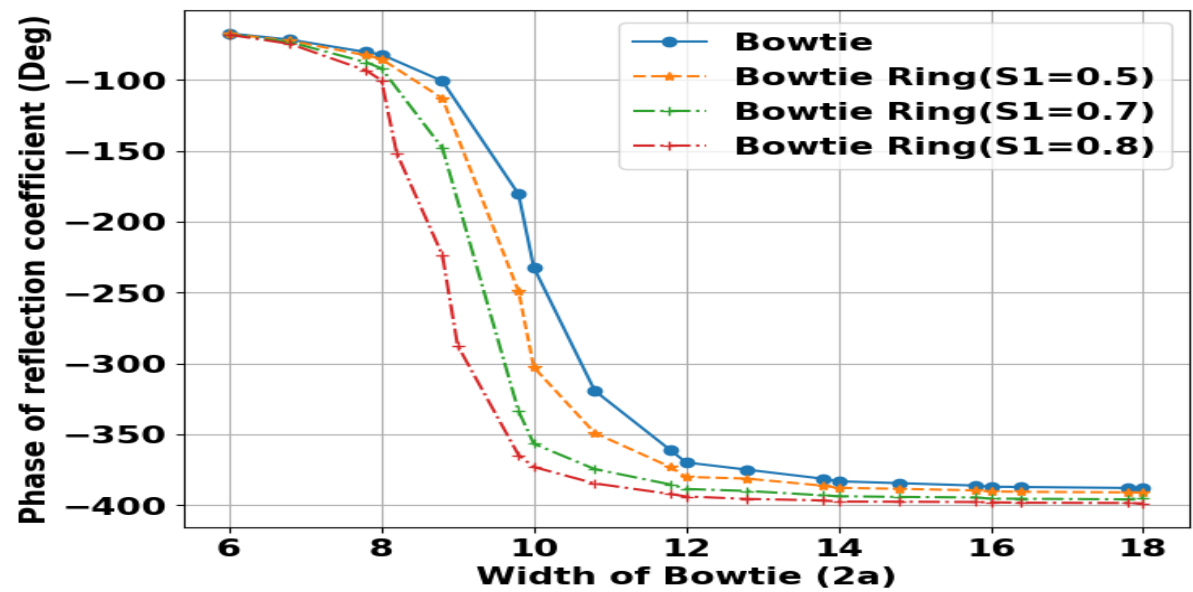


Figure 4.8. The variation of the reflection coefficient phase with width of bowtie at center frequency of 8 GHz.

Table 4.2.Phase response and characteristics of the bowtie and bowtie ring unit cell .				
Name	Bowtie	Bowtie ring S1 (0.5)	Bowtie ring S1 (0.7)	Bowtie ring S1(0.8)
Max phase	-67.2	-67.6	-68	-68.1
Min phase	-388.1	-391.1	-394.6	-397.8
Center phase	-227.6	-229.3	-231.3	-232.9
Element size	10	9.8	9.5	9
Phase range	320.9	323.5	326.6	329.7
Slope(deg /mm)	109.1	158	173.7	254.7
Slope (deg /GHz)	202.5	233.8	245.1	306.5

4.3 Bowtie Double Ring Element

When considering the design of a reflectarray, it is crucial to take into consideration the single or multiple resonating elements that compose the unit cell. To achieve multiple resonances, it is necessary for the unit cell to incorporate a significant number of resonating elements. The concept of utilizing stacked microstrip patches in multilayer microstrip reflectarrays already applies this principle [83]. This concept was extended to the design of multiple-resonant configurations within a single-layer unit cell, resembling the approach employed in multi- resonant microstrip reflectarrays [12][16][52]. As a result, dual ring element configurations were developed based on the classic bowtie shape that was investigated in Chapter Three. The performance of these double ring elements is being evaluated through simulation, as shown in the following subsections.

In the previous section, the extent to which the width of the ring affects the response was studied and analyzed. In this section, the unit cell is composed of

two rings. The inner ring is a scaled version of the outer ring. Referring to Fig. 4.5, if the outer dimensions of the outer ring are:

Width = $2a_1$, and height = $b_1=2a_1$, Then the inner ring was set as a scaled version of the outer ring, i.e. its dimensions are;

Width = $2a_2 = S_2 \times 2a_1$, and height = $b_2= S_2 b_1 = S_2 \times 2a_1$, where S_2 is a scale factor for inner ring. Due to the fact that the inner ring is a scaled version of the outer one, then the width of the inner ring W_2 will be $W_2 = S_2 \times W_1$, where the subscripts 2 and 1 refer to inner and outer rings respectively.

several cases of the double ring are analyzed in the following to select the appropriate shape.

4.3.1 First Case

Figure 4.9 shows the geometry of the proposed bowtie double ring unit cell. In this case, the two rings are connected at the center of the bowtie to form a single conducting layer as shown in Fig. 4.9, where the scale for width(W_1) of outer ring is $S_1=0.8$, inner ring $S_2=0.8$ and for height inner ring(b_2) is $S_2= 0.6$.

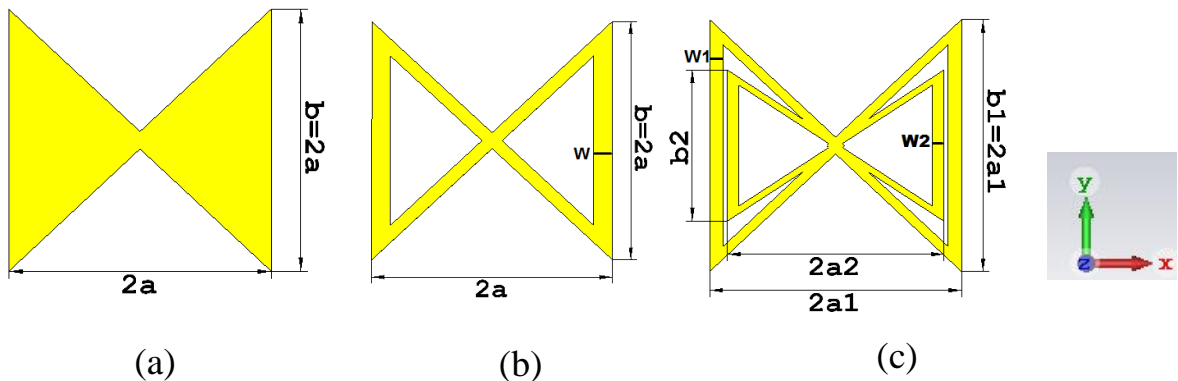


Figure 4.9. Geometry of the investigated of unit cell; (a)bowtie , (b)bowtie ring, (c) double ring bowtie element at $2a_1=b_1$.

Figures 4.10 and Fig.4.11 show the obtained results of the bowtie double ring unit cell simulations. Figure 4.10 shows the magnitude of the reflection coefficient, where it can be seen that for every size of the element there are two

resonance regions corresponding to the outer and inner rings. This finding is confirmed by examining the phase responses that are shown in Fig. 4.11, where two regions of fast changes can be easily seen. For example, when the width of the outer ring is set at ($2a_1=2 \times 7=14$ mm), the two regions are around the frequencies of 5 GHz and 7 GHz.

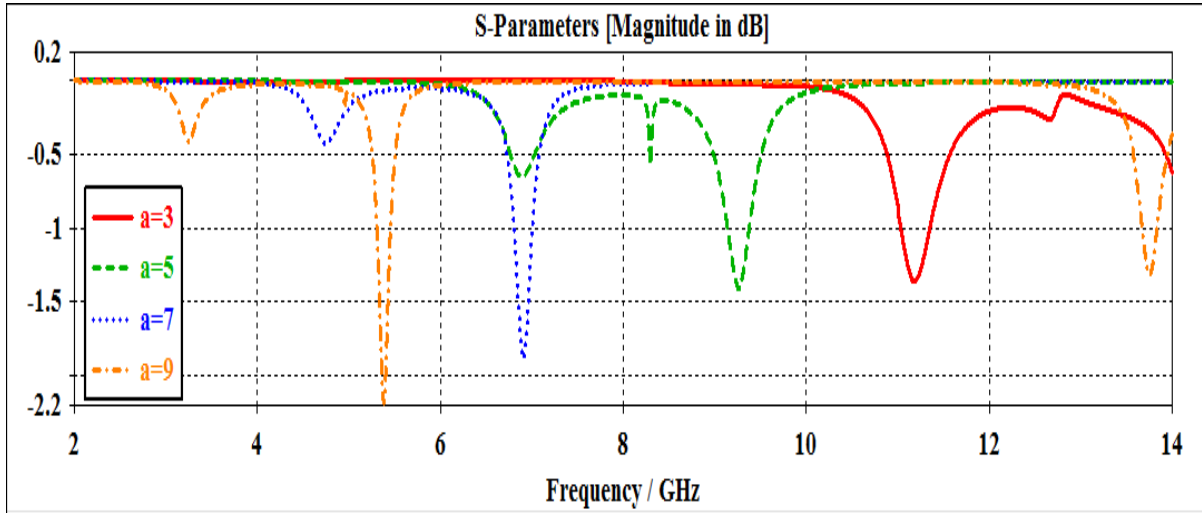


Figure 4.10: The variation of the reflection coefficient magnitude with the frequency for various double ring bowtie sizes ($2a_1=b_1$).

Figure 4.12 and Table 4.3 show the phase response of a bowtie and bowtie ring and bowtie double-ring unit cells at the center frequency of 8 GHz. Upon analysis, it becomes apparent that the bowtie double-ring has two linear regions, so the slope was calculated for the first region and the second region. It is noted that the phase of the reflection coefficient undergoes a change of more than 360° approaching 700° for the bowtie double ring.

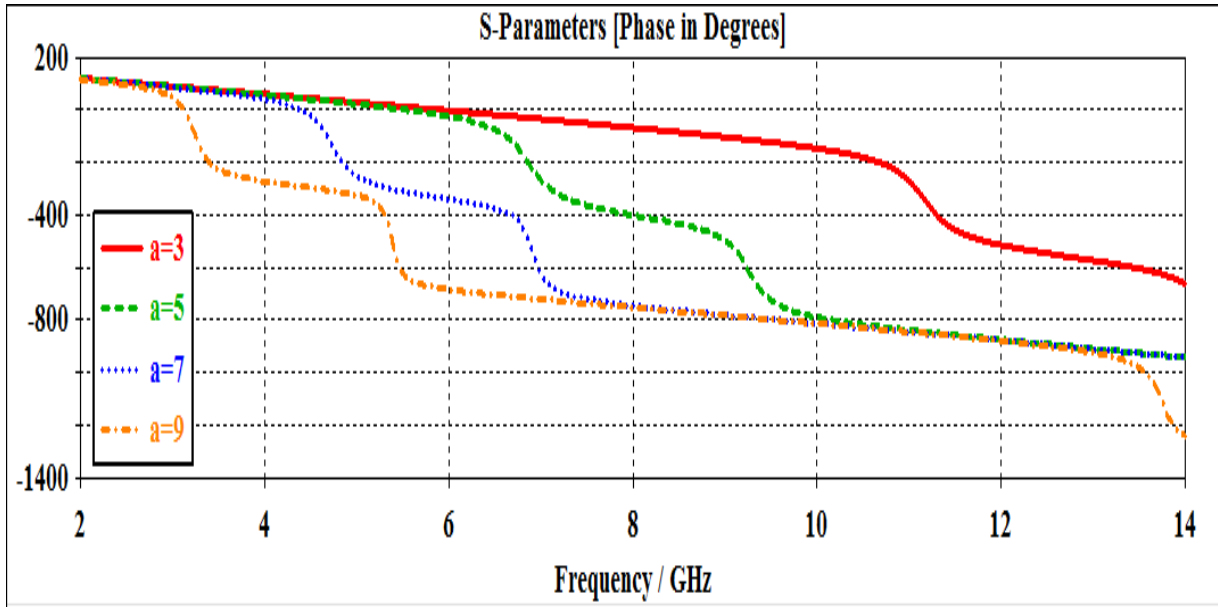


Figure 4.11. The variation of the reflection coefficient phase with the frequency for various double ring bowtie sizes ($2a_1=b_1$).

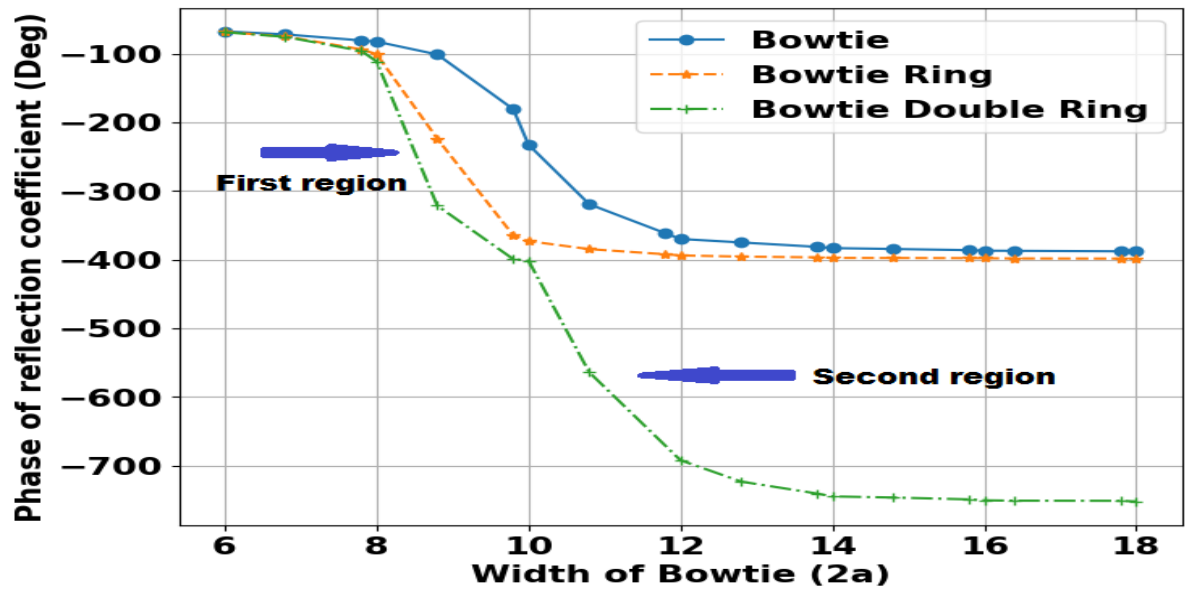


Figure 4.12. The variation of the reflection coefficient phase with the width of the bowtie at a center frequency of 8 GHz.

Table 4.3. Phase response and characteristics of the bowtie, ring bowtie, and bowtie double ring unit cells.				
Name	Bowtie	Bowtie ring	Bowtie double ring	
Max phase	-67.2	-68.1	-68.4	
Min phase	-388.1	-397.8	-752.2	
Center phase	-227.6	-232.9	-410.3	
Element size for phase center	10	9	9.8	
Phase range	320.9	329.7	683.8	
Slope(deg /mm)	109.1	254.7	Slop for First region	262.8
			Slop for Second region	145.4
Slope (deg /GHz)	202.5	306.5	Slop for First region	357.5
			Slop for Second region	473

The models in Fig.4.9 were compared to the classical shape of the bowtie under the same conditions for the inner ring dimension and the outer ring as shown in Fig.4.13. It turned out that it has a lower slope for both regions as shown in Fig.4.16 and listed in Table 4.4.

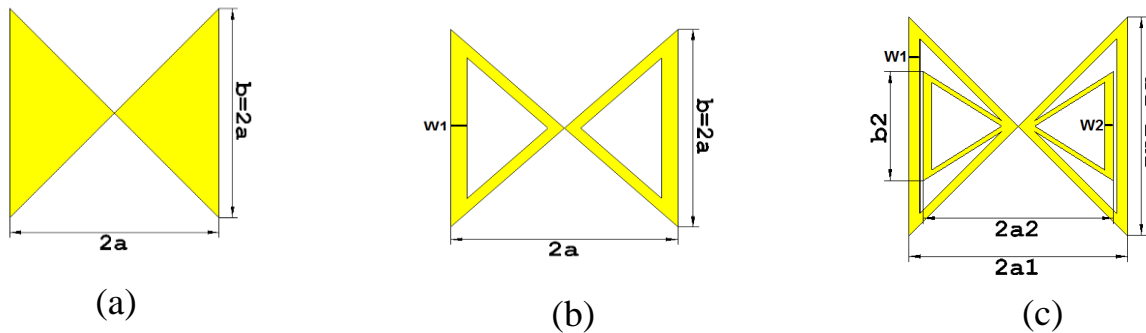


Figure 4.13. Geometry of the investigated unit cell; (a) bowtie, (b) bowtie ring, (c) double ring bowtie element at $b_1=2a_1$.

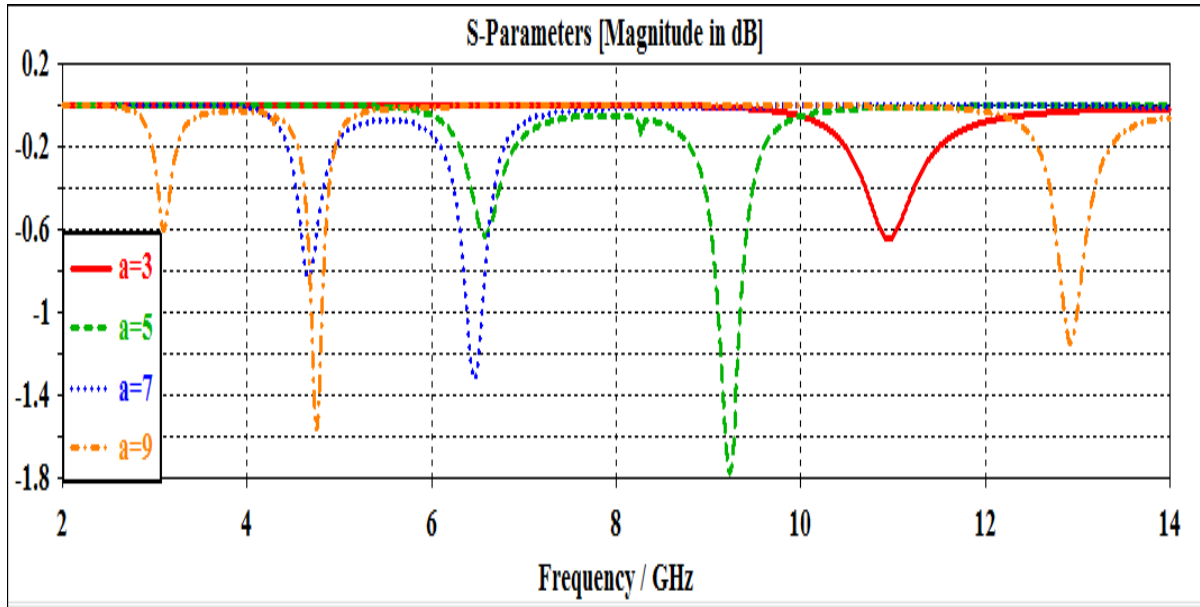


Figure 4.14. The variation of the reflection coefficient magnitude with the frequency for various double ring bowtie sizes ($2a_1 = b_1$).

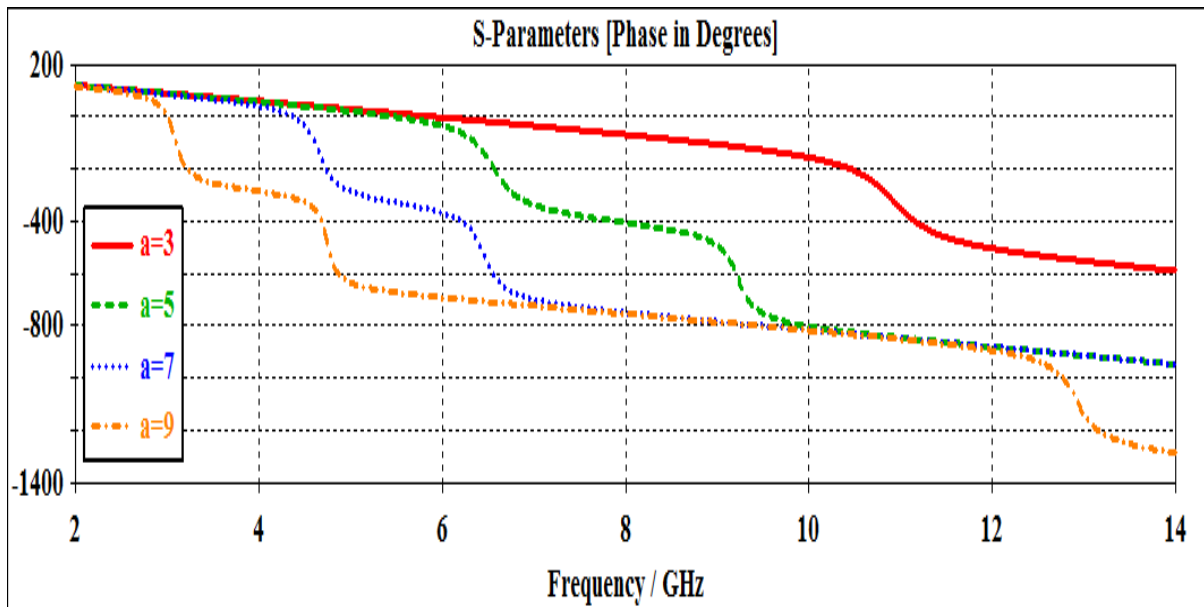


Figure 4.15. The variation of the reflection coefficient phase with the frequency for various double ring bowtie sizes ($2a_1 = b_1$).

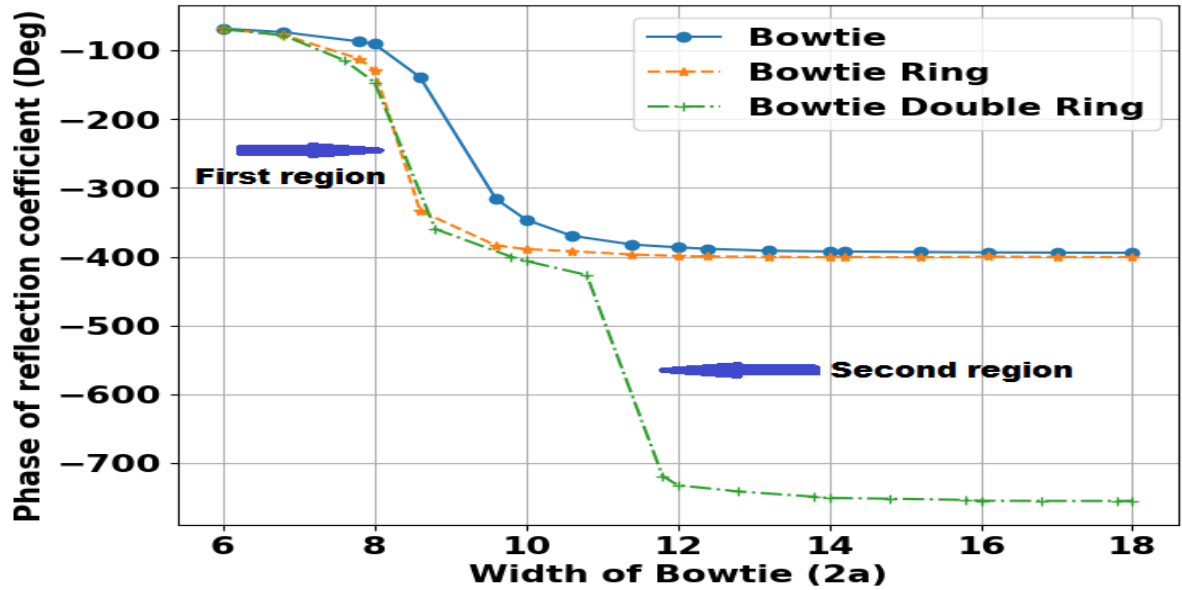


Figure 4.16. The variation of the reflection coefficient phase with width of bowtie at center frequency 8GHz.

Table 4.4. Phase response and characteristics of the bowtie , bowtie ring and bowtie double ring unit cell.

Name	Bowtie	Bowtie Ring	Bowtie double ring	
Max phase	-68.2	-68.9	-69.1	
Min phase	-394.4	-400	-755	
Center phase	-231.3	-234.4	-412	
Element size	9	8.3	10	
Phase range	326.2	331.1	685.9	
Slope(deg /mm)	176.9	340	Slop for First region	266.6
			Slop for Second region	292.3
Slope (deg /GHz)	528.7	236	Slop for First region	525.5
			Slop for Second region	482.2

4.3.2 Second Case

The difference of this case from the previous one is that the inner part is a filled bowtie, not a ring. The scale for the width of the outer ring was $S1=0.85$, while the scale for the width of the inner bowtie was $S2=0.8$ and for its height ($b2$) $S2=0.6$ as shown in Fig.4.17. From Fig 4.18 and Table 4.5, it is noted that the phase decreases with increasing slope for the first region, which indicates that it is not the most suitable model.

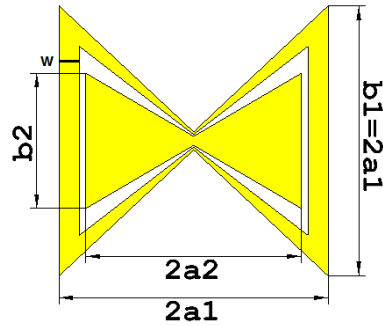


Figure 4.17. Geometry of the investigated of unit cell.

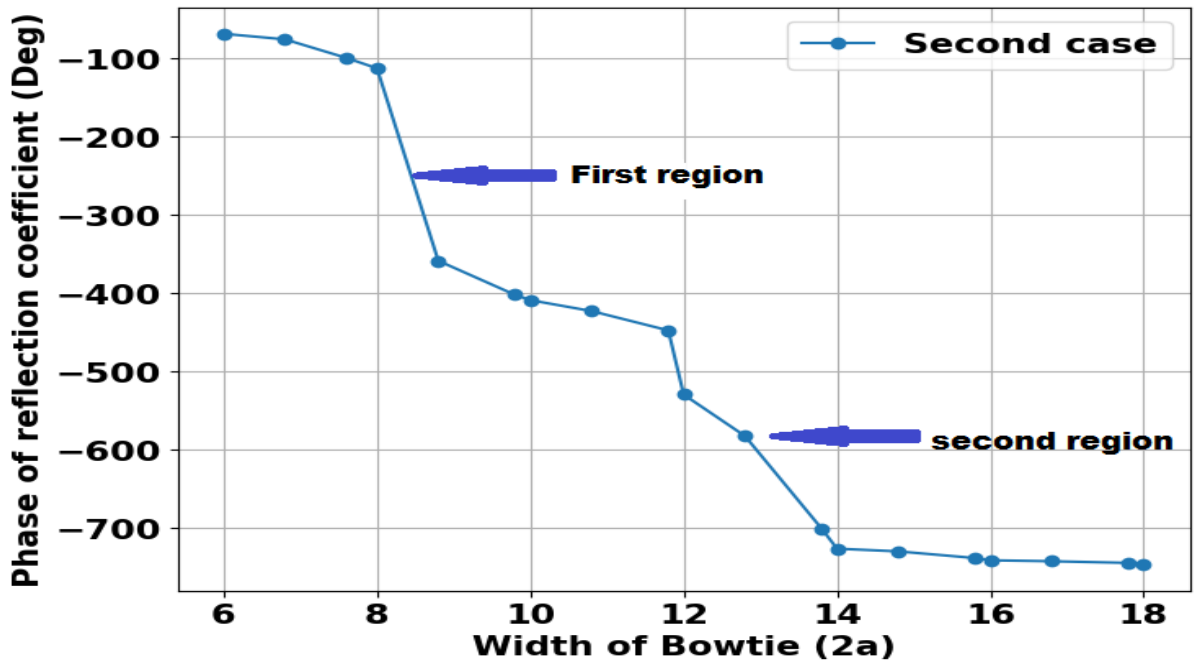


Figure 4.18. The variation of the reflection coefficient phase with width of bowtie at center frequency 8GHz.

Table 4.5. Phase response and characteristics of the Second case.		
Name	Bowtie double ring	
Max phase	-68.1	
Min phase	-745.8	
Center phase	-338.8	
Element size for center phase	8.6	
Phase range	677.7	
Slope(deg /mm)	Slop for First region	307.5
	Slop for Second region	98.4
Slope (deg /GHz)	Slop for First region	238.1
	Slop for Second region	330

4.3.3 Third case

The analysis of the wide double loop will be carried out, based on the previous results. It was reached by the fact that the wider the loop, giving the lowslope, as shown in Fig.4.19. From the results obtained in Fig.20 and table 4.6, a decrease in the phase range is observed as the second response region moves away. This happens due to the smallness of the inner ring, but it results in a lower slope.

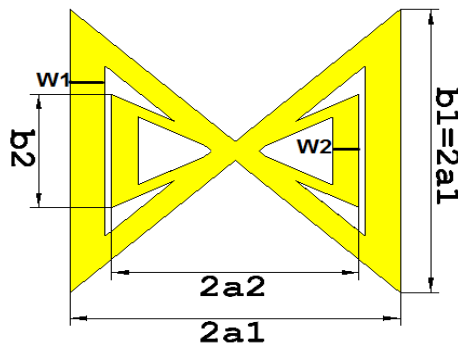


Figure 4.19. Geometry of the investigated of unit cell.

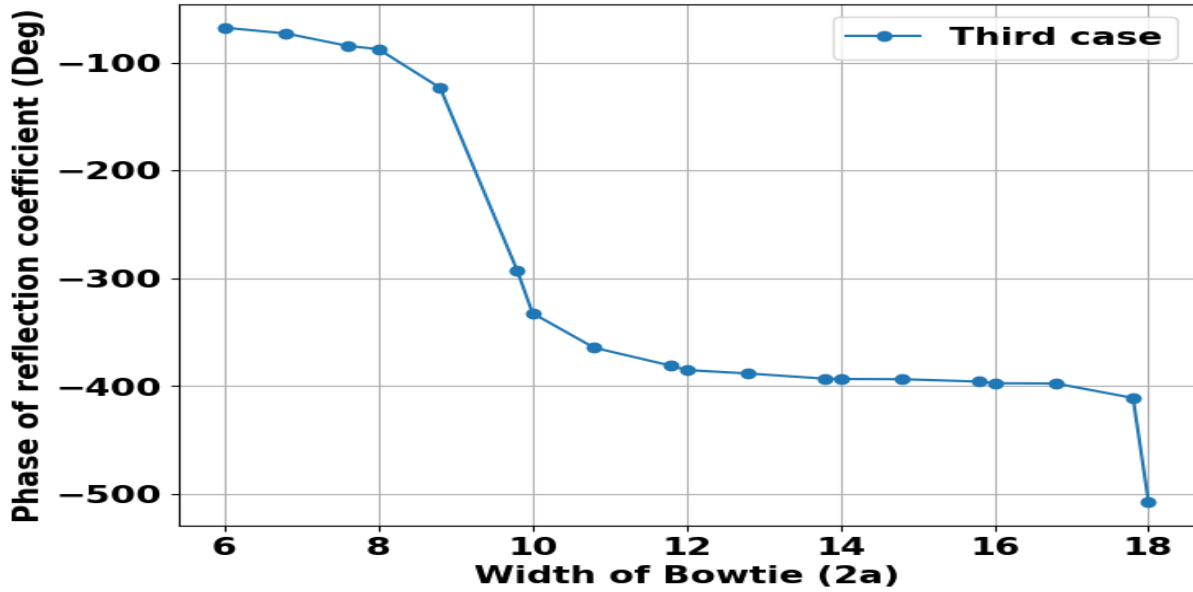


Figure 4.20. The variation of the reflection coefficient phase with width of bowtie at center frequency 8GHz.

Table 4.6 .Phase response and characteristics of the third case .	
Name	Bowtie double ring
Max phase	-67.8
Min phase	-507.2
Center phase	-287.5
Element size for center phase	9.8
Phase range	439.4
Slope(deg /mm)	122.4
Slope (deg /GHz) for First region	211.2

4.3.4 Fourth case

Based on the findings in Chapter 3, the elliptical shape exhibited a lower slope compared to the other proposed models for the bowtie. This is attributed to the reduction of sharp edges, as indicated by the research [82]. Therefore, it will also be compared here with the ring and double ring configurations, as illustrated in the following Fig.4.21. Where it was $a=b$, $S1=0.8$ and $S2=0.7$.

The figures from 4.22 to 4.27 illustrate the reflection coefficient magnitude with the frequency and reflection coefficient phase with the frequency for each model (elliptical bowtie, elliptical bowtie ring, elliptical bowtie double ring).

The width of elliptical bowtie was plotted along with the phase, as shown in the Fig.4.28. It can be observed that it yielded two linear regions, and the slope was calculated for each region, as shown in Table 4.7. It is noteworthy that it gave a lower slope compared to the other analyzed models.

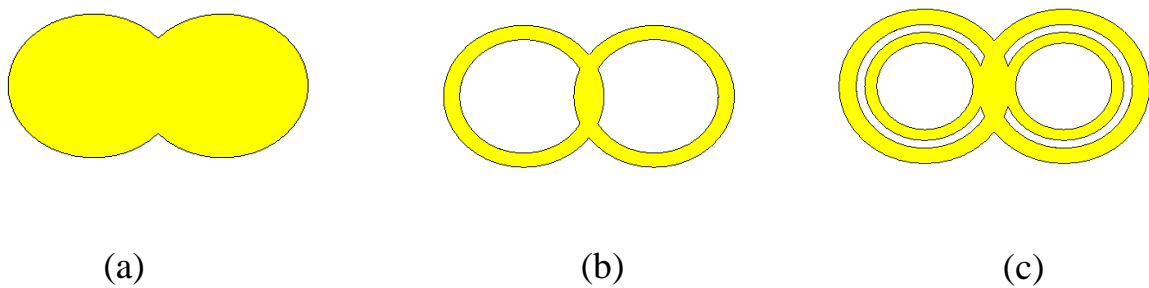


Figure 4.21. Geometry of the investigated of unit cell;(a) elliptical bowtie (b) ;elliptical bowtie ring ;(c) elliptical bowtie double ring at $a=b$.

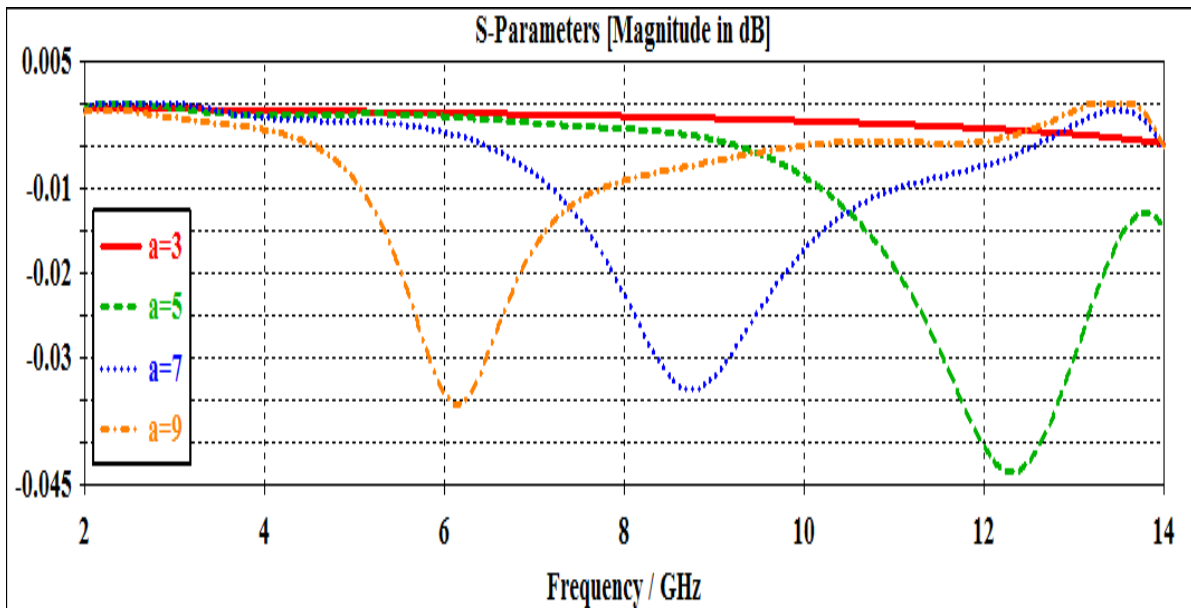


Figure 4.22. The variation of the reflection coefficient magnitude with the frequency for various elliptical bowtie sizes ($b=a$).

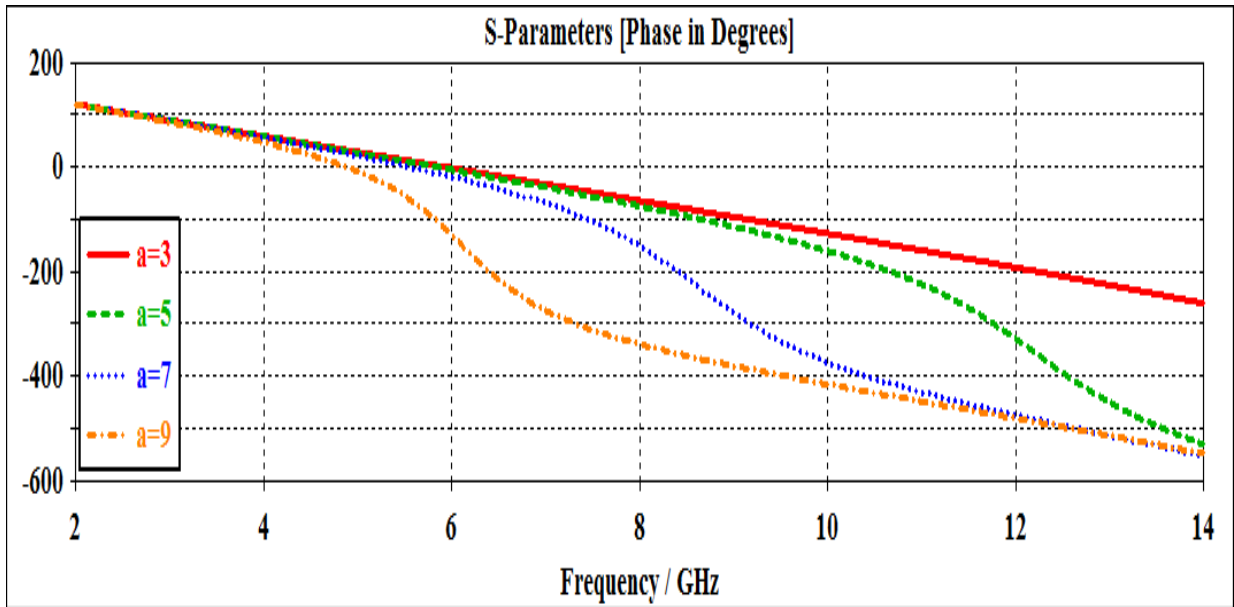


Figure 4.23. The variation of the reflection coefficient phase with the frequency for various elliptical bowtie sizes ($b=a$).

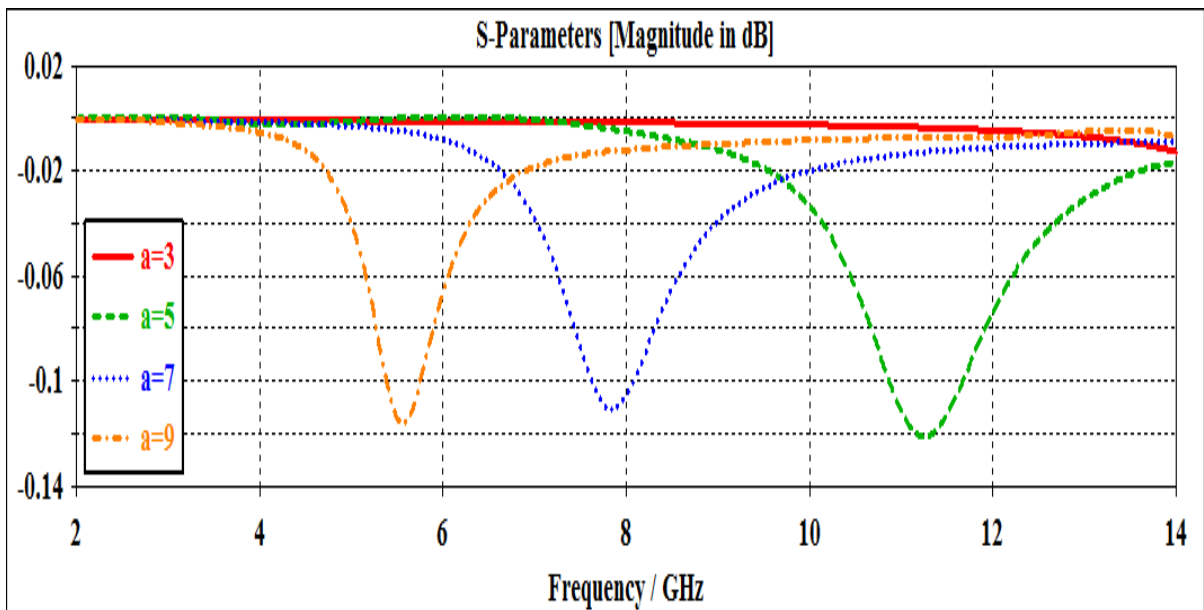


Figure 4.24. The variation of the reflection coefficient magnitude with the frequency for various elliptical bowtie ring sizes ($b=a$).

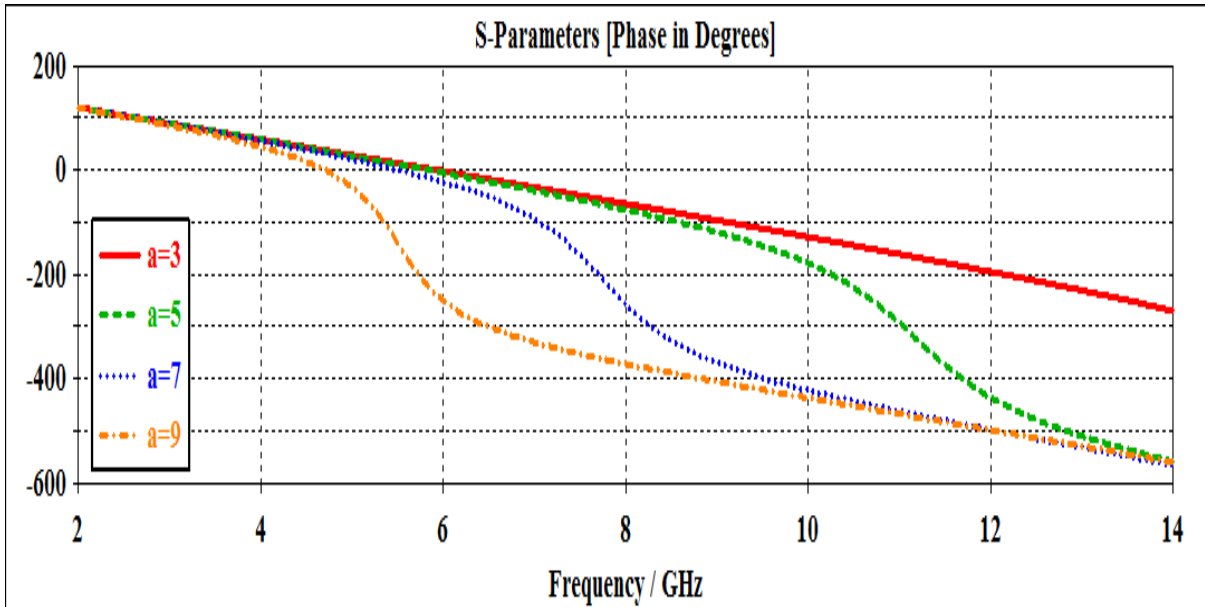


Figure 4.25. The variation of the reflection coefficient phase with the frequency for various elliptical bowtie ring sizes ($b=a$).

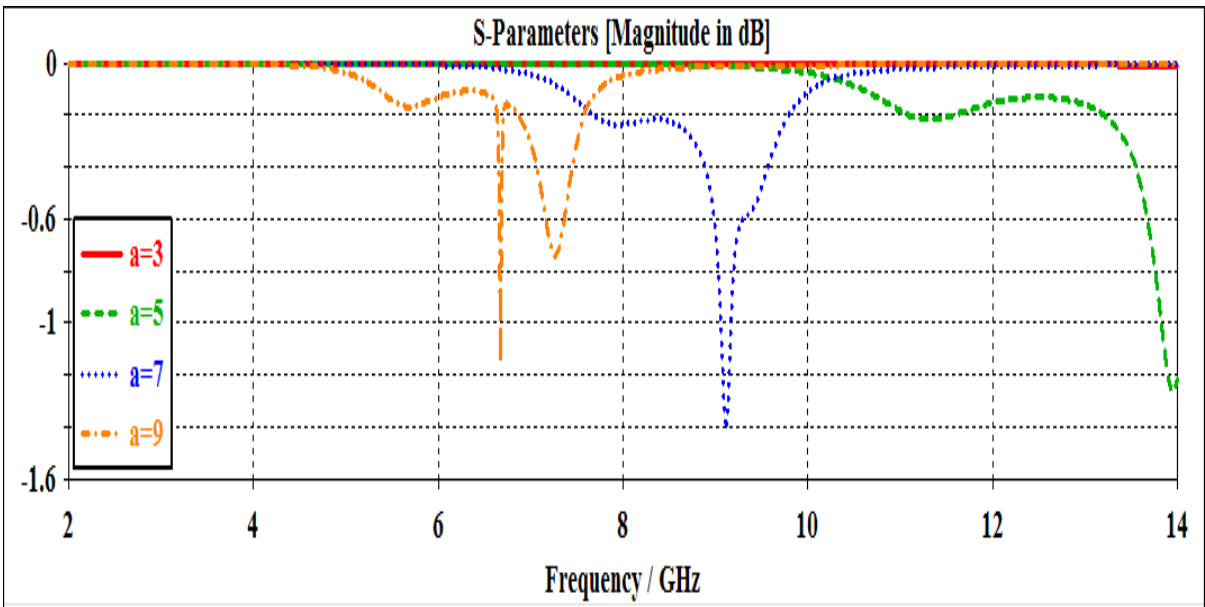


Figure 4.26. The variation of the reflection coefficient magnitude with the frequency for various elliptical bowtie double ring sizes ($b=a$).

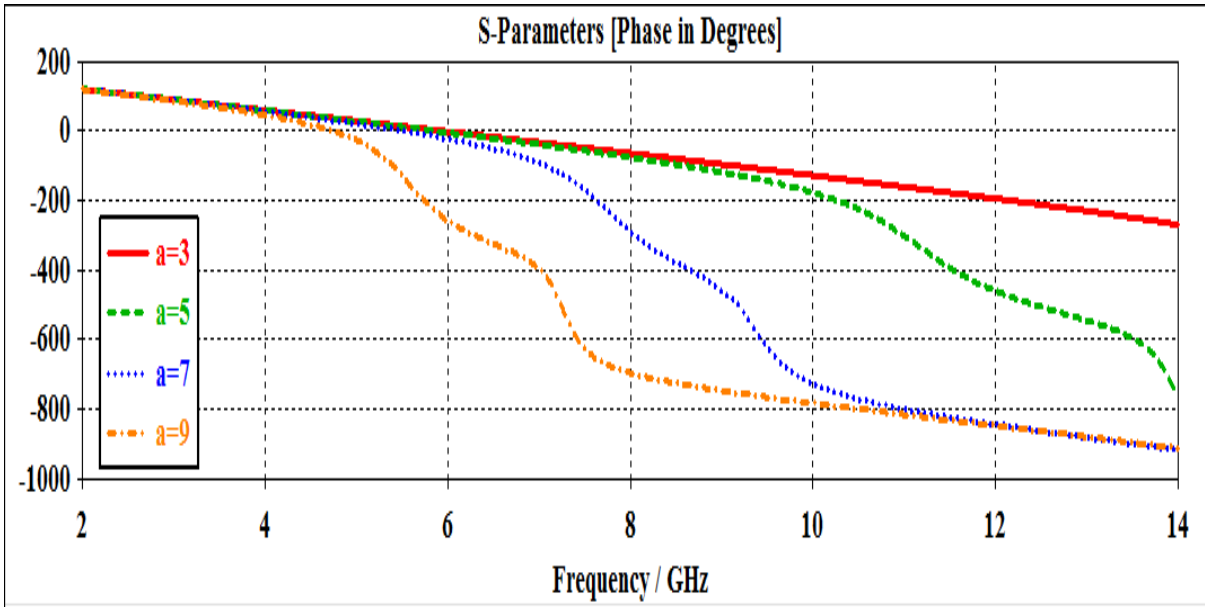


Figure 4.27. The variation of the reflection coefficient phase with the frequency for various elliptical bowtie double ring sizes ($b=a$).

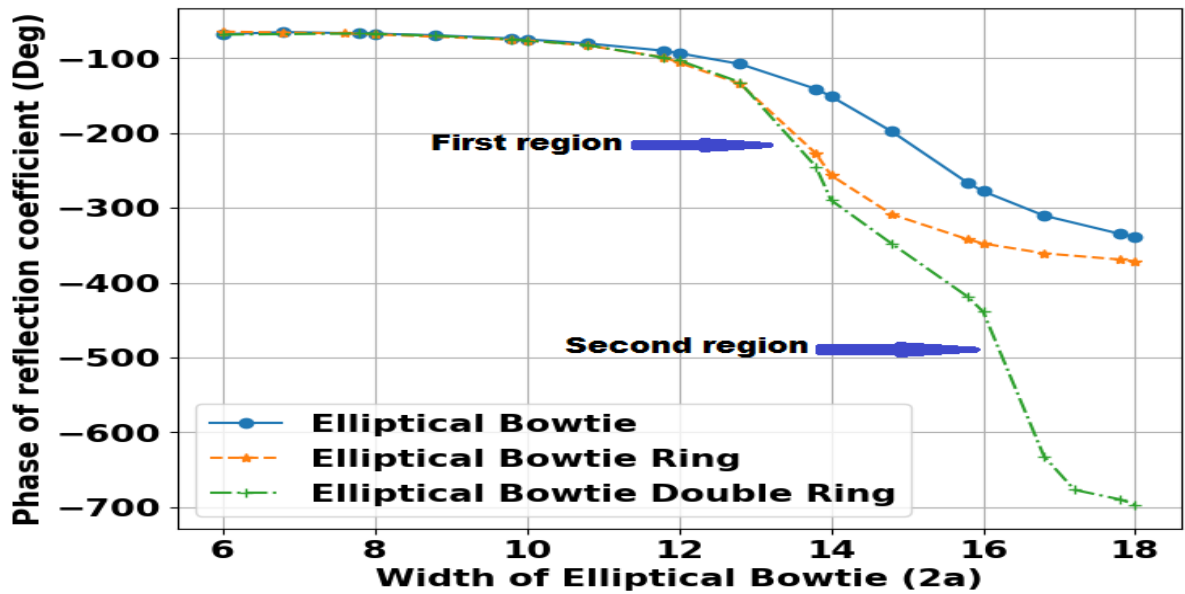


Figure 4.28. The variation of the reflection coefficient phase with width of elliptical bowtie at center frequency 8GHz.

Table 4.7. Phase response and characteristics of the elliptical bowtie , elliptical bowtie ring and elliptical bowtie double ring unit cell.				
Name	Elliptical Bowtie	Elliptical Bowtie Ring	Elliptical Double ring	
Max phase	-64.1	-64.5	-64.5	
Min phase	-338.5	-371.4	-695.9	
Center phase	-201.3	-217.9	-380.2	
Element size for center phase	14.8	12.8	14.6	
Phase range	274.4	306.9	631.4	
Slope(deg /mm)	63.4	102.1	Slop for First region	131.4
			Slop for Second region	198.3
Slope (deg /GHz)	117.5	119.1	Slop for First region	149.5
			Slop for Second region	358

CHAPTER FIVE

CONCLUSION AND FUTURE WORK

5.1 Conclusions

The reflectarray antenna combines the functions of a reflector antenna and an array antenna. The analysis of the reflectarray antenna has revealed the influence of various parameters on the phase response performance of its elements. The investigations have revealed the following conclusions:

1-The geometry of bowtie has been utilized in the construction of elements suitable for reflectarray antennas as it is known in antenna applications to have wide band compared to the thin dipole antenna.

2-The unit cell approach simplifies the analysis as only one element of the reflectarray is investigated. The assumption of the boundary conditions (perfect metallic walls and perfect magnetic walls) helped to treat the whole array through a single element. The obtained results from the unit cell were the reflection coefficient S_{11} assuming a waveguide port. The magnitude of S_{11} was used to determine the resonance frequency, while the dip (minimum value of $|S_{11}|$) gives indication about the loss incurred by the element.

3-The study demonstrated that by manipulating the shapes of elements and adjusting the dimensions, the characteristics of desired features of the phase response can be controlled and optimized. These characteristics encompass the phase range and the slope of this phase with respect either the element size or the frequency.

4-The investigations have been conducted on various bowtie element shapes, and results shown that using a single resonance element in a unit cell can result in a slower phase slope, but this comes at the cost of a limited phase range, typically less than 300° .

5- The bowtie was specially developed to achieve element shapes that generate a suitable phase response with a low slope, achieving the desired phase slope and resulted in reducing the phase range to below 360° . The slope of the phase response can be reduced by tapering the sharp corners of the element. Moreover, substrate with lower permittivity can offer lower phase response.

6-To solve the problem of the reduced phase range that results from adopting developed elements for the reduction of the phase slope, double ring elements were found a suitable solution.

7-The proposed bowtie shapes were implemented as a single ring configuration, and then further extended to a double ring configuration to achieve the desired phase range and slope. Therefore, some of the increased phase range by adopting the double ring configuration can be tolerated in the process of reducing the phase slope.

8-A double ring design of bowtie shape was investigated and compared with the conventional and single ring design.

9-The proposed double ring elements showed double resonance that were manipulated to achieve lower phase slope with a linear phase characteristic over an adequate phase range.

5.2 Future Work

Overall, reflectarray antennas continue to be an area of active exploration and development, with the potential for significant advancements in the future.

The following aspects can be considered to develop the performed work in this dissertation:

1-Investigating other shapes for the unit cell that are expected to give better performance as regards to the slope of the phase response and the range of the phase.

2- Searching among available substrates for favorable characteristics that help to achieve lower phase slopes.

3-The achieved simulation results need verification by experimental measurements.

References

- [1] J. Huang and J. A. Encinar, "Reflectarray Antennas", John Wiley & Sons, 2008.
- [2] J. Shaker, and Reza Chaharmir, "Microstrip Reflectarray Antennas", "Microstrip and Printed Antennas: New Trends, Techniques and Applications", 2010, pp.113-159.
- [3] M. Y. Ismail and M. Inam, "Resonant Elements for Tunable Reflectarray Antenna Design", "Int. J. Antennas Propag.", vol. 2012, 2012, pp. 1-8, doi: 10.1155/2012/914868.
- [4] A. Kiyani, "Design of Reflectarray Antenna Integrated With FSS Textured Configurations for Wireless Communication Applications", MSc Dissertation, Universiti Tun Hussein Onn Malaysia, 2014.
- [5] P. Nayeri, F. Yang, and A. Z. Elsherbeni, "Reflectarray Antennas: Theory, Designs, and Applications", 2018,
- [6] A. K. Awasthi and A. R. Harish, "Ultra-Wideband Tightly Coupled Dipole Phased Array Antenna," 2017 Int. Conf. Adv. Comput. Commun. Informatics, ICACCI, Udipi, India, 2017, pp. 275-278, , doi: 10.1109 /ICACCI.2017.8125852.
- [7] H. Wang, K. E. Kedze, and I. Park, "Microstrip Patch Array Antenna Using a Parallel and Series Combination Feed Network", 2018 Int. Symp. Antennas Propag. (ISAP), Busan, Korea (South), 2018, pp. 1-2.
- [8] R. Deng, F. Yang, S. Xu, and M. Li, "A Low-Cost Metal-Only Reflectarray Using Modified Slot-Type Phoenix Element with 360° Phase Coverage", IEEE Trans. Antennas Propag., vol. 64, no. 4, 2016, pp. 1556-1560, doi: 10.1109/TAP.2016.2526258.
- [9] M. Trampler, "Reconfigurable Reflectarray Antennas with Bandwidth Enhancement for High Gain, Beam-Steering Applications", PhD Thesis, Univ. Florida, 2019, pp. 2004-2019.
- [10] Y. N. Phua, E. H. Lim, and B. K. Chung, "Design of a Single-Layer Broadband Reflectarray using Circular Microstrip Patch Loaded with two Unequal Slots", "AEU - Int. J. Electron. Commun.", vol. 124, 2020, pp. 153341, doi: 10.1016/j.aeue.2020.153341.
- [11] M. Bozzi, S. Germani, and L. Perregrini, "Performance Comparison of Different Element Shapes used in Printed Reflectarrays", "IEEE Antennas

Wirel.Propag.Lett.,vol.2,2003,pp.219-222,doi:10.1109/LAWP.2003.819687.

- [12] K. H. Sayidmarie and M. E. Bialkowski, "Multi-ring unit Cells for Increased Phasing Range in Single-Layer Microstrip Reflectarrays", Conf. Proc. 2008 IEEE Int. Work. Antenna Technol. Small Antennas Nov. Metamaterials, Chiba, Japan,, 2008,pp. 163-166, doi: 10.1109/IWAT.2008.4511312 .
- [13] M. E. Bialkowski and K. H. Sayidmarie, "Investigations into Phase Characteristics of a Single-Layer Reflectarray Employing Patch or Ring Elements of Variable Size", IEEE Trans. Antennas Propag., vol. 56, no. 11, 2008,pp. 3366-3372, doi: 10.1109/TAP.2008.2005470.
- [14] P. Nayeri, M. E. Bialkowski, and K. H. Sayidmarie, "Design of Double-Ring Unit Cells for Single-Layer Microstrip Reflectarrays", Proc. 2008 Asia Pacific Microw. Conf., Hong Kong, China ,2008,pp. 8-11, doi: 10.1109 / APMC.2008.4958563.
- [15] D. L. Dou, G. Q. Zhang, F. Xing, and Z. Tu, "Broadband Microstrip Reflectarray with Multiple-Resonance Dipoles," 2010 IEEE 12th Int. Conf. Commun. Technol. Nanjing, China, 2010, pp. 262-265, doi: 10.1109 /ICCT.2010.5689256.
- [16] Y. Li, M. E. Bialkowski, K. H. Sayidmarie, and N. V. Shuley, "81-Element Single-Layer Reflectarray With Double-Ring Phasing Elements for Wideband Applications", 2010 IEEE Antennas and Propag.Society Int. Symp. ,Toronto, ON, Canada, 2010, pp. 1-4, doi: 10.1109 /APS.2010.5562103
- [17] P. Nayeri, F. Yang, and A. Z. Elsherbeni, "Bandwidth Improvement Of Reflectarray Antennas Using Closely Spaced Elements" , Progress In Electromagnetics Research, vol. 18, 2011, pp. 19–29.
- [18] K. H. Sayidmarie and M. E. Bialkowski, "Fractal Unit Cells of Increased Phasing Range and Low Slopes for Single-Layer Microstrip Reflectarrays" ,IET Microwaves, Antennas Propag., vol. 5, no. 11, , Nov. 2011 pp. 1371–1379, doi: 10.1049/iet-map.2010.0581.
- [19] M. M. Fakharian, P. Rezaei, and A. A. Orouji, "A Novel Reflectarray Based on the Folded SIR Patch-Slot Configuration", in 8th Eur. Conf. Antennas Propagation, EuCAP 2014, The Hague, Netherlands, May 2014, pp. 1931–1933. doi: 10.1109/EuCAP.2014.6902179.

- [20] L. Zhang, S. Gao, Q. Luo, W. Li, Y. He, and Q. Li, "Single-Layer Wideband Circularly Polarized High-Efficiency Reflectarray for Satellite Communications", *IEEE Trans. Antennas Propag.*, vol. 65, no. 9, Sep. 2017, pp. 4529–4538, doi: 10.1109/TAP.2017.2722824.
- [21] T. Velly, A. Yonatan, U. Umairah, and M. Alaydms, "A Reflectarray Microstrip Antenna with Rectangular Ring and Cross Patch at 28 GHz", in *Proc. 2020 27th Int. Conf. Telecommun. ICT 2020*, Bali, Indonesia, May 2020, pp. 43–46, doi: 10.1109/ICT49546.2020.9239570.
- [22] T. Bashir et al., "Design and Analysis of Reflectarray Compound Unit Cell for 5G Communication", *ACES Journal*, Vol. 35, No. 12, December 2020, pp. 1513-1518.
- [23] M. I. Abbasi, M. Y. Ismail, M. R. Kamarudin, and Q. H. Abbasi, "Reconfigurable Reflectarray Antenna: A Comparison Between Design Using PIN Diodes and Liquid Crystals", *Wirel. Commun. Mob. Comput.*, vol. 2021, no. 8, 2021, doi: 10.1155/2021/2835638.
- [24] C. Molero and P. Padilla, "Wideband Metal-only Reflectarray for Controlling Orthogonal Polarizations", *TechRxiv Prepr.*, 2022, doi: 10.36227/techrxiv.20196173.v1.
- [25] U. Sarwar, M. Amin, D. Dancila, and I. Aziz, "A Wideband Monofilar Helical Reflectarray Antenna with Large-Angle Beam-Scanning Performance", *IEEE Access*, vol. 10, 2022, pp. 25044–25050, doi: 10.1109/ACCESS.2022.3155766.
- [26] S. A. M. Soliman, A. M. Attiya, and Y. M. Antar, "Low Profile/Single Layer X-Band Circularly Polarized Reflectarray with a Linearly Polarized Feed", *Prog. Electromagn. Res. M*, vol. 113, Jul. 2022, pp. 87–99, doi: 10.2528/PIERM22070106.
- [27] W. Luo, S. Yu, N. Kou, Z. Ding, and Z. Zhang, "Design of Height-Adjustable Mechanically Reconfigurable Reflectarray", *Prog. Electromagn. Res. Lett.*, vol. 104, Mar. 2022, pp. 1–6, doi: 10.2528/PIERL 22030801.
- [28] L. Veluchamy, K. T. Selvan, R. Jyoti, and S. S. Kumar, "Wideband Reflectarray Antennas Using Concentric Ring-Based Elements for Ku-Band Applications", *IETE J. Res.*, vol. 69, no. 3, 2023, pp. 1675–1685, May. doi: 10.1080/03772063.2021.1874842.

- [29] E. Hadian, M. M. Taskhiri, S. Fakhte, and D. Ramezani, "Design of a Wideband Flower-like Shape Metamaterial Reflectarray Antenna", *IETE J. Res.*, 2023, pp. 1–8, doi: 10.1080/03772063.2023.2173671.
- [30] H. Zhang, Y. Wang, J. Wang, H. Xiao, X. Chen, and X. Wang, "A Single-Layer Circularly Polarized Reflectarray Antenna with High Aperture Efficiency for Microwave Power Transmission", *Int. J. Antennas Propag.*, vol. 2023, no. 12, 2023, doi: 10.1155/2023/1569710.
- [31] A. Palomares-Caballero, C. Molero, P. Padilla, M. Garcia-Vigueras, and R. Gillard, "Wideband 3-D-Printed Metal-Only Reflectarray for Controlling Orthogonal Linear Polarizations", *IEEE Trans. Antennas Propag.*, vol. 71, no. 3, Mar. 2023, pp. 2247–2258, doi: 10.1109/TAP.2023.3240583.
- [32] A. Ali, M. Khalily, T. Brown, and R. Tafazolli, "Beam-Steering Capability for OAM-Based Reflectarray at 5G-mmWave frequencies", *IET Microwaves, Antennas Propag.*, vol. 17, no. 2, Feb. 2023, pp. 162–168, doi: 10.1049/mia2.12333.
- [33] J. Shaker and M. R. C. J. Ethier, "Reflectarray Antenna Analysis, Design, Fabrication, and Measurement", 2014.
- [34] M. Y. Ismail, H. I. Malik, A. F. M. Zain, S. Adnan, and S. R. Masrol, "A Compact Broadband Dual Resonance Reflectarray Antenna Embedded on Organic Substrate for Space Applications", *ASM Sci. J.*, vol. 12, no. Special Issue 2, 2019, pp. 47–53.
- [35] C. Robert E. Munson, Hussain A. Haddad, and John W. Hanlen, "Microstrip Reflectarray For Satellite Communication and Radar Cross-Section Enhancement or Reduction", *United States Pat.*, no. 19, 1987.
- [36] P. N. F. Y. A. Z. Elsherbeni, "Reflectarray Antennas: Theory, Designs, and Applications", 2018.
- [37] D. M. Pozar, S. D. Targonski, H. D. Syrigos, and S. Member, "Design of Millimeter Wave Microstrip Reflectarrays", *IEEE Trans. Antennas Propag.*, vol. 45, no. 2, Feb. 1997, pp. 287–296, doi: 10.1109/8.560348
- [38] B. A., Constantine, "Antenna theory: analysis and design", 2016.
- [39] G. Kim, M. Hwang, H. Jeong, C. M. Lim, K. Y. Park, and S. Kim, "Design of a Flat-Panel Metasurface Reflectarray C-Band Antenna," *Electron.*, vol. 11, no. 17, Aug. 2022, doi: 10.3390/electronics11172729.
- [40] M. H. Dahri et al., "Aspects of Efficiency Enhancement in Reflectarrays with Analytical Investigation and Accurate Measurement", *Electron.*, vol.

- 9, no. 11, Nov. 2020, pp. 1–26, doi: 10.3390/electronics9111887.
- [41] Xingliang Zhang, F. Yang, S. Xu, and M. Li, "Single-Layer Reflectarray Antenna with Independent Dual-CP Beam Control", *IEEE Antennas Wirel. Propag. Lett.*, vol. 19, no. 4, Apr. 2020, pp. 532–536, doi: 10.1109/LAWP.2020.2969707.
- [42] P. Nayeri, F. Yang, and A. Z. Elsherbeni, "Beam-Scanning Reflectarray Antennas: , A technical overview and state of the art," in *IEEE Antennas and Propagation Magazine*, vol. 57, no. 4, Aug. 2015, pp. 32-47, doi: 10.1109/MAP.2015.245388.
- [43] R. D. Javor, X. Wu, and K. Chang, "Design and Performance of a Microstrip Reflectarray Antenna", *IEEE Transactions on Antennas and Propagation*, vol. 43, no. 9, Sep. 1995, pp. 932–939 ,doi: 10.1109/8.410208.
- [44] H. Hasani, M. Kamyab, and A. Mirkamali, "Broadband Reflectarray Antenna Incorporating Disk Elements With Attached Phase-Delay Lines", *IEEE Antennas Wirel. Propag. Lett.*, vol. 9, 2010, pp. 156–158, doi: 10.1109/LAWP.2010.2044473.
- [45] I. Derafshi, N. Komjani, and M. Mohammadirad, "A Single Layer Broadband Reflectarray Antenna by Using Quasi-spiral Phase Delay Line," vol. 1225, no. c, 2014, pp. 10–13, doi: 10.1109/LAWP.2014.2355496.
- [46] C. Han, Y. Zhang, and Q. Yang, "A Broadband Reflectarray Antenna Using Triple Gapped Rings with Attached Phase-Delay Lines", in *IEEE Transactions on Antennas and Propagation*, vol. 65, no. 5, pp. 2713-2717, May 2017, doi: 10.1109/TAP.2017.2679493
- [47] D. M. Pozar and T. A. Metzler, "Analysis of a Reflectarray Antenna using Microstrip Patches of Variable Size", *Electron. Lett.*, vol. 29, no. 8, 1993, pp. 657–658. doi: 10.1049/el:19930440.
- [48] D. M. Pozar, S. D. Targonski, and R. Pokuls ",A Shaped-Beam Microstrip Patch Reflectarray", *IEEE Trans. Antennas Propag.*, vol. 47, no. 7, 1999, pp. 1167–1173, doi: 10.1109/8.785748.
- [49] M. Y. Ismail, H. I. Malik, and M. Amin, "Design and Analysis of Dual U Slot Reflectarray Antenna for X-band Applications" ,*J. Phys. Conf. Ser.*, vol. 852, no. 1, 2017, doi: 10.1088/1742-6596/852/1/012035.
- [50] K. H. Sayidmarie and M. E. Bialkowski, "Investigation into Bandwidth Limitations of Microstrip Reflectarrays" ,in 2008 3rd Int. Conf. Inf. Commun. Technol. From Theory to Appl. ,Damascus, Syria,, 2008, doi:

10.1109/ICTTA.2008.4530140.

- [51] M. Y. Ismail, M. F. M. Shukri, U. Tun, and H. Onn, "Study Of Phasing Distribution Characteristics Of Reflectarray Antenna Using Different Resonant Elements", *International Journal of Integrated Engineering* vo.1,no.3,2009.
- [52] K. H. Sayidmarie and A. M. Saleh, "Comparison of Phase Responses of Proposed Element Shapes for Reflectarray Unit Cells", 2011 4th IEEE Int. Symp. Microwave, Antenna, Propag. EMC Technol. Wirel. Commun. Beijing, China, 2011, pp. 367-371, doi: 10.1109/MAPE.2011.6156273.
- [53] X. Chen, Q. Chen, P. Feng, and K. Huang, "Efficient Design of the Microstrip Reflectarray Antenna by Optimizing the Reflection Phase Curve", *International Journal of Antennas and Propagation* ,2016, pp. 6–8 ,doi.org/10.1155/2016/8764967.
- [54] M. R. Chaharmir, J. Shaker, M. Cuhaci, and A. Ittipiboon, "Wideband Reflectarray Research at the Communications Research Centre Canada", 2009 13th International Symposium on Antenna Technology and Applied Electromagnetics and the Canadian Radio Science Meeting, 2009.pp. 1–4, doi: 10.1109/ANTEMURSI.2009.4805053.
- [55] M. R. Chaharmir, J. Shaker, M. Cuhaci, and A. Ittipiboon, "Broadband Reflectarray Antenna With Double Cross Loops", *Electronics Letters*, vol. 42, no. 2, 19th January 2006,pp. 1–2, doi: 10.1049/el.
- [56] K. Q. Henderson and N. Ghalichechian, "Circular-Polarized Metal-Only Reflectarray with Multi-Slot Elements", *IEEE Trans. Antennas Propag.*, vol. 68, no. 9, 2020,pp. 6695–6703, doi: 10.1109/TAP.2020.2993229 .
- [57] S. F. Qotolo, H. R. Hassani, M. Naser-moghadasi, and I. Azad, "A Novel Broadband Reflectarray Antenna with Lattice Stubs on Square Element For KU-band", vol. 57, no. 11, 2022, pp. 471–473, doi: 10.1002/mop.
- [58] R. S. Malfajani and Z. Atlasbaf, "Design and Implementation of a Dual-Band Single Layer Reflectarray in X and K Bands", *IEEE Transactions on Antennas and Propagation* ,vol. 62, no. 8, 2014,pp. 4425–4431, doi: 10.1109/TAP.2014.2327137.
- [59] Soliman, Shimaa AM, Eman M. Eldesouki, and Ahmed M. Attiya. "Analysis and design of an X-band Reflectarray Antenna for Remote Sensing Satellite System" ,*Sensors* ,vo.22,no.3, 2022,pp.1166, doi .org/10.3390/s22031166 .

- [60] A. Gómez Álvarez, B. Imaz Lueje, D. Rodríguez Prado, M. Arrebola Baena, and M. Rodríguez Pino, "Comparative Study of Different Approaches to Analyze Unit Cells of Reflectarray Antennas", in 15th Eur. Conf. Antennas Propag., (EuCAP). European Association on Antennas and Propagation (EuCAP) 2021. Available: <http://hdl.handle.net/10651/61852>.
- [61] M. R. Chaharmir, J. Shaker, M. Cuhaci, and A. Ittipiboon, "A Broadband Reflectarray Antenna with Double Square Rings as the Cell Elements", 2006 First European Conference on Antennas and Propagation. Nice, France, 2006, pp. 1-4, doi: 10.1109/EUCAP.2006.4584613.
- [62] K. H. Sayidmarie and M. E. Bialkowski, "Phasing of a Microstrip Reflectarray using Multi-Dimensional Scaling of its Elements ", Progress In Electromagnetics Research B 2 ,vol. 2, 2008,pp. 125–136.
- [63] I. Bulu and H. Caglayan, "Single-Layer Microstrip Reflectarray with Double Elliptical Ring Elements for Bandwidth Enhancement", *Microw. Opt.*, vol. 48, no. 12, 2006 ,pp. 1083-1087, doi: 10.1002/mop.
- [64] Fernandez, Santiago RC, and Marcos RR Gesualdi., "Possibilities for Realization of Optical Non-Diffracting Beams by Holographic Metasurfaces using Surface Impedance.
- [65] A. Y. I. Ashyap et al., "An Overview of Electromagnetic Band-Gap Integrated Wearable Antennas", *IEEE Access*, vol. 8, 2020,pp. 7641–7658, doi: 10.1109/ACCESS.2020.2963997.
- [66] S. Li, Y. Cai, Y. Cao, B. Zhang, and T. Wu, "Design of a Wideband Bowtie-Shaped Reflectarray Antenna Loaded with Parasitic Split Rings", *Microw. Opt. Technol. Lett.*, vol. 64, no. 1, 2022,pp. 154–160, doi: 10.1002/mop.33072.
- [67] Qu, Shi-Wei, and Cheng-Li Ruan, "Effect of round corners on bowtie antennas." *Progress In Electromagnetics Research " ,vo. 57,2006,pp.179-195*, doi.org/10.2528/PIER05072103.
- [68] R. Gonçalves Licursi de Mello, A. C. Lepage, and X. Begaud, "The Bowtie Antenna: Performance Limitations and Improvements", *IET Microwaves, Antennas Propag.*, vol. 16, no. 5, 2022,pp. 283–294. doi: 10.1049/mia2.12242.
- [69] O. W. Ata and M. I. Jawadeh, "Double-Slotted Multiband Bowtie Antenna," in 2019 Int. Symp. Adv. Electr. Commun. Technol. ISAECT, Rome, Italy, 2019, pp. 1–6, doi: 10.1109/ISAECT47714.2019.9069692.

- [70] M. Asgari and A. Shahzadi, "Metallic Cross Bow-ties on Low-Cost Substrate as a Broadband Reflectarray Antenna", *Int. J. RF Microw. Comput. Eng.*, vol. 32, no. 9, 2022, pp. 1–9, doi: 10.1002/mmce.23288.
- [71] M. M. Tahseen and A. A. Kishk, "Ka-Band Circularly Polarized High Efficiency Wide Band Reflectarray Using Cross Bow-Tie Elements", *Progress In Electromagnetics Research* vol. 153, October, 2015, pp. 1–10, doi.org/10.2528/PIER15072305.
- [72] K. H. Sayidmarie and Y. A. Fadhel, "UWB Fractal Monopoles of Rectangular and Triangular Shapes", 2011 4th IEEE Int. Symp. Microwave, Antenna, Propag. EMC Technol. Wirel. Commun. , 2011, pp. 709–712, doi: 10.1109/MAPE.2011.6156214.
- [73] A. C. Durgun, S. Member, C. A. Balanis, L. Fellow, C. R. Birtcher, and D. R. Allee, "Design, Simulation, Fabrication and Testing of Flexible Bow-Tie Antennas", *IEEE Transactions on Antennas and Propagation* , vol. 59, no. 12, 2011, pp. 4425–4435, doi: 10.1109/TAP.2011.2165511.
- [74] Sagiroglu, Seref, and Kerim Güney., "Calculation of Resonant Frequency for an Equilateral Triangular Microstrip Antenna with the use of Artificial Neural Networks", *Microwave and Optical Technology Letters* , vo.14, no.2 ,1997, pp. 89-93, doi.org/10.1002/(SICI)1098-2760(19970205) 14:2% 3C89::AID-MOP5%3E3.0.CO;2-H.
- [75] S. H. Yusop, N. Misran, and M. T. Islam, " Analysis of Concentric Split Ring Square Reflectarray Element for Bandwidth Enhancement", 2009 International Conference on Space Science and Communication. Port Dickson, Malaysia, 2009, pp.62-66, doi:10.1109/ICONSPACE2009 5352670.
- [76] N. Misran, R. Cahill, and V. F. Fusco, "Design Optimization of Ring Elements for Broadband Reflectarray Antennas", *IEE Proc. Microwaves, Antennas Propag.*, vol. 150, no. 6, 2003, pp. 440–444, doi: 10.1049/ip-map:20030857.
- [77] R. Florencio, J. A. Encinar, R. R. Boix, V. Losada and G. Toso, "Reflectarray Antennas for Dual Polarization and Broadband Telecom Satellite Applications," in *IEEE Transactions on Antennas and Propagation*, vol. 63, no. 4, pp. 1234-1246, April 2015, doi: 10.1109 / TA P.2015.2391279.
- [78] J. A. Encinar. , "Design of two-layer Printed Reflectarrays for Bandwidth Enhancement", *IEEE Antennas and Propagation Society International Symposium. 1999 Digest. Held in conjunction with: USNC/URSI National*

- Radio Science Meeting (Cat. No. 99CH37010), vol. 2,1999, pp. 1164-1167
vol.2, doi: 10.1109/APS. 789520.
- [79] J. H. Yoon and Y. J. Yoon, "Bandwidth Enhancement of Single-layer Microstrip Reflectarrays with Multi-Dipole Elements", *J. Electromagn. Eng.Sci.*,vol.19,no.2,2019,pp.130–139,doi: 10.26866/ JEES.2019.19.2.130.
- [80] Guo, Lu, Peng-Khiang Tan, and Tan-Huat Chio. , "Bandwidth Improvement of Reflectarrays using Single-Layered Double Concentric Circular Ring Elements on a Subwavelength Grid" ,*Microwave and Optical Technology Letters* vo.56,no.2 ,2014,pp. 418-421 ,doi .org /10 .10 02/mop.28111
- [81] Q. Y. Li, Y. C. Jiao, and G. Zhao, "A Novel Microstrip Rectangular-Patch/ring-Combination Reflectarray Element and its Application", *IEEE Antennas Wirel. Propag. Lett.*, vol. 8, 2009,pp. 1119–1122, doi: 10.1109 /LAWP.2009.2033620 .
- [82] P. Priyalatha, P. Choudhary, and R. Kumari, "Ultra-Wideband Edge Trimmed Bowtie Antenna for X-band Radar Communication", 2023 IEEE 13th Annu. Comput. Commun. Work. Conf. CCWC Las Vegas, NV, USA,June2023, pp. 1231–1235, doi: 10.1109 /CCWC5 7344.2023. 100 99062.
- [83] Tsai, F-CE, and Marek E. Bialkowski, "Designing a 161-Element Ku-Band Microstrip Reflectarray of Variable Size Patches Using an Equivalent Unit Cell Waveguide Approach", *IEEE transactions on antennas and propagation* ,vo.51,no.10 ,2003,pp. 2953-2962, doi: 10.1109/TAP.2003.818001.